Numerical Modeling of the Performance of Highway Bridge Approach Slabs

by

Gregory S. Rajek

A thesis in partial fulfillment of the requirements for the degree of

Master of Science

(Civil Engineering)

UNIVERSITY OF WISCONSIN - MADISON

2010

Numerical Modeling of the Performance of Highway Bridge Approach Slabs

APPROVED BY:

_____ _____

Dr. Michael G. Oliva Date

Major Advisor

Professor of Civil and Environmental Engineering

University of Wisconsin - Madison

Abstract

The primary purpose of the highway bridge approach slab is to create a smooth transition from the roadway to the bridge. This transition becomes rough when deterioration of the approach slab occurs. Several state department of transportation's have noted the formation of a void under the approach slab that contributed to the deterioration. Void formation is typically the result of erosion, expansion joint, movement of the abutment from cyclic loading, and poor compaction methods. Previous research has identified other causes of approach slab deterioration and recommended methods to mitigate the problem.

The finite element program, Abaqus, was used for the numerical analysis of the roadway, approach slab, abutment, and fill as they related to approach slab deterioration. The void under the approach slab was incorporated into each model. Parametric studies were performed to determine the influential parameters that contribute to the deterioration of the approach slab. The parameters investigated were:

- Void geometry
- Abutment height
- Approach slab length
- Soil stiffness
- Concrete stiffness
- Joint restrictions (the joint between the roadway and approach slab)

This research concluded that abutment height, soil stiffness, and concrete stiffness had the largest impact on approach slab deterioration.

Acknowledgements

I would like to express my sincere gratitude to my advisors, Dr. Michael G. Oliva and Dr. James A. Schneider, for their support and guidance throughout my graduate studies. This thesis would not have been possible without the advice and direction provided by these individuals.

I would also like to thank my fellow students who have provided me with feedback on this research. Thanks to Demirhan, Jake, Pinar, Dave, Mike, Han, Derek, David, Kevin, and Miguel.

Most importantly, I would like to thank my wife Mary for her love, understanding, support, and encouragement she has given me during the time spent conducting this research. None of this could have been achieved without her in my life, I am eternally grateful to have her in my life.

Table of Contents

List of Figures

List of Tables

Chapter 1: Introduction

1.1 Background

Approach slab settlement and deterioration has been studied by various researchers throughout the past 20 years. Specifically, researchers have studied differential settlement in approach slabs, as this has been cited as the main cause for failure of approach slabs (Seo, 2003).

As the primary purpose of the approach slab is to create a smooth transition from the roadway to the bridge, failure of an approach slab is evidenced by a "bump" experienced by roadway users when they enter or exit a bridge. Differential settlement occurs when one end of the approach slab (typically supported by soil) settles a different amount than the other end (typically supported by a bridge abutment). Previous research attributes some causes of differential settlement to consolidation of backfill materials, poor drainage, poor construction methods (Seo, 2003), expansion joint failure, and the type of abutment (Helwany, et al., 2007).

Once differential settlement reaches a depth of ½ inch, roadway users are able to distinguish a "bump" at the time of the bridge exit / entry (Wahls, 1990). Differential settlement of 1 inch becomes problematic to the Department of Transportation (DOT), as repair or replacement of the approach slab is recommended for this amount of differential settlement (Zaman, et al., 1991); serious rider discomfort is experienced when a differential

settlement of 2 inches or more exists (Stark, et al., 1995). Several DOTs have noted the formation of a void space beneath problematic approach slabs (CTC & Associates, LLC, 2010). Research performed on cyclically loaded loose backfill discovered the maximum geometry of the void was dependent on abutment geometry (Cosgrove & Lehane, 2003)

In order to assess the ubiquitousness of approach slab failure rates across multiple States, a survey was sent to various state DOTs to assess the problems associated with expansion joint failures occurring between the approach slab and bridge in their region. Thirteen (13) of the eighteen (18) DOT respondents utilized expansion joints between the approach slab and bridge; 12 of the 13 DOTs that use expansion joints have reported expansion joint failures (CTC & Associates, LLC, 2010).

1.2 Objectives

The main objective of this research was to determine an expected range of end rotation for the approach slab at the abutment-approach slab interface. Secondary objectives of this research are:

- Determining which variables influence approach slab cracking.
- Determining a modified impact factor that would cause approach slab cracking for each case considered.
- Identifying parameters that have the largest impact on approach slab end rotation.

1.3 Scope

This work investigated the end rotational behavior of approach slabs as well as approach slab cracking. Parametric studies that varied the geometry of the settlement trench, abutment height, approach slab length, soil stiffness, concrete stiffness, and joint restrictions placed between the roadway and approach slab were used to determine their effect on the behavior of the approach slab. These investigations were limited to:

- **Loading**
  - One American Association of State Highway and Transportation Officials (AASHTO) HL93 tandem design truck without lane loading.
    - The use of this truck is discussed in Section 3.2.
  - No dynamic or cyclic loading.
    - Cyclic loading was not used in the model but an AASHTO impact/dynamic load factor could have been used to account for dynamic loading.
  - Pile and pile-abutment connections were considered to be rigid.
    - The large variety of pile and abutment connection types and methods were not the focus of this study.

- **Geometry**
  - Non-skewed approach slabs.
    - The two-dimensional analyses conducted in this study prevented the consideration of approach slab skew.
  - One lane width.
  - Non-integral abutments were only considered.
    - Only non-integral abutments are used in Wisconsin.

- **Concrete Properties**
  - Elastic properties were used for all concrete members.
    - Inelastic behavior of the concrete members is influence by the type and quantity of reinforcement placed in the concrete. Inelastic properties were not used due to the large variability allowed in the design of concrete components.
    - Inelastic (post-cracking) behavior was not of interest in this study, only the joint rotation and the presence of concrete cracking were of interest.
    - Cracked moment of inertia was used in areas of the approach slab that exceeded the cracking strain as defined by ACI.
      - The use of the cracked moment of inertia instead of a modified moment of inertia was considered to be conservative as the cracked moment of inertia would be smaller than the modified moment of inertia.
  - Variations of Poisson's ratio were not considered.
    - Variations in Poisson's ratio are discussed in Section 3.1.1.2.
  - Volume changes from shrinkage, creep, and thermal changes were not considered.
    - Volumetric changes from shrinkage were assumed to have occurred before the formation of the void beneath the approach slab.

- **Soil**
  - Natural soil type and location was not considered.
    - The natural soil and fill were assumed to have equivalent properties.
    - It was not possible to do extensive soil modeling within the pilot study scope.
  - The location of the water table was not considered.
    - The location would vary depending on site specific conditions.
  - Volume changes from creep and thermal changes were not considered.

Chapter 2: Literature Review

2.1 Problems Associated with Highway Bridge Approach Slabs

Highway bridge approach slabs are intended to create a smooth transition between the roadway and bridge. Differential settlement often occurs between the bridge and roadway facilitating the need for approach slab implementation (Ha, et al., 2002). An expansion joint is typically placed between the approach slab and abutment to accommodate volumetric changes in the approach slab and bridge as well as preventing surface water from infiltrating the fill beneath the approach slab.

Problems associated with bridge approach slabs have been investigated by a large number of researchers and transportation officials. On average, 25% of all bridges in the United States have problems associated with approach slabs (Seo, 2003). The most noticeable problem that users experience is the bump that is created by differential settlement of the approach slab. Previous research has identified the settlement of the embankment due to a weak natural soil, compression of the embankment fill, voids under the pavement due to erosion, abutment displacement due to pavement growth, slope instability, and temperature cycles (Seo, 2003) as the main reasons for the formation of the bump. The same study noted the bump became more severe if a high embankment, an abutment constructed on piles, high average daily traffic, soft natural soil, intense rain storms, extreme temperature cycles, and steep approach gradients existed. Conclusions

gathered from a Federal Highway Administration (FHWA, 1990) study attribute some approach slab deterioration problems to;

1. Movement of the natural soil under the embankment due to expansive soils, frost heave, or settlement.
2. Construction practices that fail to meet design requirements.
3. Inadequate or poor quality fill.
4. Vehicular overloading or inadequate designs attributing to excessive deflection.
5. Inadequate or poor drainage.
6. Loss of underlying fill due to erosion.
7. Inadequate or poor joints between the approach slab and bridge deck.
8. Thermal expansion and contraction of the approach slab.

The problems outlined above can be summarized into four categories (Helwany, et al., 2007);

1. Poor pavement performance
2. Abutment type
3. Soil deformation
4. Poor drainage

Previous research performed by Wahls (1990), Zaman (1991), Stark (1995), Ha (2002), Seo (2002), White et al. (2007), and Helwany et al. (2007) identified many of the problems associated with highway bridge approach slabs and methods to mitigate those problems. Figure 2.1 summarizes some of the most common problems encountered at bridge sites by White et al. (2007).

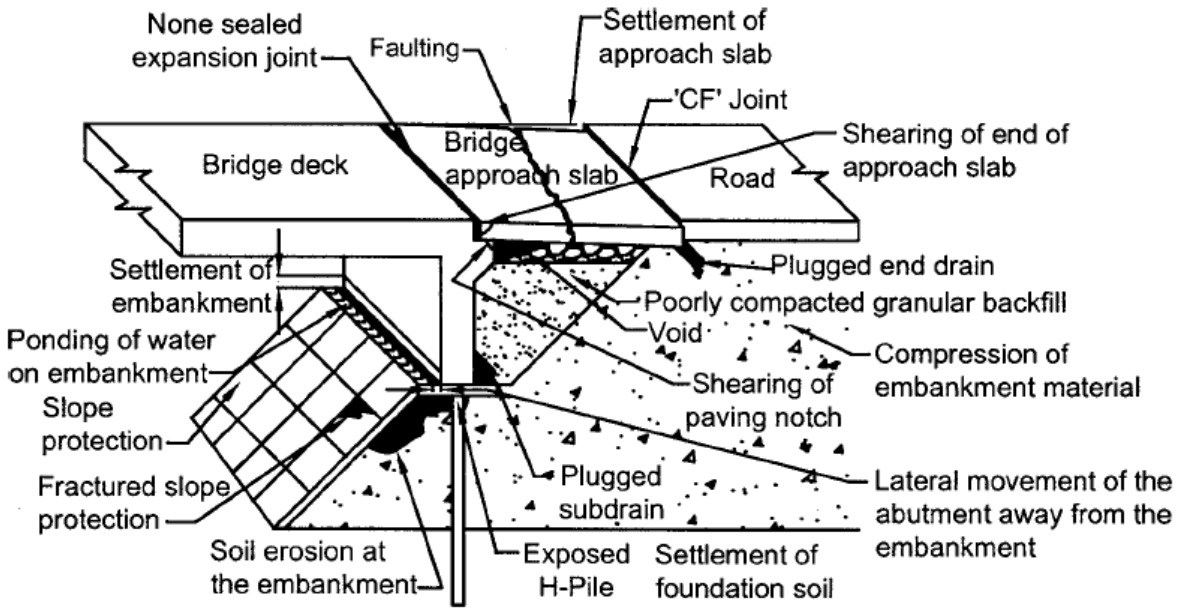

Figure 2.1 – Common problems encountered at bridge sites (White et al. 2007)

2.1.1 Pavement Performance

Poor performance of the pavement may be caused by changes in temperature, improper reinforcement, joint deterioration, and/or actual loads exceeding the design load of the pavement (Helwany, et al., 2007).

Precast approach slabs have been implemented in Iowa in an attempt to maximize the performance of the approach slab. Pre-tensioning and post-tensioning were utilized in the construction of the approach slab. This approach slab was designed to 'span' a maximum 6.1 foot void (Merritt, et al., 2007). The long term behavior of this precast approach slab was unknown at the time of this paper.

2.1.2 Abutment Type

Previous research has identified the behavior of the approach slab as influenced by the geometry and type of abutment used for the bridge. The performance of the approach slab and bridge is structurally affected when the lateral deflection exceeds 2" and/or the vertical deflection exceeds 4" (Wahls, 1990).

Wisconsin Department of Transportation (WisDOT) identifies three main abutment types as closed, stub/sill, and spill-through (Wisconsin Department of Transportation, 2009). These abutments are constructed on both deep and shallow foundations but most foundations in Wisconsin are deep. Deep foundations were only considered in this paper.

Closed type abutments are designed to retain the full soil pressure created from the entire height of the embankment. For this reason, the closed type abutments are commonly known as full height abutments. Figure 2.2 displays a closed type abutment as described by Helwany et. al, 2007.

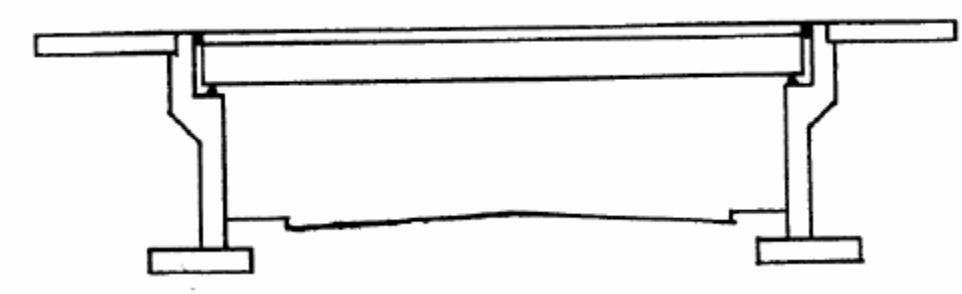

Figure 2.2 – Closed abutment (Helwany et al. 2007)

Stub/sill type abutments are designed to resist a portion of the soil pressure created from the embankment. These abutments are commonly called partial height abutments and generally utilize a slope to retain the embankment. Figure 2.3 displays a stub/sill type abutment as described by Helwany et. al, 2007.

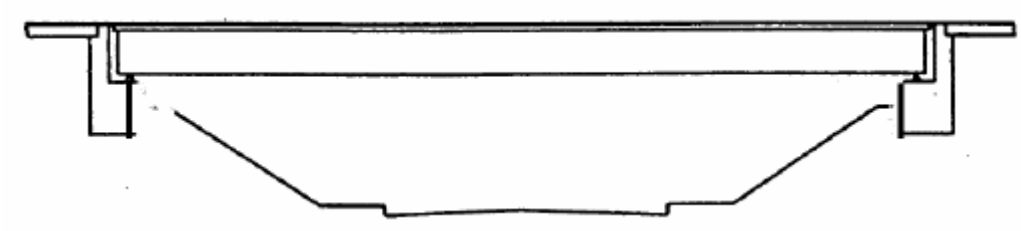

Figure 2.3 – Stub abutment (Helwany et al. 2007)

Spill-through abutment types are initially designed to be stand-alone abutments as well as having some capacity to resist soil pressure. They are commonly used in locations were future expansion would remove the embankment. These abutment types are designed to act as piers when the embankment is removed. Spill-through abutments are

not used by WisDOT. Figure 2.4 displays a typical spill-through type abutment as described by Helwany et. al, 2007.

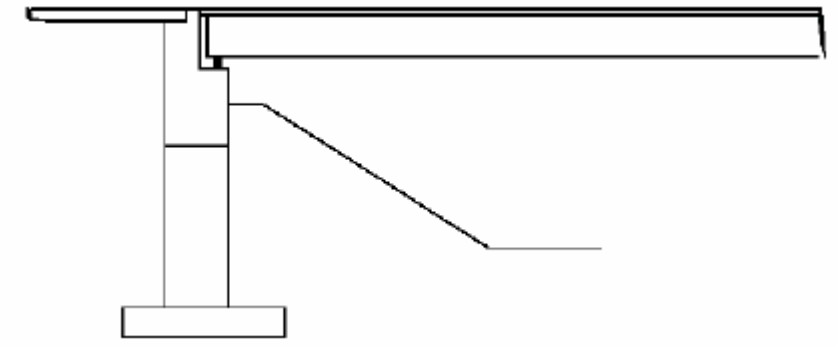

Figure 2.4 – Spill-through abutment (Helwany et al. 2007)

2.1.3 Soil Deformation

Helwany et al. identified multiple construction problems encountered during the compaction of the fill under the approach slab. These problems include:

- Too thick of lifts.
    - Fill layers are too thick resulting in poor compaction.
- The use of improper compaction equipment.
- Limited access near the abutment.
- Compacting outside of the optimum moisture content.
- Lack of inspection or testing of the relative density of the soil.
- The use of low permeability clayey soils.

The effects of cyclic loading on loose sand placed near integral abutments that utilized an approach slab was studied by Cosgrove and Lehane (2003). Multiple tests were performed that simulated active and passive conditions. These tests concluded large

volumetric changes in the soil near the abutment were observed (Cosgrove & Lehane, 2003). Surface approach slab settlement reached the maximum at a horizontal distance of 75% of the total embedment depth. Figure 2.5 displays the normalized surface settlement with respect to abutment height.

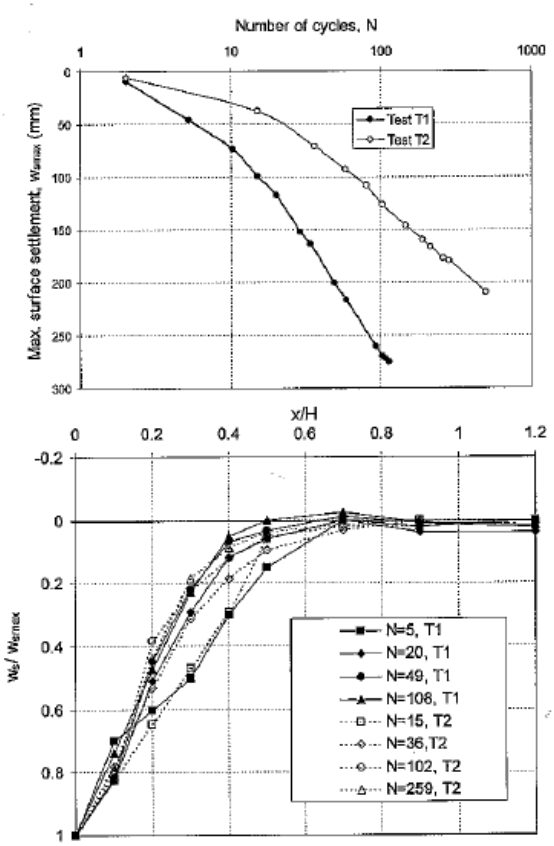

Figure 2.5 – Variation with number of cycles of the maximum settlement (w_{smax}) and the normalized surface settlement profile (plots provided from Cosgrove & Lehane, 2003)

Their study concluded the geometry of the settlement trench was dependent on abutment height.

The Iowa Department of Transportation (Iowa DOT) noted the settlement trench while performing approach slab rehabilitation. Iowa DOT noticed settlement trenches up to 15 feet in length (Merritt, et al., 2007). The depth of these trenches, soil type, and abutment geometry was not reported. Figure 2.6 displays a settlement trench observed under an approach slab discovered during rehabilitation.

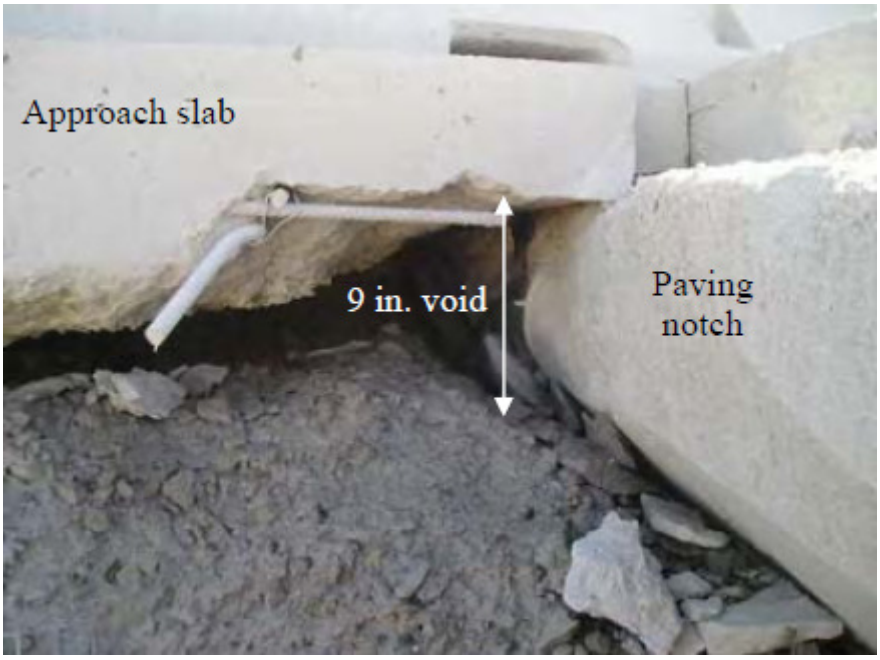

Figure 2.6 – Settlement trench observed from rehabilitation project (White et al. 2005)

2.1.4 Drainage

Improper drainage leads to erosion and weakening of the fill beneath approach slabs. Typical devices used for drainage include plastic drainpipes, weep holes in the abutment, and geosynthetic materials (Hoppe, 1999). When these devices fail, water infiltrates the underlying fill. Water can also invade the fill from weak/dysfunctional expansion joints or cracks in the approach slab (Puppala, et al., 2008). This water can cause erosion of the fines facilitating the creation of a void space beneath the approach slab.

2.2 AASHTO Guidelines

The 2007 AASHTO LRFD Bridge Design Specifications specifies 26 loads to be considered in bridge design in addition to vehicular loads. The loads defined in AASHTO were used to analyze the approach slab as the future intent is to connect the approach slab integrally to the bridge. When this is done, the approach slab will become a part of the bridge and will influence the behavior of the abutment/bridge. These loads consider earth pressures, vehicular (braking, collision, dynamic loading, etc…), pedestrian, environmental (ice, seismic, wind, etc…), and volume change forces. Vehicular loads utilize the HL-93 vehicle load that is identified in Section 3.6.1.2.2 of the code.

The HL-93 vehicle load consists of the following trucks:

- Standard Truck
- Tandem Truck
- Special Truck (Negative Moment Truck)
- Fatigue Truck
- Extreme Event Truck (Overload Truck)

The AASHTO LRFD design code identifies 12 limit states that must be considered during design. The limit states are:

- **Strength 1:** Normal vehicle loads without wind loading.
- **Strength 2:** Special vehicle loads without wind loading.
- **Strength 3:** No vehicular loading but wind loading (> 55 mph) is present.
- **Strength 4:** High dead load with respect to live load (used for large bridges)
- **Strength 5:** Normal vehicle loads with 55 mph wind load.

- **Extreme 1:** Flooding and earthquake loads.
- **Extreme 2:** Vehicular collision and ice loading with reduced live load.

- **Fatigue:** Special repeating vehicular traffic.

- **Service 1:** Normal vehicle loads with 55 mph wind load.
- **Service 2:** Establishes limits on steel yielding.
- **Service 3:** Establishes tension limits in prestressed superstructures.
- **Service 4:** Establishes tension limits in prestressed substructures.

Specific load factors are applied to each load depending on the limit state.

The dynamic allowance factor (also known as the impact factor) is applied to multiple limit states to account for the dynamic loading effects created from surface

imperfections and the natural vibration of the structure. This factor is applied to Strength 1, Strength 2, Strength 5, Extreme 1, Extreme 2, Service 1, Service 2, Service 3, and Fatigue limit states.

Chapter 3: Numerical Modeling

3.1 Detailed Model Introduction

The finite element analysis program, Abaqus[1], was used for the numerical analysis. Components considered in the model included the roadway, approach slab, abutment, soil (both the assumed natural sandy soil and fill), settlement trench, bridge, and truck. An adaptation of the void formation determined from the study performed by Cosgrove and Lehane (2007) was modeled as the settlement trench. Figure 3.1 identifies the components considered in the model.

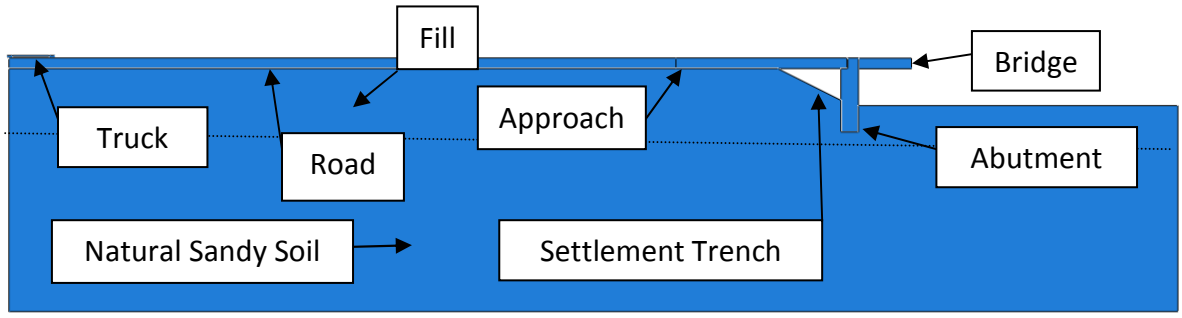

Figure 3.1 – Components considered in numerical model

The finite element model evolved from an initial model. The flaws are described in detail in Section 3.2. Some of the problems encountered with the initial model were:

- Inaccurate boundary conditions placed on the approach slab.
- Improper loading.
  - Incorrect design vehicle axle loads and spacing were used.
  - Axle loads were not placed at critical locations.
- The paving notch was neglected.

[1] Abaqus Finite Element Analysis software was created by Simulia, Inc. Version 6.9 was used for all analyses.

3.1.1 Material Properties

3.1.1.1 Soil Properties

The soil was modeled as a compacted sandy soil using the elastoplastic Mohr-Coulomb material model within Abaqus. Compacted sands are common in Wisconsin (Edil, et al., 2007). The sand emulated in the model was modeled after Portage Sand, as discussed by Schuettpelz et al. (2010). Seven properties were required by Abaqus to define a soil. The seven properties, with appropriate units, were:

- Mass density, lb/in^3 (kg/m^3)
- Young's modulus, psi (Pa)
- Poissons ratio
- Friction angle, degrees
- Dilation angle, degrees
- Meridional eccentricity
- Cohesion, psi (Pa)

Soil properties for three cases are summarized in Table 3.1.

Table 3-1 – Soil properties

Classification	Mass Density (lbm/ft^3)	Young's Modulus (psi)	Poisson's Ratio	Friction Angle (deg)	Dilation Angle (deg)	ϕ'_{cv} (deg)	Meridional Eccentricity	Cohesion (psi)
Stiff	129	14500	0.3	45	12	35	0.1	0.145
Moderately Stiff	124	8700	0.3	37	5.6	32.5	0.1	0.145
Loose	121	1450	0.3	30	0	30	0.1	0.145

Schuettpelz et al. (2010) indicated that Portage sand at a relative compaction of 93% had an equivalent relative density (D_r) of 52%, or a medium dense sand ($0.35 < Dr < 0.65$). At low stresses, the dilation angle (ϕ) of medium dense sands is often on the order of 5^o to 6^o (i.e., Bolton 1986), leading to a peak friction angle of 37^o for a constant volume (ϕ'_{cv}) friction angle of 32.5^o ($\phi'_{pk} \approx \phi'_{cv} + 0.8\psi$). The most critical parameter for the analysis was the Young's modulus (E) of the soil. Young's modulus is often referred to as the elastic modulus.

In pavement design, the resilient modulus (M_r) is often used to characterize 'elastic' behavior during cyclic loading. The resilient modulus is conceptually similar to the elastic modulus, except it is based on 'recoverable' strain (ε_r) instead of axial strain. Schuettpelz et al. (2010) illustrated that when corrections are taken into consideration for void ratio, strain level, and stress level, unload-reload resilient modulus are typically higher than (secant) elastic modulus values at low (< 29 ksi (200MPa)) values of E. The 'correction' of Schuettpelz et al. (2010) was used to increase estimated E values to those appropriate for modeling highway basecourse properties. Figure 3.2 illustrates the difference between the elastic and resilient moduli (Schuettpelz, et al., 2010).

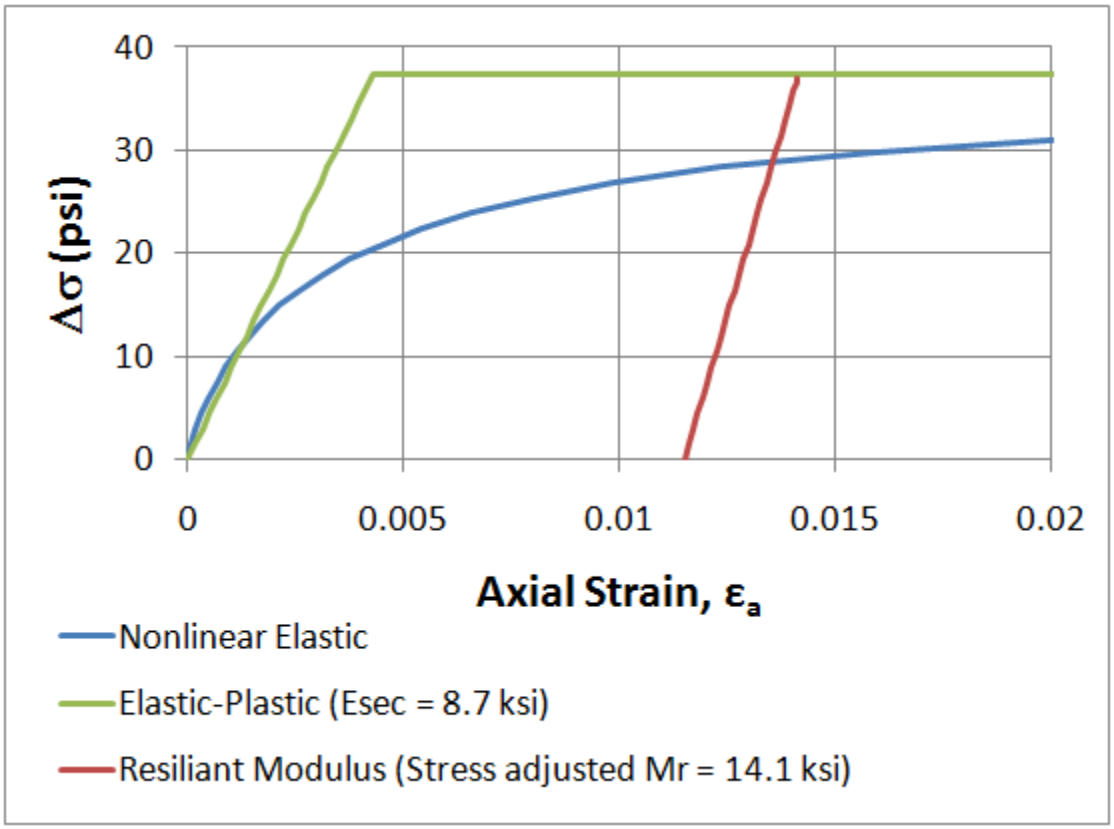

Figure 3.2 – Comparison of nonlinear elastic model with use of secant elastic and secant (stress corrected) resilient moduli (after Schuettpelz et al. 2010)

3.1.1.2 Concrete Properties

Concrete was modeled using the elastic material model within Abaqus. Four concrete properties needed to be defined in Abaqus for each analysis. The four properties, with appropriate units, were:

- Mass density, lb/in^3 (kg/m^3)
- Concrete compressive strength, psi (Pa)
- Young's' Modulus, psi (Pa)
- Poissons Ratio

Table 3.2 displays the concrete properties used to define Type 1 and Type 2 concrete in the model.

Table 3-2 – Concrete properties

Concrete Type	Density (lb/ft^3)	fc' (psi)	Young's Modulus (ksi)	Poissons Ratio
1	145	4000	3605	0.3
2	145	8000	5098	0.3

Mass density of concrete was determined from recommendations specified in ACI 318-08. According to section 2.2 of ACI 318-08, the density of concrete is typically between 135 pcf and 160 pcf. The density of the concrete was taken from the recommendations provided in ACI 318-08, section C2.2, as 145 pcf (2300 kg/m^3).

The 28 day concrete compressive strength (f_c') for Type 1 concrete was based on a report submitted to the Wisconsin Highway Research Program. Concrete studied in WHRP 06-14 had an approximate median 28 day compressive strength of 4000 psi (Naik, et al., 2006). Using this information, the 28 day concrete compressive strength used for the analyses was 4000 psi. Type 2 concrete was used to compare the effects of concrete stiffness on the model. A 28 day compressive strength of 8000 psi was used for Type 2 concrete and is representative of the concrete that could be used if the approach slab was a precast-prestressed concrete slab.

Young's modulus was determined according to the guidelines presented in section 8.5.1 of ACI 318-08. Section 8.5.1 of ACI 318-08 directs the utilization of Equation 3.1 to determine the modulus of elasticity.

$$E = 57000\sqrt{f_c'} \tag{3.1}$$

where:

E	=	Concrete modulus of elasticity, psi (Pa)
f_c'	=	Concrete compressive stress, psi (Pa)

The impact of differing Poisson's ratios was explored. An acceptable range of Poisson's ratio for concrete is from 0.15 to 0.25 (Hall & Mainey, 2008). Analyses were performed with a Poisson's ratio of 0.2 and 0.3 to determine how sensitive the model was to Poisson's ratio. Strain of the approach slab as determined from each analysis was then compared. Less than a 1% difference in strain was noticed between the two models. From the Poisson ratio sensitivity study, it was determined that either value of Poisson's ratio had little effect on the model. A Poisson's ratio of 0.3 was used for all analyses.

Reinforcement was not defined and gross moment of inertia was used for all sections unless the concrete cracking strain was exceeded. Concrete cracking stress was determined using the modulus of rupture as defined in section 9.5.2.3 in ACI 318-08. Equation 3.2 displays the equation presented in ACI 318-08 to determine the modulus of rupture.

$$f_r = 7.5\sqrt{f_c'} \quad (3.2)$$

where:

f_r	=	Modulus of rupture (psi)
f_c'	=	Concrete compressive stress (psi)

Concrete cracking strain was then calculated using Hookes Law. Hookes Law was determined to be valid due to the elastic assumption. Equation 3.3 displays the Hookes Law relationship used to determine the cracking strain. The cracking strain was 132 με for Type 1 and Type 2 concrete.

$$\varepsilon_{crack} = \frac{f_r}{E} \quad (3.3)$$

where:

ε_{crack}	=	Concrete cracking strain (in/in)
f_r	=	Modulus of rupture (psi)
E	=	Modulus of elasticity (psi)

Strain in the concrete members was compared to the cracking strain after each analysis. The moment of inertia was modified for all concrete members that exceeded the cracking strain. The moment of inertia of the cracked section was modified to be 66% of the gross moment of inertia. The resulting strain was again compared to the cracking strain as determined by Equation 3.3.

3.1.2 Modeled Parts

3.1.2.1 Abutment

The abutment used in the Abaqus model was designed to geometrically conform to the A5 abutment described in the WisDOT standard specifications. The abutment incorporated a standard WisDOT paving notch to support the approach slab. Appendix 1 contains the standard A5 abutment drawing provided by WisDOT. Figure 3.3 displays the geometry used to define the abutment in Abaqus.

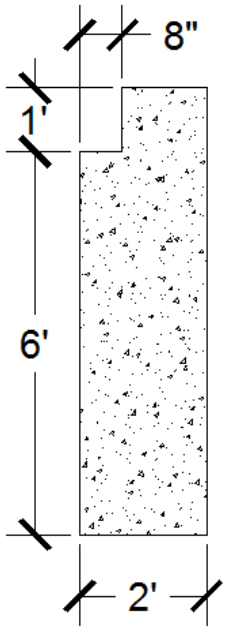

Figure 3.3 – Abutment geometry

All analyses utilized the concrete previously identified as Type 1 concrete (f_c' = 4000 psi) and neglected all superstructure loads placed on the abutment.

3.1.2.2 Roadway

Cross-sectional area of the roadway was determined using guidelines outlined in AASHTO. The width of the roadway was equal to the minimum recommended lane width (12 ft) as defined in the AASHTO 2007 LRFD Bridge Design Specifications. Thickness was maintained at a constant 1 ft thickness throughout the length of the roadway.

To minimize the effects of boundary conditions on the soil under the approach slab during the truck loading, several analysis iterations of models with varying roadway length were conducted. From these analyses, it was determined that the roadway needed to be approximately a minimum of 58 ft long to avoid any disturbance of the soil beneath the approach slab during the initial design truck loading. The minimum length of the roadway analyzed in Abaqus was 59 ft for all of the analysis cases investigated.

All analyses utilized the concrete previously identified in the concrete properties section (Section 3.5.2) at Type 1 concrete (f_c' = 4000 psi).

3.1.2.3 Approach Slab

The non-skewed approach slab analyzed in the model was made to conform to WisDOT standard specifications. WisDOT specified a length of 15'-8" and a thickness of 1 ft for the standard approach slab. The width of the approach slab was the minimum lane

width (12 ft) as defined by the 2007 AASHTO code. The standard drawing of the approach slab provided by WisDOT can be found in Appendix 2.

The initial analysis utilized the concrete previously identified in the concrete properties section (Section 3.1.1.2) as Type 1 concrete (f_c' = 4000 psi).

3.1.2.4 Interaction

Friction was the primary constraint utilized in the model to control all concrete-to-concrete and soil-to-concrete interactions. The coefficient of friction used to define all concrete-to-concrete interactions was taken from section 11.6.4.3 of ACI 318-08. It was assumed that each concrete member was placed against hardened concrete that was not intentionally roughened. Using this assumption, the coefficient of friction (μ_{conc}) was equal to 0.6. The coefficient of friction used to define the soil to concrete interaction was 0.577 (Jardine, et al., 1993).

A coupling restraint was placed at the roadway-approach slab interface. The coupling allowed rotation between the two parts but prevented both horizontal and vertical displacement of the approach slab relative to the roadway. This coupling was placed at the quarter point down from the top of the approach slab. The interaction properties prohibited any overlap of the approach slab onto the roadway. Figure 3.4 displays the location of the coupling between the roadway and approach slab.

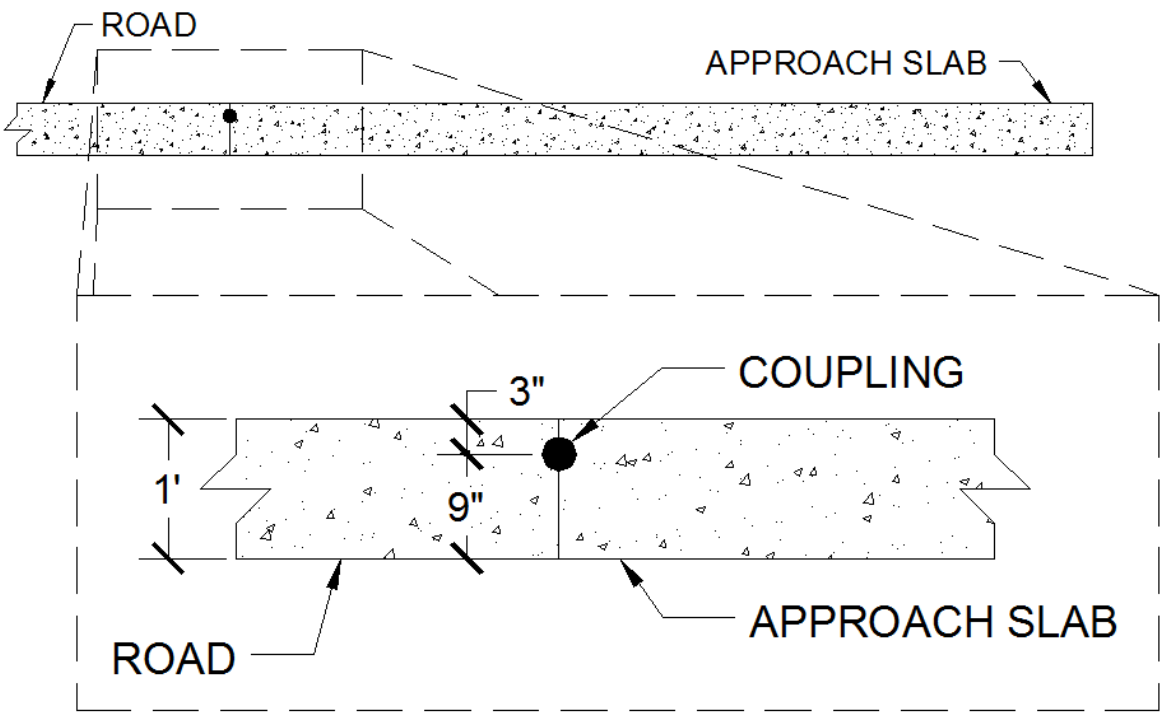

Figure 3.4 – Roadway-approach slab coupling location

3.1.3 Analysis Steps

Each model used four steps to complete the analysis. Gravity was applied to the model during the first analysis step. Boundary conditions placed on the abutment were altered during the second analysis step. Axle loads were applied to the truck during the third analysis step. The last step modified the boundary conditions placed on the truck. Detailed descriptions of the tasks performed in each analysis step are described in Section 3.1.4.

3.1.4 Boundary Conditions and Loading

3.1.4.1 Boundary Conditions

Boundary conditions placed on the fill, roadway, abutment, truck, and bridge were created to best simulate realistic restraints imposed on the approach slab and surrounding components. Improper boundary conditions could drastically affect any finite element model.

Boundary conditions imposed on the fill were determined using recommendations provided by Seo (2003). Seo recommends a 22'-11 ½" (7 m) minimum depth of soil to minimize the adverse effects the boundary condition on approach slab response. The depth of the soil complied with the recommendations provided by Seo. A vertical displacement restraint was implemented at the bottom of the soil to simulate very stiff natural soils or bedrock at depth. Horizontal displacement restraints were placed at the sides of the soil. These boundary conditions did have an effect on the displacement of the roadway near the edge of the model and the impact of this on the approach slab was minimal due to the length of the roadway. Figure 3.5 displays the boundary conditions placed on the model.

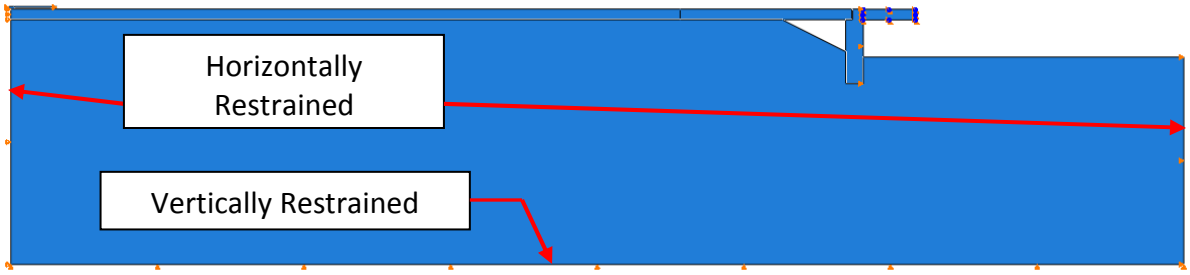

Figure 3.5 – Boundary conditions placed on the soil

A horizontal displacement boundary condition was placed on the end of the roadway. This boundary condition simulated the remaining portion of the roadway not modeled. Figure 3.6 displays the location of this boundary condition.

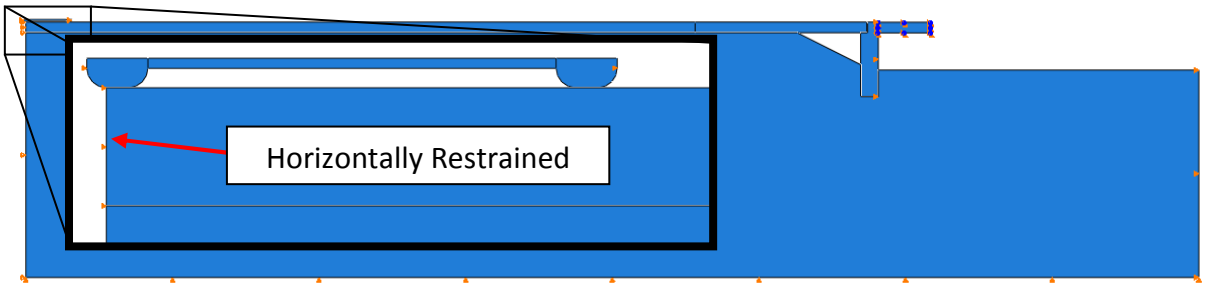

Figure 3.6 – Roadway boundary condition location

Boundary conditions on the abutment were varied depending on the analysis step. Initial boundary conditions were placed on the side of the abutment that allowed vertical displacement while gravity was applied to the model. This boundary condition prevented

rotation of the abutment as the soil was compressed from gravity loading. Figure 3.7 displays this initial boundary condition placed on the abutment.

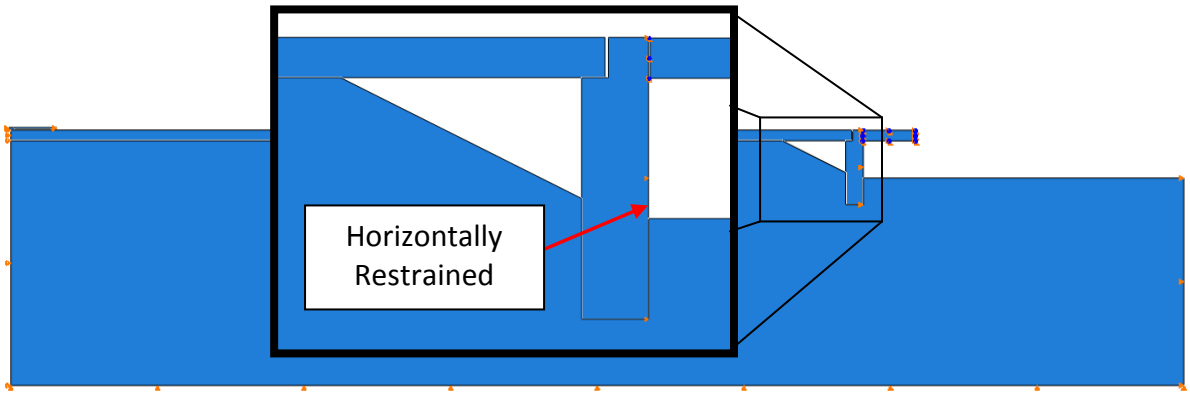

Figure 3.7 – Initial boundary conditions placed on the abutment

The next step in the analysis fixed the bottom of the abutment to simulate a rigid pile and pile connection. The boundary condition placed on the side of the abutment was removed after the boundary condition placed on the bottom of the abutment was applied. The horizontal restraint placed on the side of the abutment was removed so the increase in lateral earth pressure created from the axle loads could be accounted for in the analysis. The flexibility of the pile or connection between the pile and abutment was not considered in any analysis.

The boundary conditions placed on the truck varied depending on the analysis step. Premature movement of the truck during gravity loading was controlled by a horizontal

restraint placed on the tires of the truck. This boundary condition remained in effect until the HL93 tandem truck axle loads were applied to the 'tires'. Figure 3.8 displays the location of the initial boundary conditions prescribed on the 'tires' of the truck.

Figure 3.8 – Modeled truck initial boundary conditions

A second boundary condition applied to the entire truck invoked a controlled horizontal displacement. The chassis material of the truck was given zero density and very low stiffness to allow the wheels to deflect while traversing the gap between the approach slab and abutment. The truck moved horizontally across the roadway and approach slab in 4 inch maximum increments. Abaqus was allowed to automatically reduce this increment if convergence problems were encountered during the analysis. Figure 3.9 displays the final location of the truck.

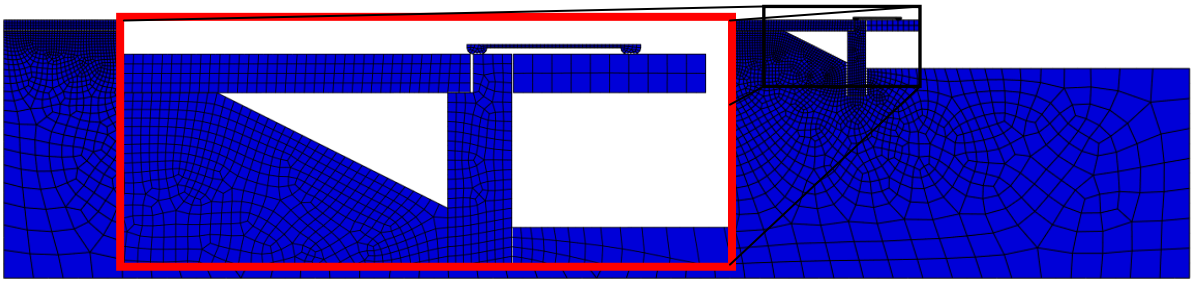

Figure 3.9 – Final location of truck

Initial boundary conditions prescribed on the bridge restricted horizontal, vertical, and rotational displacement. Boundary conditions initially placed on the bridge remained in effect throughout the analysis.

3.1.4.2 Loading

The model was subjected to vertical loads alone. Dynamic, horizontal, or impact loading was not considered in any analysis.

The first analysis step applied gravity to the model. A gravitational acceleration of 32.2 ft/s^2 (9.81 m/s^2) was applied to the entire model. Gravity was required to model the increase in effective vertical stress with depth in the soil. The strength of the granular soil used in the model was dependent on soil particle contact and friction. The gravity load was required to be the first load in the model to ensure proper soil particle friction created from the normal force between the particles. Gravity loading was used for each analysis.

Axle loads applied to the modeled truck conformed to the HL93 tandem design truck outlined by AASHTO. AASHTO specified two 25 kip axle loads spaced 4 ft apart for the HL93 tandem design truck. These axle loads were kept constant while the truck was moved along the roadway and approach slab. Though the model used the AASHTO Service 1 tandem live load, the effect of dynamic impact may be seen by multiplying the results by the AASHTO

impact factor and results for other limit states may be obtained by multiplying by the appropriate factors since the model is assumed to remain elastic (superposition is acceptable). Figure 3.10 displays the axle loading and spacing modeled after the design truck.

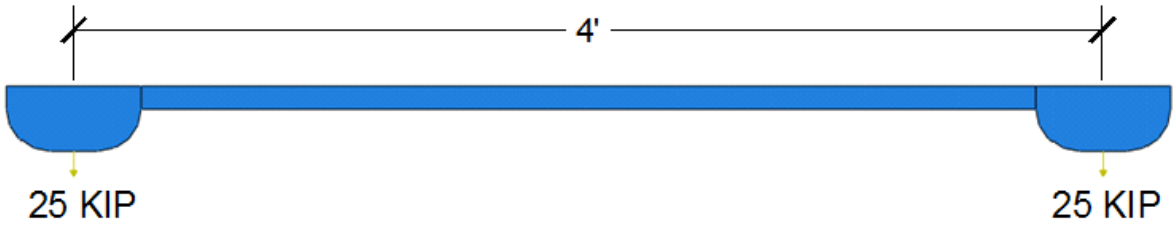

Figure 3.10 – Modeled truck with HL93 axle loading

A separate analysis was performed that considered gravity and uniform lane loading alone. This analysis utilized a vertical distributed load with a magnitude of 640 lb/ft along the lane as defined by AASHTO. The lane load was applied to entire length of the roadway and approach slab.

3.1.5 Mesh

The mesh implemented in the model utilized multiple meshing schemes. Nodal seeding of all concrete parts was governed by size. This seeding ensured the creation of uniformly sized elements when the parts were meshed. Seeding of the fill was governed by a combination of size and biased seeding techniques. The size of the seeds that were in

contact with concrete and the bottom of the fill were governed by size. Biased seeding techniques were used on the edges of the fill and on the fill under the bridge. Figure 3.11 identifies the locations on the fill where the differing seeding techniques were used.

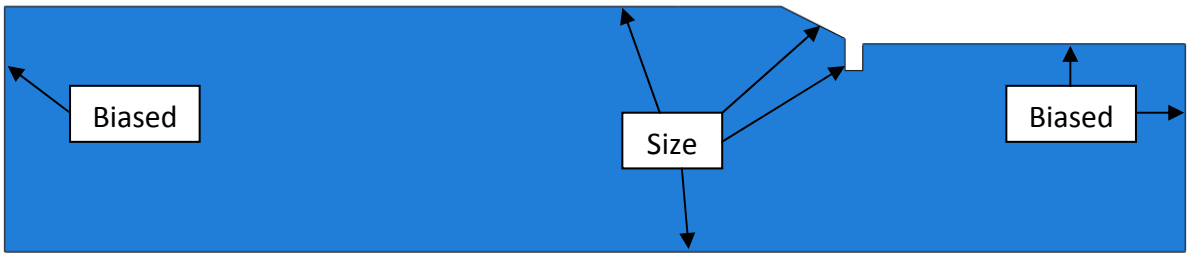

Figure 3.11 – Seeding techniques used to define the mesh on the fill

Figure 3.12 displays the mesh used to analyze the model.

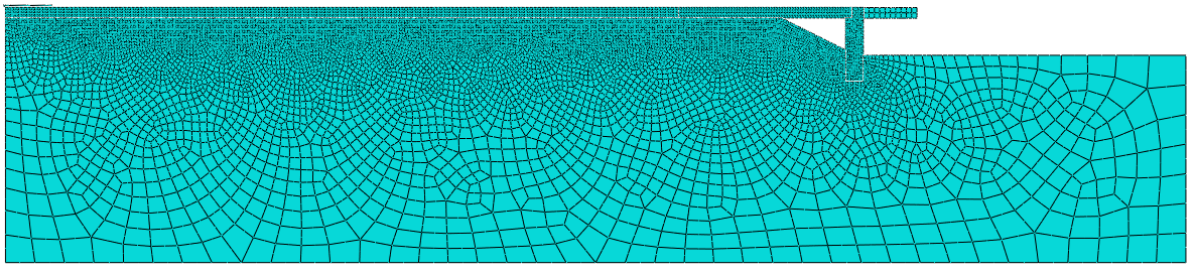

Figure 3.12 – Mesh defined in the model

3.1.5.1 Elements

Plane strain and plane stress elements were used in the model. Plane strain quadrilateral quadratic elements with reduced integration were used for the soil region

(Helwany, 2007). Plane stress quadrilateral quadratic elements with reduced integration were used for all concrete parts.

3.1.5.2 Mesh Refinement Study

A mesh refinement study was performed to determine an acceptable mesh density. The mesh refinement study utilized Richardson's extrapolation formula to determine a quantity of interest calculated with an infinitely fine mesh (Cook, et al., 2002). Richardson's extrapolation formula is shown as Equation 3.4.

$$\phi_\infty = \frac{\phi_1 h_2^q - \phi_2 h_1^q}{h_2^q - h_1^q} \tag{3.4}$$

where:
- ϕ_∞ = Quantity from infinite mesh
- ϕ_1 = Quantity from 1st mesh
- h_2 = Characteristic length *(longest line segment that fits within an element)* of 2nd mesh
- q = Extrapolation exponent
- ϕ_2 = Quantity from 2nd mesh
- h_1 = Characteristic length of 1st mesh

Multiple analyses conducted with a minimum of three different sized mesh densities were required to use Richardson's extrapolation formula. Analyses were conducted with 1.5 inch, 3 inch, and 6 inch sized elements (the length of one side of the element) on the approach slab. Figures 3.13 – 3.15 display the meshes used in the mesh refinement study.

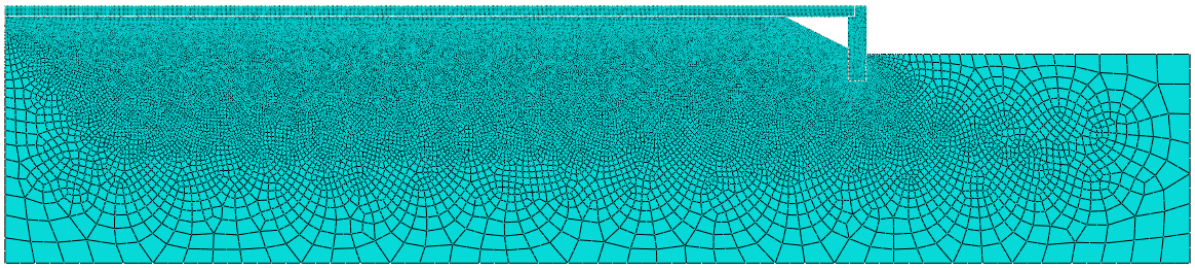

Figure 3.13 – 1.5 inch elements used in mesh refinement study

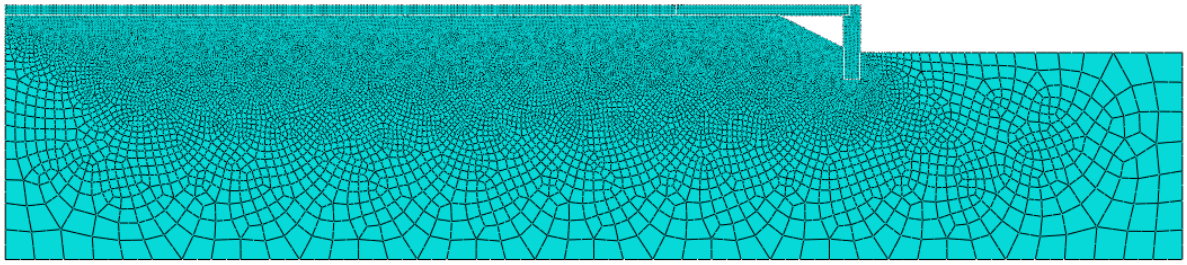

Figure 3.14 – 3 inch elements used in mesh refinement study

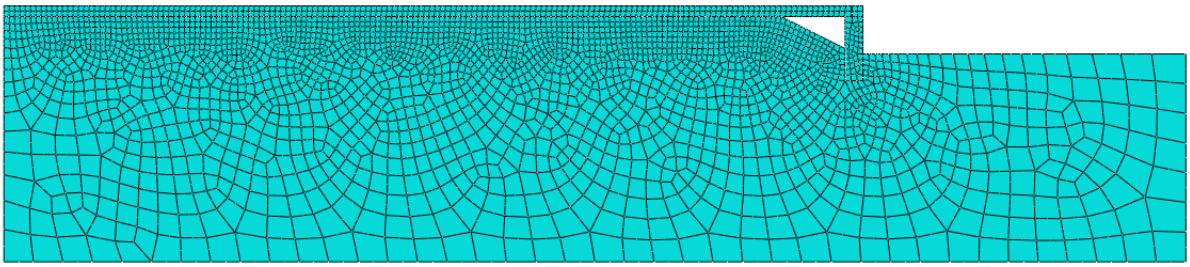

Figure 3.15 – 6 inch elements used in mesh refinement study

Deflection of the approach slab was used as the quantity to compare the mesh densities. The bottom corner of the approach slab, near the roadway, was selected as the

point that would be used for the comparison. Figure 3.16 displays the location of the point used in all comparisons.

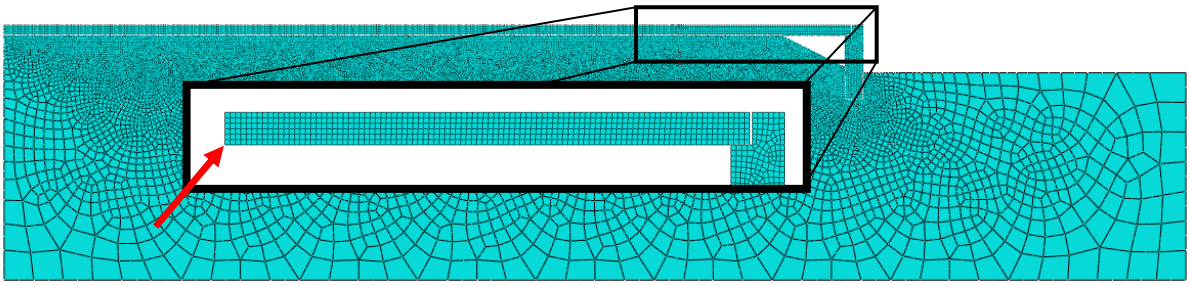

Figure 3.16 – Control point used in mesh refinement study

The extrapolation exponent (q) was determined using methods outlined by Cook et al. (2002). Cook recommended finding the value of q graphically. Deflection (ϕ) taken at the control point identified in Figure 3.16 was plotted against the characteristic length (h) raised to the q power. The value of q was altered until the plot of ϕ vs. h^q plotted a straight line. A value of 2.47 for q was used to plot the straight line. The calculations used to determine q can be found in Appendix 3. Figure 3.17 displays the plot used to determine q.

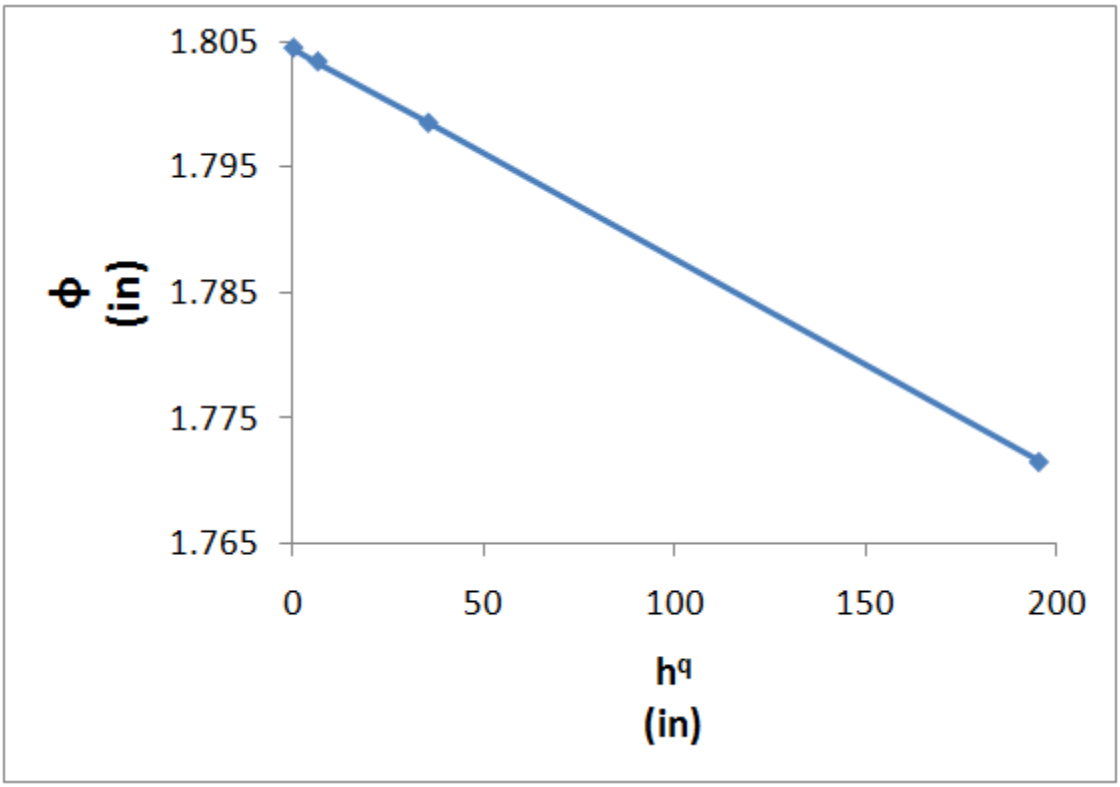

Figure 3.17 – h^q vs. ϕ plot used to determine q for Richardson's extrapolation

The displacement of the point with an infinitely fine mesh could be extrapolated by Equation 3.4 and the variables found above. Equation 3.6 yielded a displacement of 1.804 inches.

The error between the extrapolated displacement and the model containing the 1.5 inch elements was calculated to determine the accuracy of the model. Error was determined using the percent error formula. This formula is presented as Equation 3.5.

$$e_2 = \frac{\phi_2 - \phi_\infty}{\phi_\infty} \times 100\% \quad (3.5)$$

where: e_2 = Error in 2nd mesh
ϕ_2 = Deflection from 2nd mesh
ϕ_∞ = Deflection from infinite mesh

The calculated error between the model with 1.5 inch elements and the same model with an infinitely small mesh was 0.06%.

Richardson's extrapolation formula was applied to the model with 3 inch elements. The runtime of the model with 3 inch elements was reduced by approximately 1.5 hours when compared to the model with 1.5 inch elements. The calculation steps previously defined resulted in a 0.33% error between the model with 3 inch elements and the model with an infinitely fine mesh. This error is considered acceptable and this mesh density was used for all subsequent analyses.

3.1.6 Parametric Studies

A series of parametric studies was performed to determine which variables had the largest impact on concrete cracking and end rotation of the approach slab near the abutment. The parameters investigated were:

- Settlement Trench / Void Geometry
- Approach Slab Length
- Abutment Height
- Soil Stiffness
- Concrete Stiffness
- Approach Slab-Roadway Joint Restrictions

All parametric studies were variations of an established baseline model unless otherwise noted. There was nothing essentially "unique" about the baseline model. It was not assumed to be the best model for the physical slab and bridge, but was simply used as the reference case used to evaluate the effects of changing modeling parameters. The characteristics selected for the baseline model were:

- Soil
  - One homogeneous layer of moderately stiff soil
  - Settlement trench geometry
    - 1 ft vertical gap
    - 2 ft horizontal gap
- Abutment
  - 6 ft height (measured from bottom of approach slab to base of abutment)
  - 4 ksi concrete
- Approach slab
  - 15'-8" length (the standard approach slab length used in Wisconsin)
  - 1 ft thick
  - 4 ksi concrete
  - Shear coupling placed at quarter point utilized to connect approach slab to roadway

- Roadway
  - 59 ft minimum length
  - 1 ft thick
  - 4 ksi concrete
- Truck
  - AASHTO HL93 tandem design truck axle spacing and loads
- Bridge
  - Rigid material
  - Fixed boundary conditions

3.1.6.1 Settlement Trench / Void Geometry

The geometry of the settlement trench formed under the approach slab was varied in this parametric study. Settlement trench geometries analyzed are shown in Figure 3.18, which are in general agreement with observations of Cosgrove & Lehane (2003).

X (ft)	Y (ft)
0	0
2	1
4	2
6	3
8	4

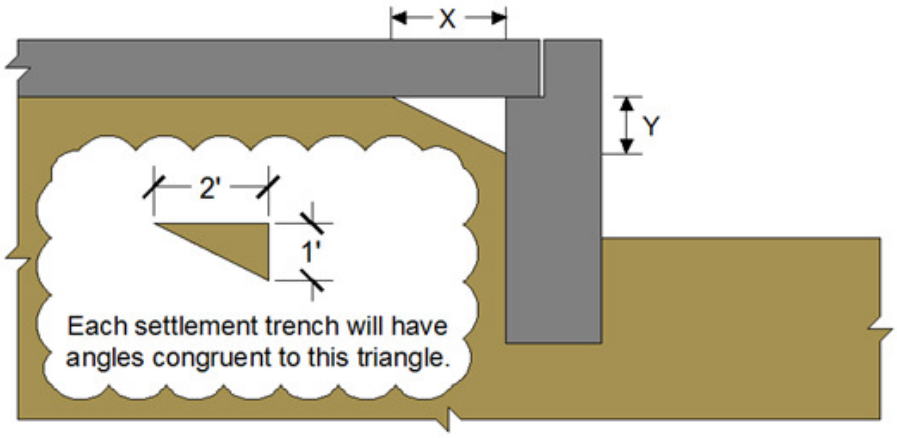

Figure 3.18 – Settlement trench geometries considered in parametric study

While standard practice dictates that the angle of the settlement trench be equal to the constant volume friction angle (32.5 degrees), the model utilized for this study set the

angle of the settlement trench at approximately 26.5 degrees. This was assumed accurate as the saturation of the soil and water pressure buildup within the soil would cause an increase in pore pressures. The effective stress of the soil would decrease as a result of the increase in pore pressure.

3.1.6.2 Approach Slab Length

Differing approach slab lengths were analyzed to determine the impact on concrete cracking and end rotation of the approach slab near the abutment. Approach slabs of 10 ft and 20 ft were analyzed in addition to the baseline model. The length of the roadway was modified to accommodate differing approach slab lengths. Roadway length did not violate the minimum recommended length of 58 ft that was determined in Section 3.1.2.2.

3.1.6.3 Abutment Height

Two differing abutment heights were analyzed to determine their effect on the approach slab. Abutment heights of 8 ft and 12 ft were considered in addition to the 6 ft high abutment used in the base model.

3.1.6.4 Soil Stiffness

The stiffness of the soil under the concrete parts was varied to include a layered soil profile and homogeneous layers of loose and stiff soil. Homogeneous soil layer properties are displayed in Table 3.3.

Table 3-3 – Homogeneous soil layer properties

Classification	Mass Density (lbm/ft^3)	Young's Modulus (psi)	Poisson's Ratio	Friction Angle (deg)	Dilation Angle (deg)	Meridional Eccentricity	Cohesion (psi)
Stiff	129	14500	0.3	45	12	0.1	0.145
Moderately Stiff	124	8700	0.3	37	5.6	0.1	0.145
Loose	121	1450	0.3	30	0	0.1	0.145

The homogeneous soil layers properties do not reflect changes in effective stress with respect to depth and assume uniform compaction throughout the entire layer. A layered soil profile that simulated a stiff soil over loose soil model was analyzed in addition to the homogeneous soil layer analyses to account for changes in effective stress with depth. A graphical representation of the soil layering and a table displaying the layered soil properties is displayed as Figure 3.19 and Table 3.4, respectively.

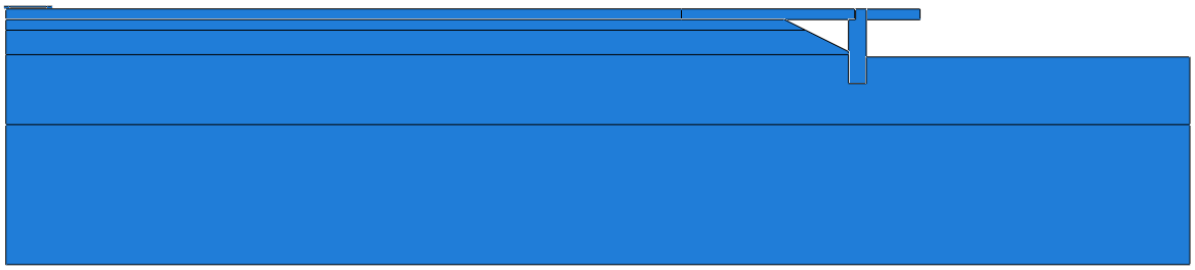

Figure 3.19 – Layered soil profile

Table 3-4 – Layered soil properties

Layer	Depth (ft)	Mass Density (lbm/ft^3)	Young's Modulus (psi)	Poisson's Ratio	Friction Angle (deg)	Dilation Angle (deg)	Meridional Eccentricity	Cohesion (psi)
1	1.0	124	8700	0.3	37	5.6	0.1	0.145
2	2.3	122	3625	0.3	32.1	1.68	0.1	0.145
3	6.6	123	5800	0.3	34.2	3.36	0.1	0.145
4	23.0	124	8700	0.3	37	5.6	0.1	0.145

3.1.6.5 Concrete Stiffness

The stiffness of the approach slab was manipulated with the loose homogeneous soil analysis to test the influence of stiffer concrete. The baseline used the type 1 concrete as defined in Table 3.5. This parametric study utilized concrete type 2, shown in Table 3.5, to define the concrete properties of the approach slab alone. All other concrete members utilized type 1 concrete.

Table 3-5 – Concrete properties used in concrete stiffness parametric study

Concrete Type	Density (lb/ft^3)	fc' (psi)	Young's Modulus (ksi)	Poissons Ratio
1	145	4000	3605	0.3
2	145	8000	5098	0.3

3.1.6.6 Joint Restrictions

Coupling constraints applied to the approach slab at the roadway-approach slab interface were varied from the baseline model to determine how they influenced the behavior of the approach slab. The coupling used on the baseline model allowed rotation but restricted horizontal and vertical displacement of the approach slab relative to the roadway. An unrestricted and moment coupling was analyzed and compared to the baseline model. The moment coupling restricted rotational, vertical, and horizontal displacement of the approach slab relative to the roadway. Surface-to-surface friction was the only constraint allowed for the unrestricted coupling case. The control point of the coupling is shown in Figure 3.20.

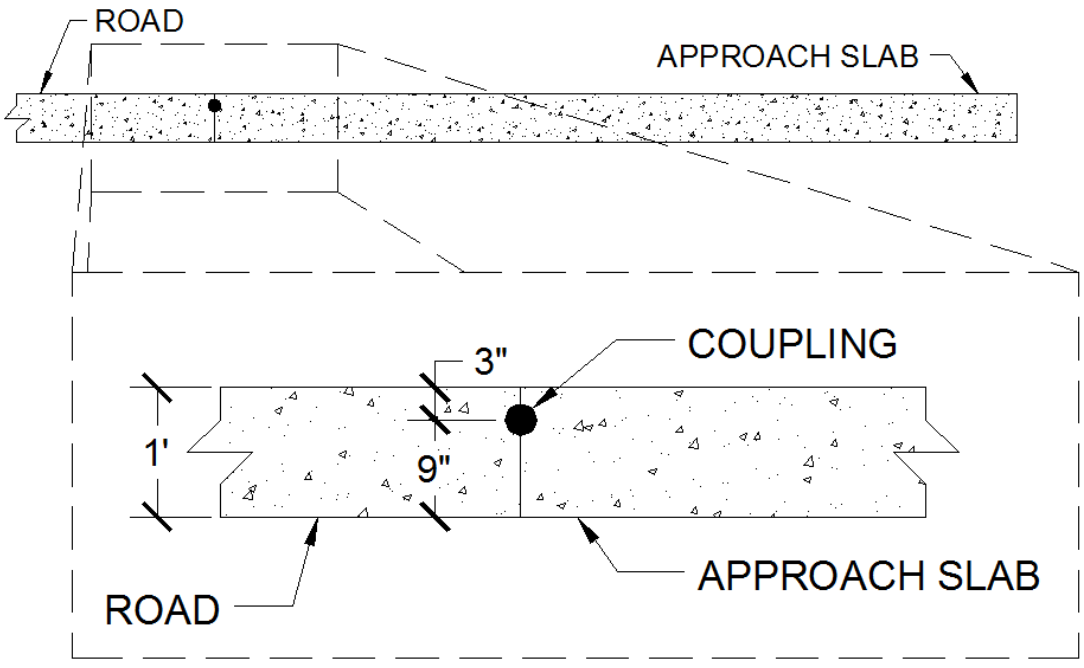

Figure 3.20 – Roadway-approach slab coupling location

3.2 Initial Models

Initial models that were created had inaccurate boundary conditions imposed on the approach slab. The approach slab was connected to the abutment with a shear coupling (horizontal and vertical displacement of the approach slab relative to the abutment was restricted) placed at the bottom edge of the approach slab. Another shear coupling connected the roadway to the approach slab. This coupling was placed at the top of the roadway-approach slab joint. Figure 3.21 displays the initial model and location of each shear coupling.

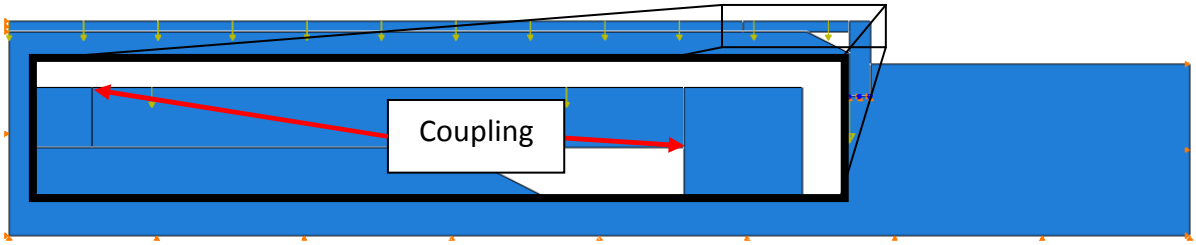

Figure 3.21 – Approach slab restraints placed on initial model

Both couplings allowed excessive approach slab end rotation. Figure 3.22 displays a scaled picture of the deformed approach slab.

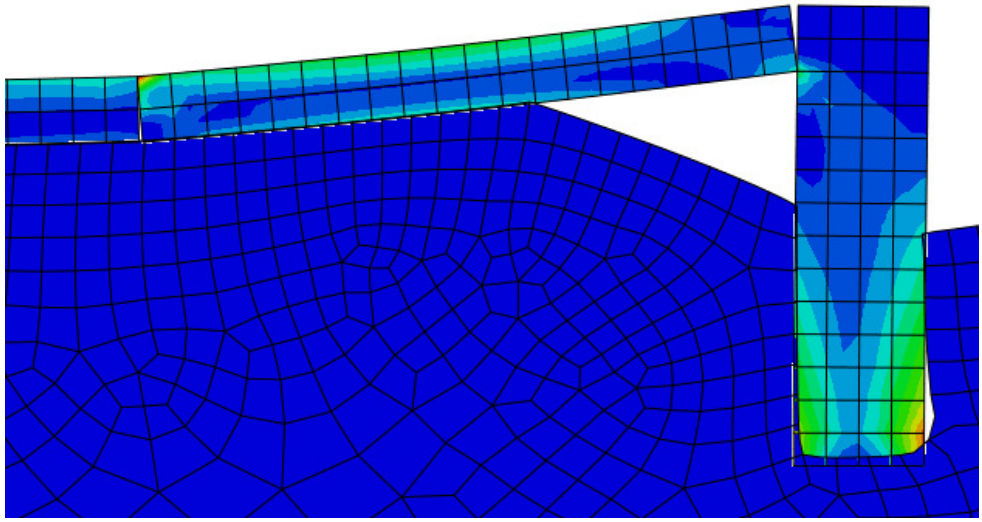

Figure 3.22 – Deformed approach slab calculated in initial model

The model was modified to better accommodate construction practices. The location of the coupling between the roadway and approach slab was moved to the quarter point to better simulate the effect of dowel bars which are usually placed near mid-depth of the slab. Abutment geometry was altered to allow the approach slab to be supported by a paving notch. The paving notch allowed the shear coupling between the approach slab and abutment to be removed from the analysis.

Loading was the second major flaw with the initial model. The initial loading scheme applied axle loadings and spacing's for a standard HL93 AASHTO truck (shown in Figure 3.23) to the roadway and approach slab at seven foot intervals.

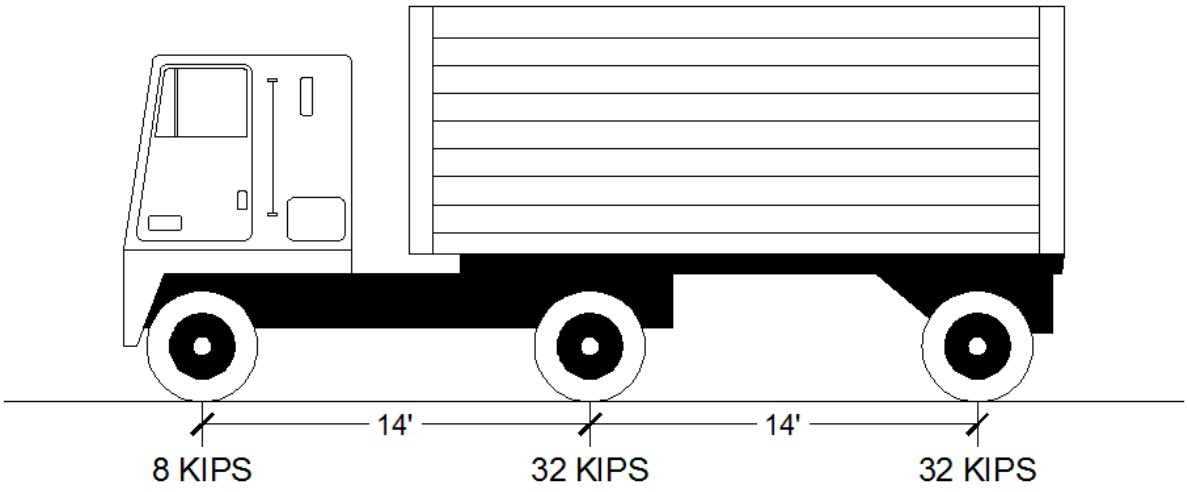

Figure 3.23 – HL93 standard design truck

Axle loads were applied at two locations along the baseline approach slab. These locations are shown in Figure 3.24. This loading scheme failed to apply the axle load(s) at the critical location of the approach slab.

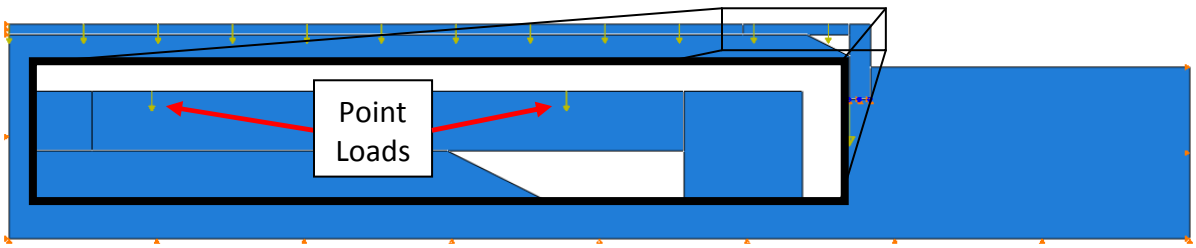

Figure 3.24 – Approach slab point loads used in initial model

The initial model considered the axle load and spacing of the AASHTO HL93 standard truck alone. The axle loads and spacing of the AASHTO HL93 standard truck were compared

to the AASHTO HL93 tandem truck, shown in Figure 3.25, over the short span (the maximum approach slab considered in this work) to determine which truck produced the largest moments.

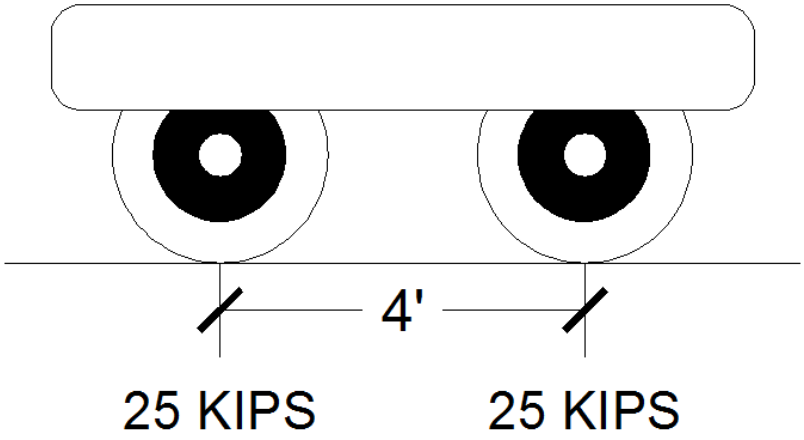

Figure 3.25– HL93 tandem design truck

Maximum moment was calculated for multiple approach span lengths using axle loads and spacing from each design truck. Figure 3.26 displays the maximum moment vs. span length created by each truck.

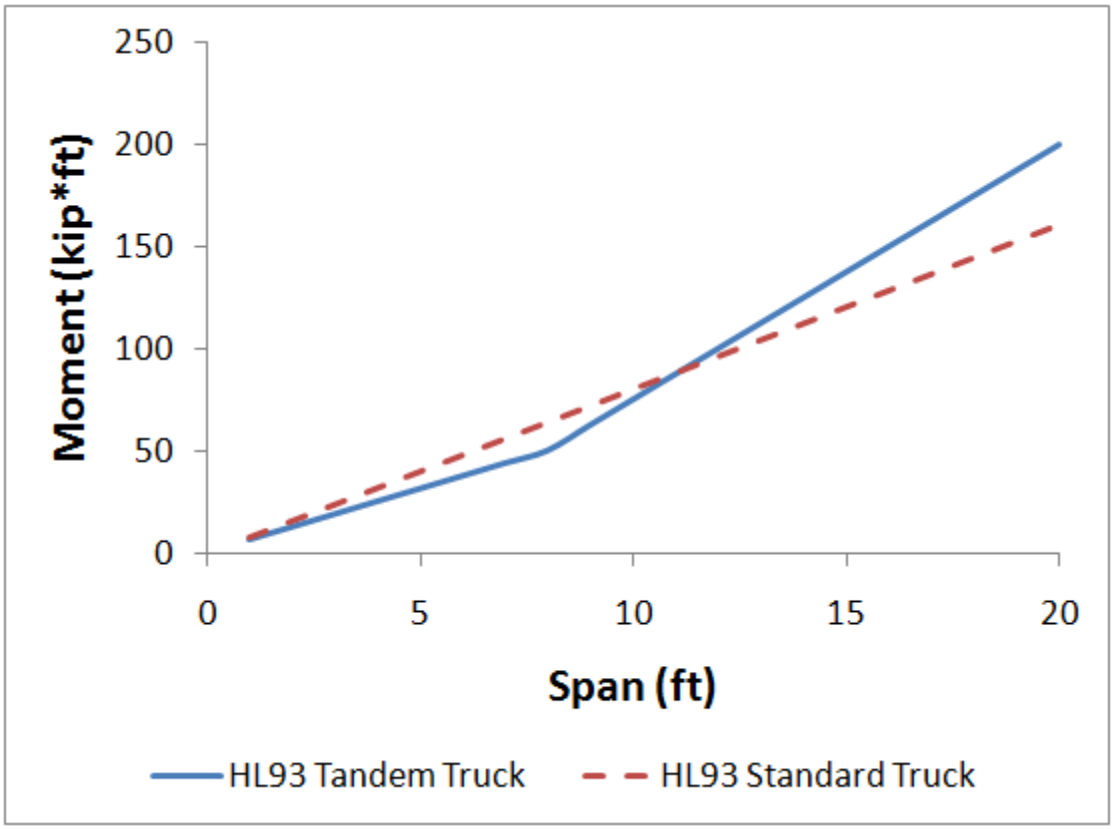

Figure 3.26– HL93 design truck moments

The moment created from the standard truck would control for spans shorter than 11 ft. Moments created from the HL93 tandem truck control for spans between 12 ft and 20 ft. The shortest approach slab considered in this work was 10 ft. The HL93 tandem truck was even used for the analyses conducted on models with 10 ft approach slabs considering the small 6% underestimate in maximum moment. It is assumed that the 6% difference will not have a substantial impact on the results.

3.3 Validation

3.3.1 Approach Slab Deformation

A validation was performed on the truck and approach slab parts used in the corrected model. Axle spacing and bending flexibility of the 'chassis' of the truck was checked to ensure the behavior complied with the guidelines defined in AASHTO (two independent axles spaced 4 ft apart). The verification model incorporated gravity and HL93 tandem truck axle loads to generate deflection of the approach slab; however, the influence of soil was neglected for this validation. Validation of soil response is included in the next section. The deflection of the approach slab as determined from the analysis was compared to a theoretical beam with similar loading and boundary conditions. Figure 3.27 displays the model used for validation.

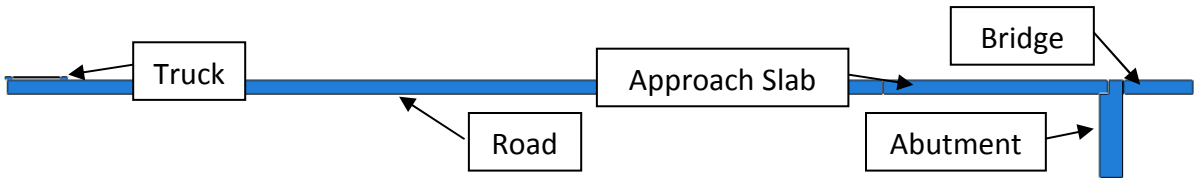

Figure 3.27– Model used for approach slab deflection verification

3.3.1.1 Loading and Boundary Conditions

Unique boundary conditions were utilized on the model due to the absence of soil. Displacement based boundary conditions were placed along the bottom of the roadway, abutment, and bridge to restrict horizontal and vertical displacement. Rotational displacement of the bottom of the abutment was restrained in addition to the boundary

conditions previously mentioned. This fixed restraint simulated a rigid pile and pile connection at the base of the abutment.

Interaction between the approach slab and roadway was controlled by a shear coupling placed at a distance of *t*/4 from the top of the approach slab with *t* being the approach slab thickness. Figure 3.28 displays the location of the coupling.

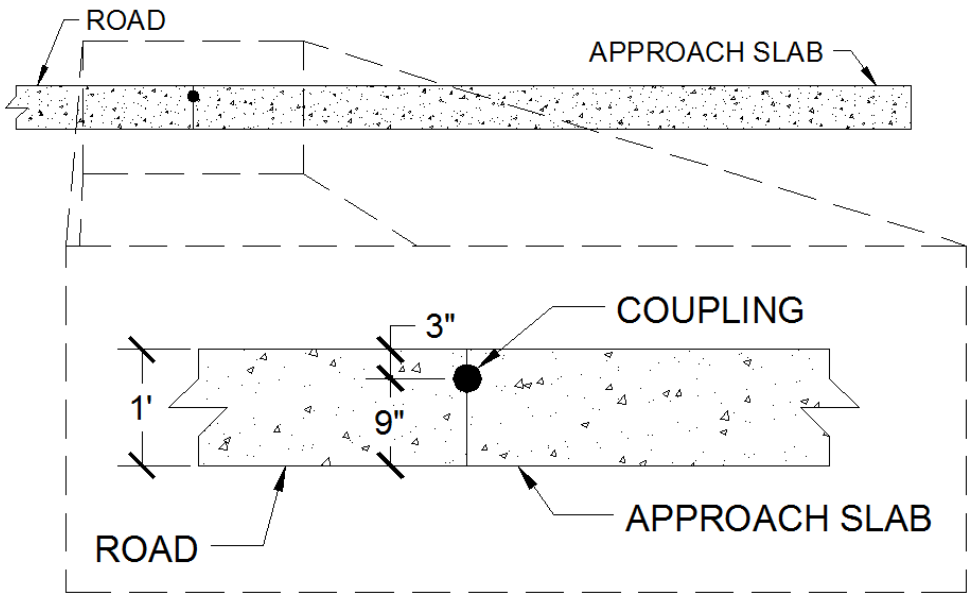

Figure 3.28 – Coupling location used in model verification

A thickness (*t*) of 12” was used for the thickness of the approach slab and roadway. The location and restraints placed on the shear coupling acted as a fixed support for the approach slab. This was due to the formation of a couple as shown in Figure 3.29.

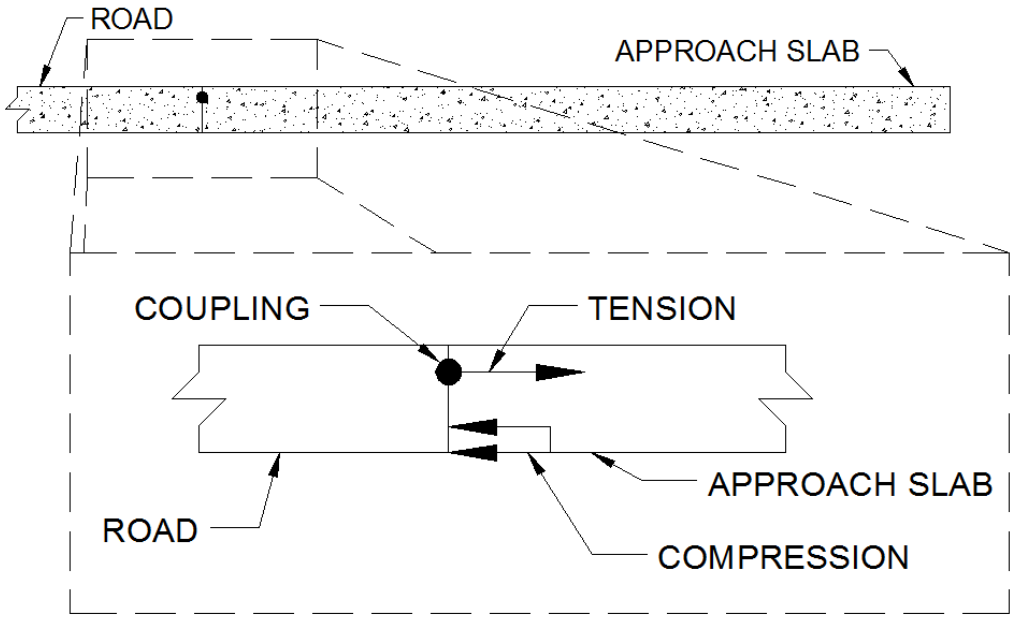

Figure 3.29 – Roadway-approach slab support

The contact between the approach slab and abutment was controlled by a frictionless surface-to-surface contact constraint. The frictionless contact allowed the paving notch to behave like a roller during the analysis.

Gravity and HL93 tandem truck axle loads were used in the analysis. The design vehicle was placed on the left side of the roadway, as depicted in Figure 3.30, while gravity was applied to the model. After gravity and the axle loads were applied, the truck was moved towards the approach slab in increments less than or equal to 4 inches until the both

axles had traveled the full length of the approach slab. Figure 3.31 shows the final position of the truck after the analysis.

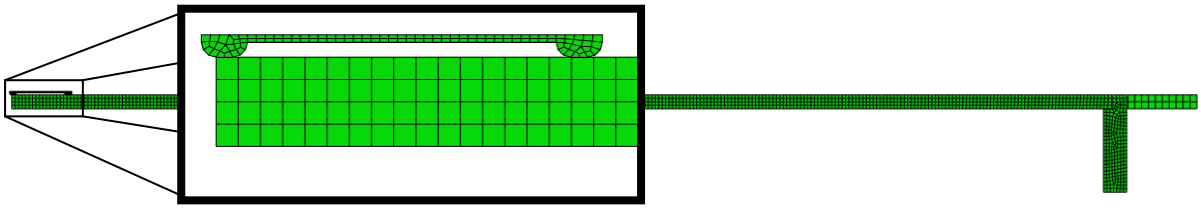

Figure 3.30 – Initial position of the HL93 tandem design truck

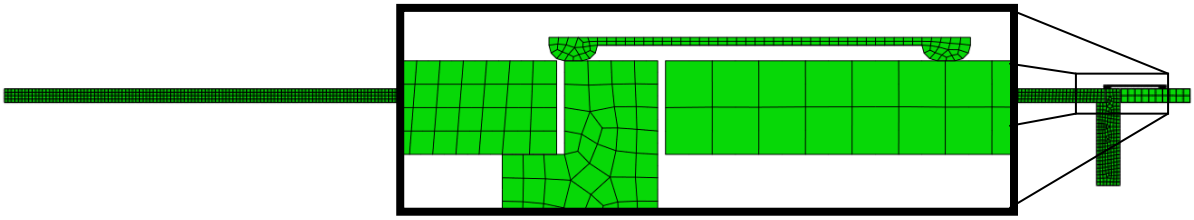

Figure 3.31 – Final position of the HL93 tandem design truck

3.3.1.2 Approach Slab Deformation Results and Discussion

Deflection of the approach slab determined from the analysis was compared to the theoretical deflection of a beam with similar loading and boundary conditions. The deflection of the approach slab was compared to the theoretical beam when the left axle of the truck had traveled 7'-1 1/8" on the approach slab. Figure 3.32 displays the position of the truck and theoretical beam used in the validation.

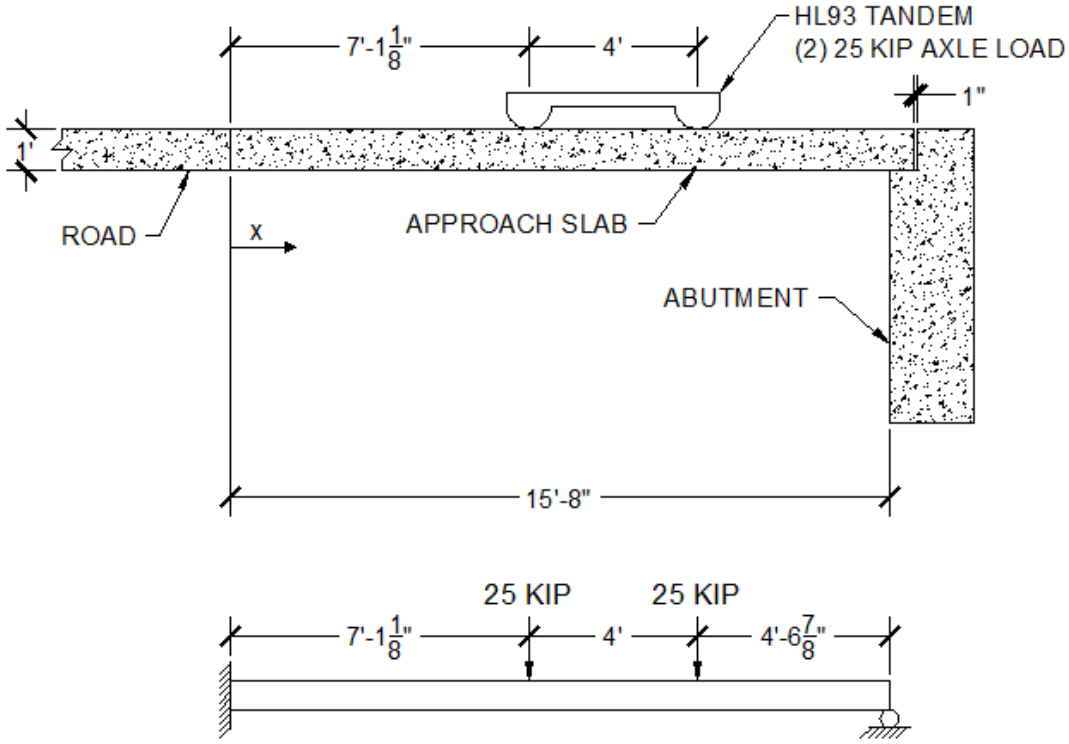

Figure 3.32 – Position of truck and theoretical beam used for model validation

Superposition was used to determine theoretical deflection of the beam. The calculations for the theoretical deflection can be found in Appendix 4. Figure 3.33 compares the deflection calculated from the finite element analysis and the theoretical beam deflection.

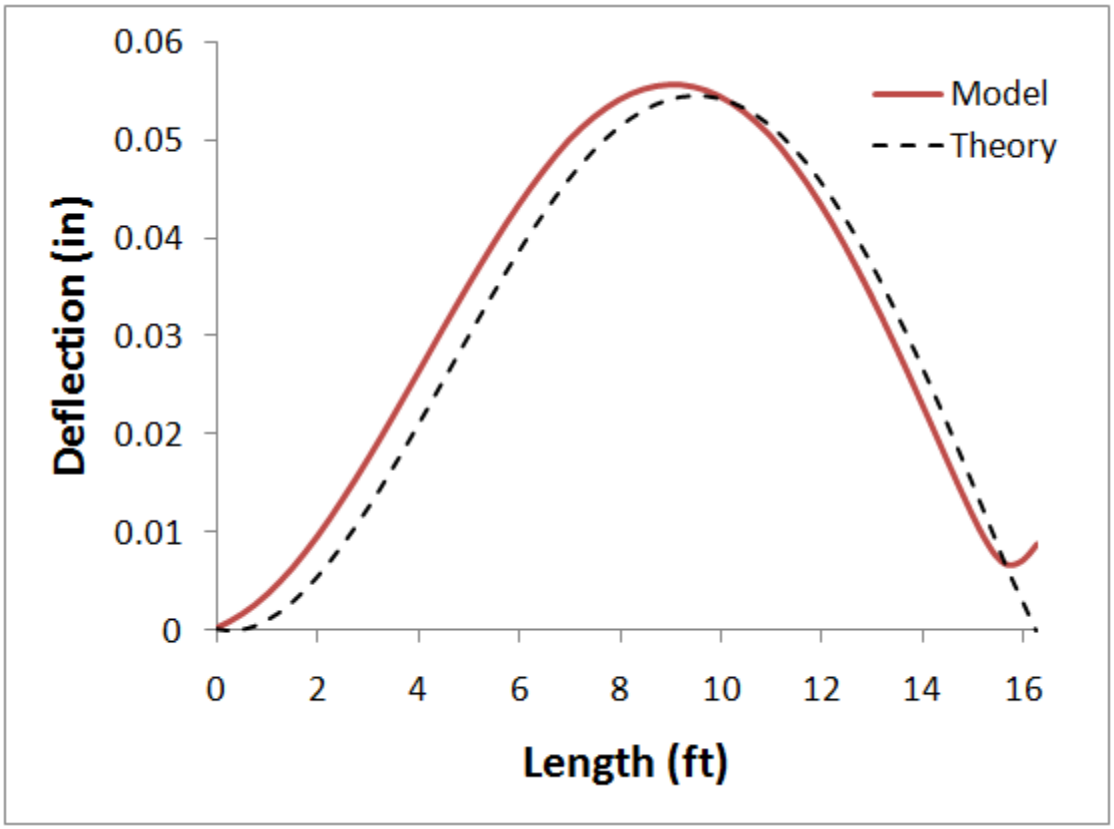

Figure 3.33 – Theoretical deflection vs. finite element analysis deflection

The maximum deflection computed in the numerical analysis was 0.0556 inches at 8'-11 7/16" from the roadway-approach slab joint while the maximum deflection calculated from the theoretical beam was 0.0545 inches as 9'-5 3/8" form the roadway-approach slab joint.

The deflection between the numerical analysis and the theoretical calculation show similar trends. Differences that exist between the two models can be attributed to the differing boundary conditions placed on the approach slab in the model. The slope of the deflection computed at the beginning of the approach slab is not zero in the numerical

analysis. This behavior is the result of the left support of the approach slab not being a truly fixed support. The amount of rotation of this joint in the numerical analysis was $8.13*10^{-5}$ radians. This is larger than the amount of rotation assumed in the theoretical analysis (no rotation is assumed in the theoretical analysis).

The second cause of the difference between the two models is due to the presence of the paving notch. In the numerical analysis, the approach slab initially rested on the paving notch. Deflections occurred as the approach slab was loaded. These deflections caused some rotation of the approach slab from the paving notch support. When these rotations occurred, a portion of the approach slab was lifted off the paving notch. This can be seen in Figure 3.33 by the portion of the model curve that bends upward near the right edge of the graph. The resulting cantilever would create some negative moment in the approach slab which would reduce deflection.

3.3.2 Soil Behavior Validation

3.3.2.1 Introduction

The behavior of the soil in the model was compared to a plane strain theoretical solution. Boussinesq's method for determining the change in vertical stress for any point (x,z) under a strip foundation was used as the theoretical solution Figure 3.34 identifies all variables used by Boussinesq's method.

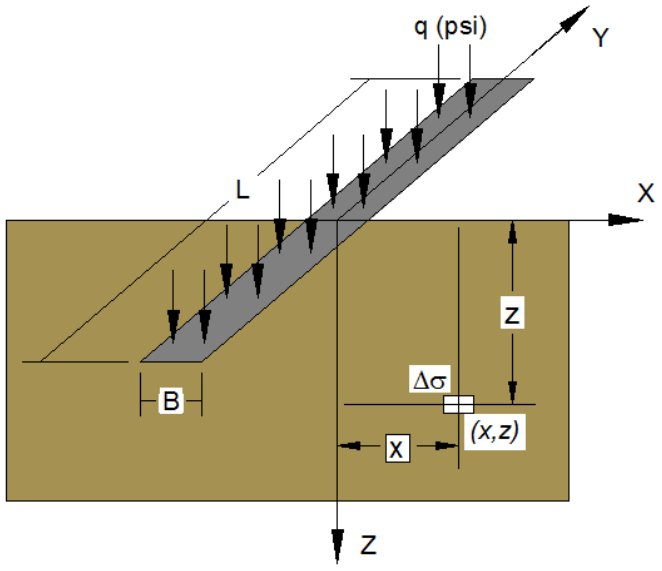

Figure 3.34 – Variables used to analyze strip foundation loads (after Helwany 2007)

Boussinesq's equation, per Helwany (2007), is presented as Equation 3.6.

$$\Delta\sigma_z = \frac{q}{\pi}\left\{tan^{-1}\left(\frac{x}{z}\right) - tan^{-1}\left(\frac{x-B}{z}\right) + sin\left[tan^{-1}\left(\frac{x}{z}\right) - tan^{-1}\left(\frac{x-B}{z}\right)\right] * cos\left[tan^{-1}\left(\frac{x}{z}\right) + tan^{-1}\left(\frac{x-B}{z}\right)\right]\right\} \quad (3.6)$$

where:

$\Delta\sigma_z$	=	Vertical stress increase of point, psi (Pa)
q	=	Applied pressure
B	=	Strip load width
x	=	Horizontal distance of the point from the center of the strip load
z	=	Vertical distance of the point from the center of the strip load

3.3.2.2 Loading and Boundary Conditions

Displacement based boundary conditions were placed on the soil and abutment for the validation. Both sides of the soil were restrained from horizontal displacement while the bottom surface of the soil was restrained from vertical displacement. Boundary conditions placed on the bottom of abutment restricted prevented rotational, vertical, and horizontal displacements. The boundary condition placed on the base of the abutment simulated a rigid pile and pile connection. Figure 3.35 displays the boundary conditions placed on the soil and abutment.

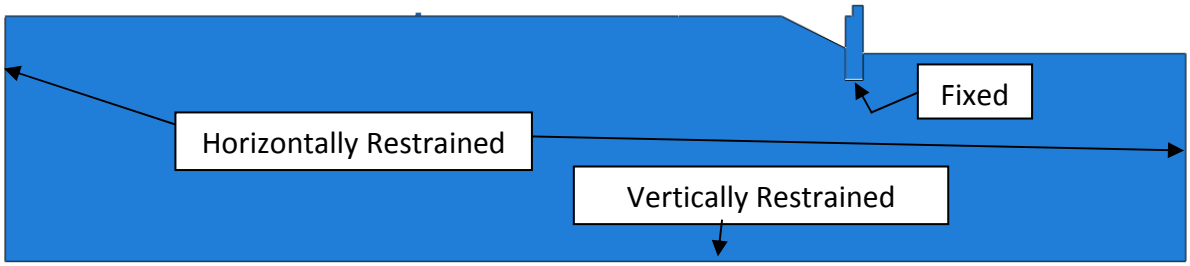

Figure 3.35 – Boundary conditions placed on soil and abutment

Boundary conditions placed on the 'strip foundation' restricted horizontal displacement for the duration of the analysis. This boundary condition was applied to the left side of the 'foundation' as shown in Figure 3.36.

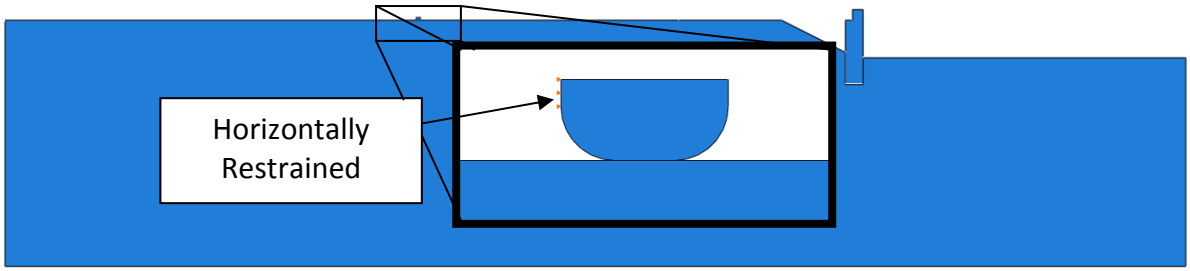

Figure 3.36 – Boundary conditions placed on the 'foundation'

Loading of the verification consisted of the strip foundation loading alone. The width (into the paper) of the foundation was 12 ft. The foundation was loaded with a 225 lb (1 kN) downward force to compress the soil. Figure 3.37 displays the contact surface and loading of the foundation.

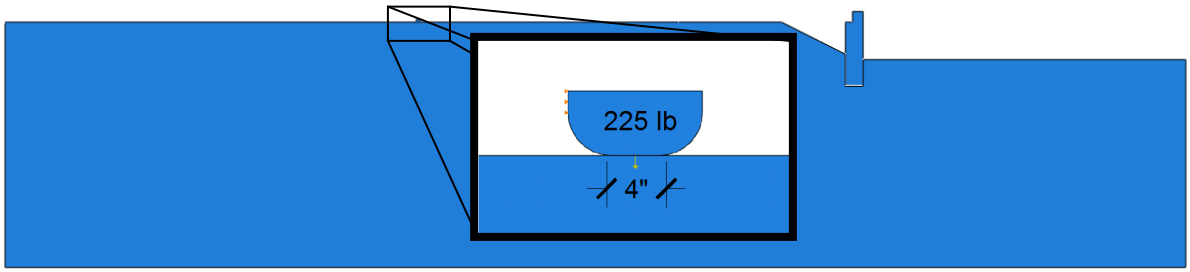

Figure 3.37 – Strip foundation loading use for soil validation

3.3.2.3 Results and Discussion

Vertical stress of the soil under the strip foundation computed from the finite element analysis was compared to vertical stress calculated with Boussinesq's equation for

strip foundations. The path feature found within the Abaqus software was used to determine the locations of the elements used for the stress comparison. Figure 3.38 displays the path.

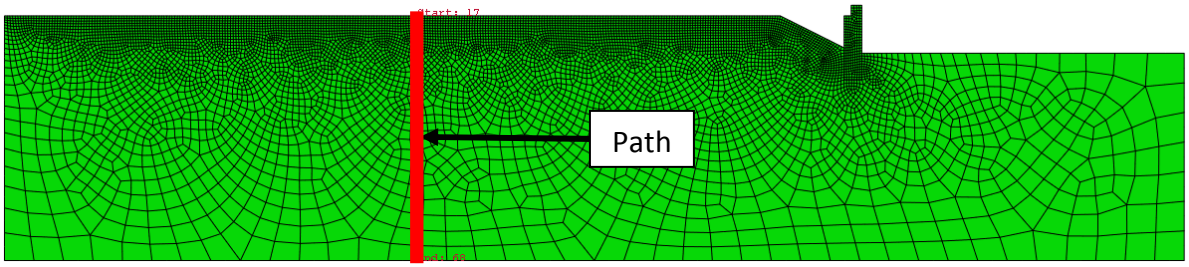

Figure 3.38 – Path used to define elements used for soil validation

Vertical stress and integration point locations of the elements located along the path were compared to the theoretical vertical stress computed with Boussinesq's equation. Figure 3.39 displays the stress calculated in both the finite element analysis and theoretical equation.

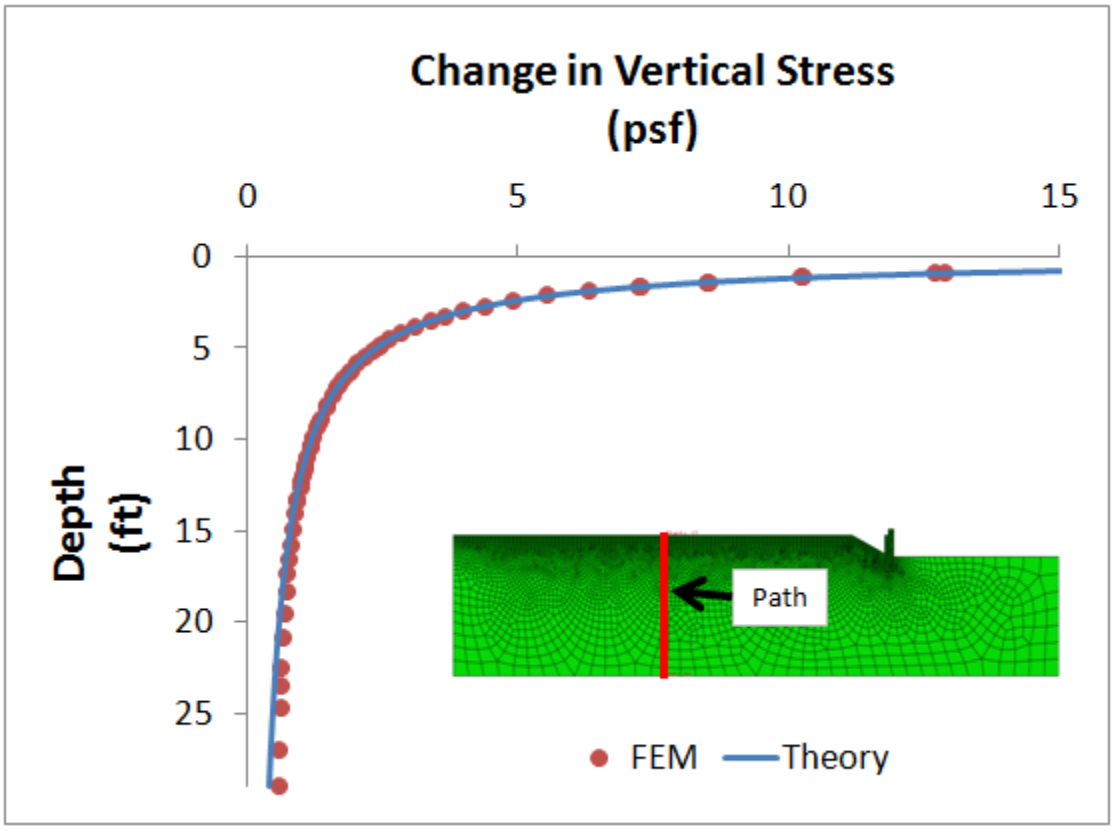

Figure 3.39 – Theoretical stress and finite element analysis stress comparison

The vertical stress determined from the finite element analysis shows a trend that resembles the trend seen from the theoretical calculations. Less than 10% error existed between the two solutions from the surface to a depth of approximately 17'-6". The error between the two methods gradually increases to a maximum error of 44% at an approximate depth of 29 ft. A spreadsheet showing the comparison of the two methods can be located in Appendix 5.

Differences between the two methods seen at deeper depths may be due to the boundary conditions imposed on the finite element model. The bottom of the soil was prescribed a boundary condition that restrained vertical displacement. This boundary condition may have caused an abnormal increase in vertical stress near the boundary condition. The theoretical solution only considered the increase in vertical stress from the strip load alone and did not have any conditional restraints. The low error (less than 10%) between the two methods observed from the ground surface to a depth of 17’-6” is considered acceptable as the zone of influence of the strip is within the upper 17’-6”. The depth of soil for the model is considered adequate to minimize the influence of the lower boundary condition on model results.

Chapter 4: Results

4.1 Introduction

Rotational deformation at the approach slab-to-bridge deck interface was the primary characteristic of interest in this study. To determine the relative rotation at the end of the approach slab, displacements of the top and bottom nodes located along the slab's vertical edge were used with an assumption of plane section behavior in calculating a rotation. The rotation of the joint near the abutment was determined for each analysis case. Rotation of the approach slab located near the roadway was not of primary interest, but was determined for one analysis case only.

Possible cracking of the approach slab was also of concern. Envelopes of the maximum (tensile) and minimum (compressive) principle strains were created for nodes located along the top and bottom fibers of the approach slab. The compressive strain was compared to the concrete crushing strain defined in ACI 318-08. Tensile strains were compared with the rupture strains to determine if cracking had occurred.

Datum was located at the joint between the roadway and approach slab. All resulting strain plots use this point as datum. Figure 4.1 displays the datum and the coordinate system used in the interpretation of all results.

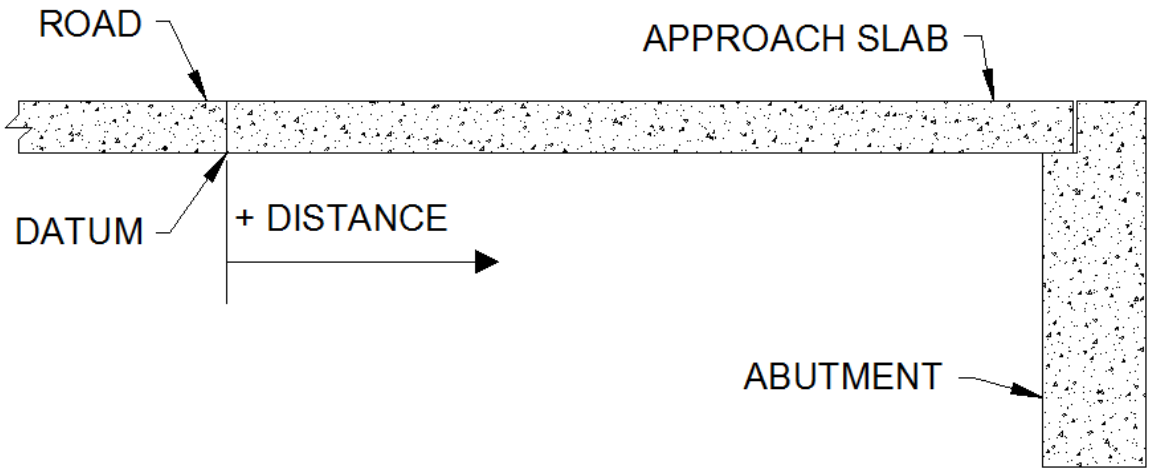

Figure 4.1 – Datum location and axis for distance measurement

Concrete cracking strain was determined in Section 3.1.1.2. The concrete cracking strain calculated in Section 3.1.1.2 was 132 με.

Crushing strain was taken as 0.003 as defined in the ACI 318-08. None of the analysis exhibited concrete crushing.

4.2 Base Model Behavior

4.2.1 Base Model Results

The base model with the HL-93 tandem loading did not exhibit any cracking of the approach slab and the maximum rotation of the joint near the abutment was 0.001086 radians. The minimum principle (compressive) strain in the approach slab was 90 με at a distance of 11’-9” from datum. The maximum principle (tensile) strain was 82 με (or 62% of

the 132 με for cracking) at 11’-2 ¼” from datum. No crushing or cracking occurred. Figure 4.2 displays the tensile strain envelope of the bottom surface of the approach slab.

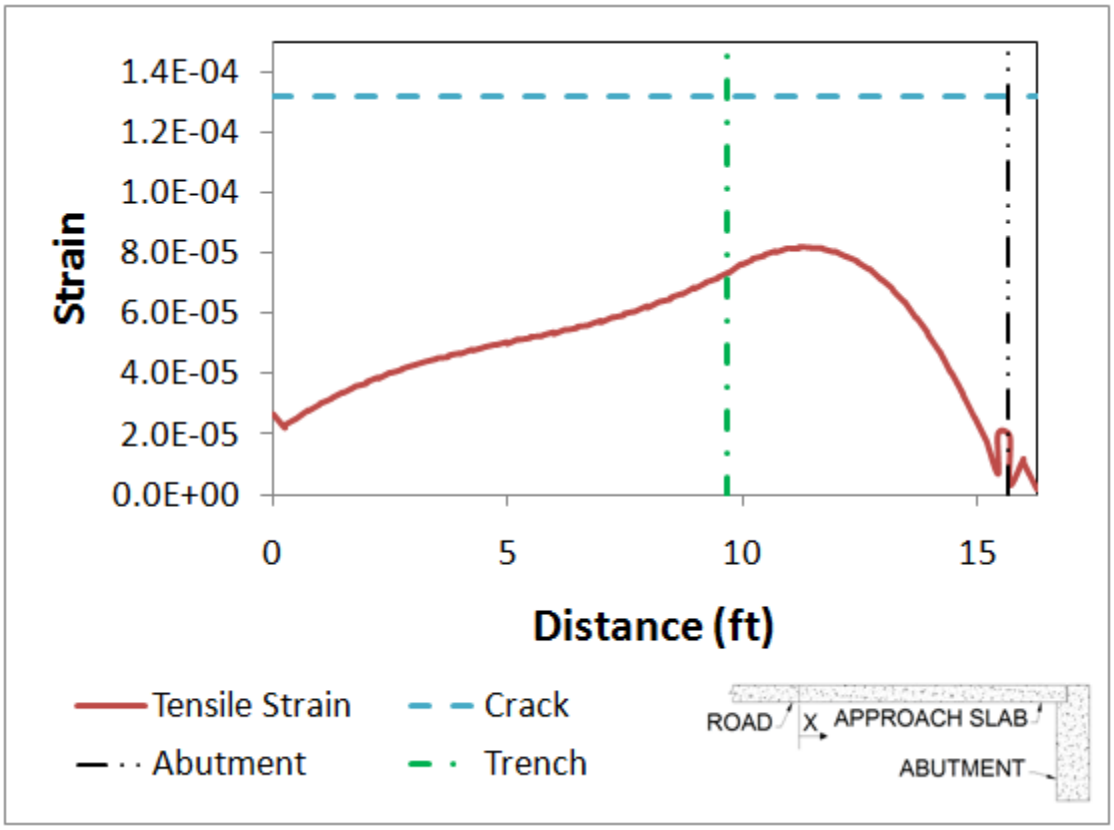

Figure 4.2 – Maximum principle (tensile) strain envelope for the baseline approach slab

4.2.2 Results from lane loading

Strain and rotation of the approach slab was also determined from the model consisting of uniform lane loading alone. The lane loading analysis incorporated the standard 640 lb/ft distributed load placed along the entire length of the roadway and approach slab as defined in the 2007 AASHTO design code. The largest maximum principle

(tensile) strain in the approach slab was 36 με measured at 11'-2 ¼" from datum (44% of the tension strain obtained from the tandem truck load). The maximum rotation of the joint between the approach slab and abutment was 0.000796 radians (73% of the rotation from the tandem truck load). The largest minimum principle (compressive) strain in the approach slab was 37 με at 11'-3" from datum. Figure 4.3 displays the maximum principle strain envelope for the bottom fiber of the approach slab. No crushing or cracking occurred.

If the HL-93 tandem and uniform lane load were superimposed, the tensile strain would reach 118 με or 89% of the cracking strain. The joint rotation would reach 0.001882 radians.

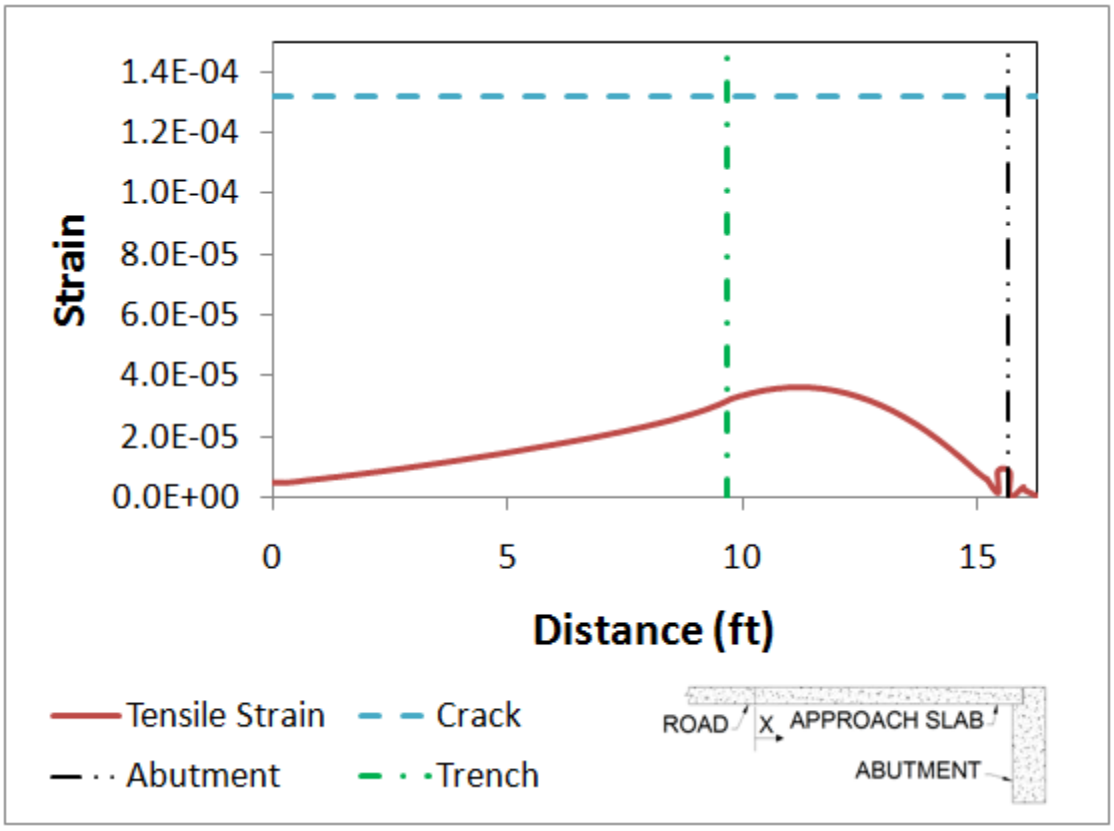

Figure 4.3 – Maximum principle strain of approach slab under lane loading

4.3 Results from parametric studies

4.3.1 Fill Properties

Soil properties were varied to encompass the loose and very dense states of the soil that may exist under the approach slab. A total of four different analyses were conducted with different soil properties. Three of these analyses assumed a homogeneous soil layer under the roadway and approach slab. The homogeneous soil layer had varied density, modulus of elasticity, friction angle, and dilation angle for each analysis case. Table 4.1 shows the soil properties used for homogeneous soil layered analysis cases.

Table 4-1 – Homogenous soil layered analysis properties

Classification	Mass Density (lbm/ft^3)	Young's Modulus (psi)	Poisson's Ratio	Friction Angle (deg)	Dilation Angle (deg)	Meridional Eccentricity	Cohesion (psi)
Stiff	129	14500	0.3	45	12	0.1	0.145
Med.	124	8700	0.3	37	5.6	0.1	0.145
Loose	121	1450	0.3	30	0	0.1	0.145

An additional analysis was performed with a layered soil profile that was intended to account for changes in effective stress with depth. The layered soil profile mimicked a stiff-over-soft-over-stiff layering scheme. Layer 1 was the surface layer of the model while Layer 4 was the deepest soil layer in the model. Table 4.2 displays the thickness and soil properties for each layer. Figure 4.4 displays the layered soil model and identifies the soil layer numbering scheme.

Table 4-2 – Layered soil analysis properties

Layer *	Depth (ft)	Mass Density (lbm/ft^3)	Young's Modulus (psi)	Poisson's Ratio	Friction Angle (deg)	Dilation Angle (deg)	Meridional Eccentricity	Cohesion (psi)
1	1.0	124	8700	0.3	37	5.6	0.1	0.145
2	2.3	122	3625	0.3	32.1	1.68	0.1	0.145
3	6.6	123	5800	0.3	34.2	3.36	0.1	0.145
4	23.0	124	8700	0.3	37	5.6	0.1	0.145

** Layer 1 is the upper-most layer. The numbering increases with increasing depth.*

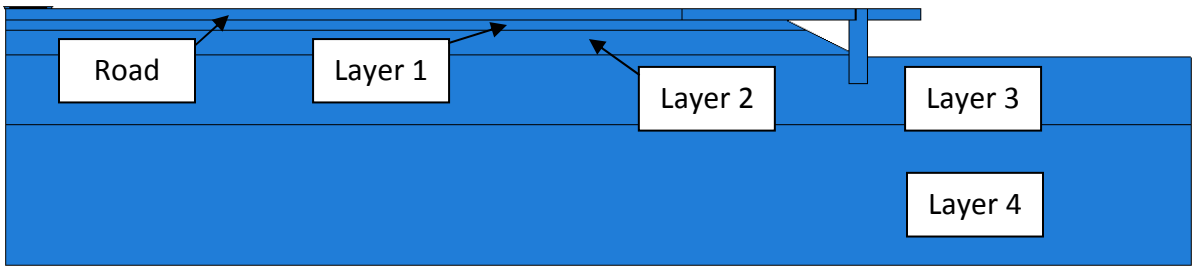

Figure 4.4 – Layered soil analysis

The loose homogeneous soil layer case was the only case where high tensile strains indicated that cracking would occur. As such, the slab stiffness in the model would be incorrect. After that was realized, the moment of inertia of the slab region that had strains above the cracking limit was modified according to ACI 318-08 to represent a cracked moment of inertia. The analysis was performed again and was repeated until only the region of the approach slab that had exceeded the cracking strain had the cracked moment of inertia. Figure 4.5 displays the final maximum principle strains along the bottom of the approach slab. Table 4.3 displays the location and magnitude of the maximum (tensile) principle strains calculated from this parametric study. Table 4.4 displays the location and magnitude of the minimum (compressive) principle strains calculated from this parametric study.

Table 4-3 – Maximum principle (tensile) strains with location for soil parametric study (13.2E-05 is cracking)

Case	Strain	Location
Stiff Soil	7.06E-05	11'-8 1/4"
Moderately Stiff	8.23E-05	11'-2 1/4"
Layered Soil	9.36E-05	10'-11 1/4"
Loose Soil	3.29E-04	10'-2 3/8"

Table 4-4 – Minimum principle (compressive) strains with location for soil parametric study

Case	Strain	Location
Stiff Soil	-7.97E-05	11'-9"
Moderately Stiff	-9.04E-05	11'-9"
Layered Soil	-1.02E-04	11'-3"
Loose Soil	-3.63E-04	10'-11 1/4"

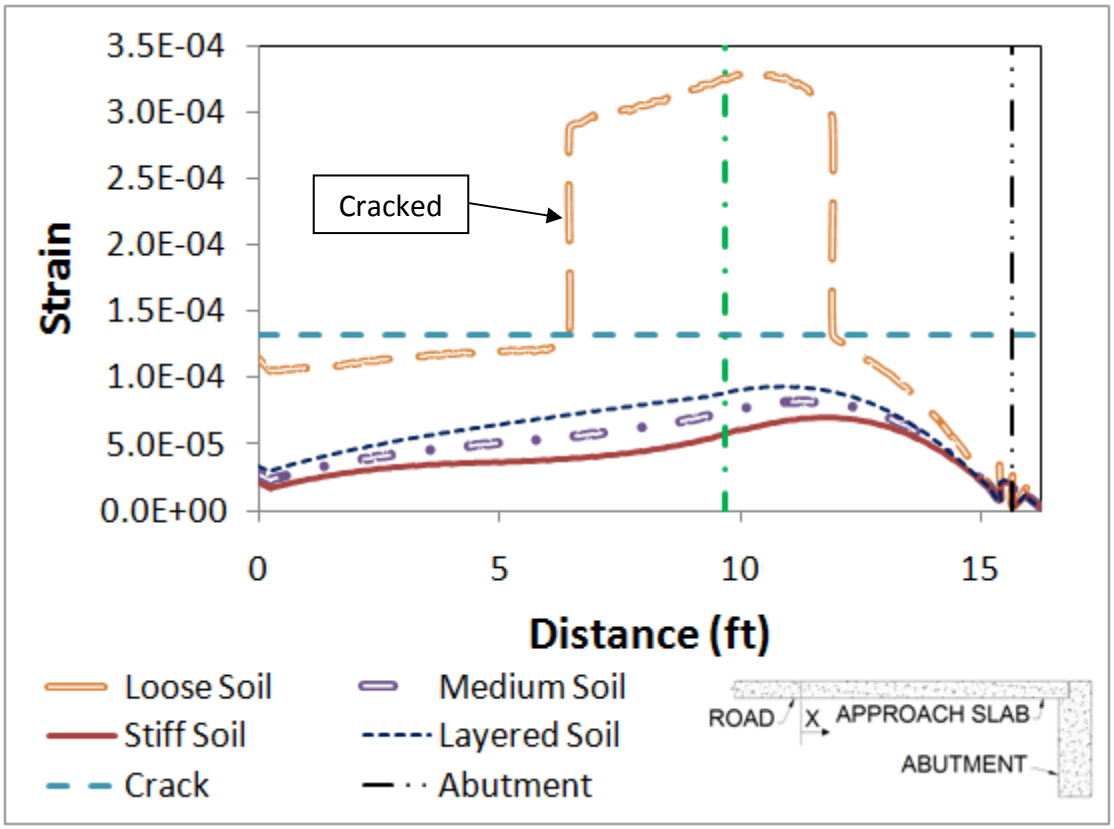

Figure 4.5 – Maximum principle (tensile) strain envelope for soil parametric study

The joint rotations for each case analyzed were determined from the nodal displacement of the approach slab at the joint with the bridge. Figure 4.6 displays the maximum calculated values of approach slab end rotation. With the loose soil and slab cracking, the end rotation reached 4.5×10^{-3} or 414% of the rotation in the baseline case.

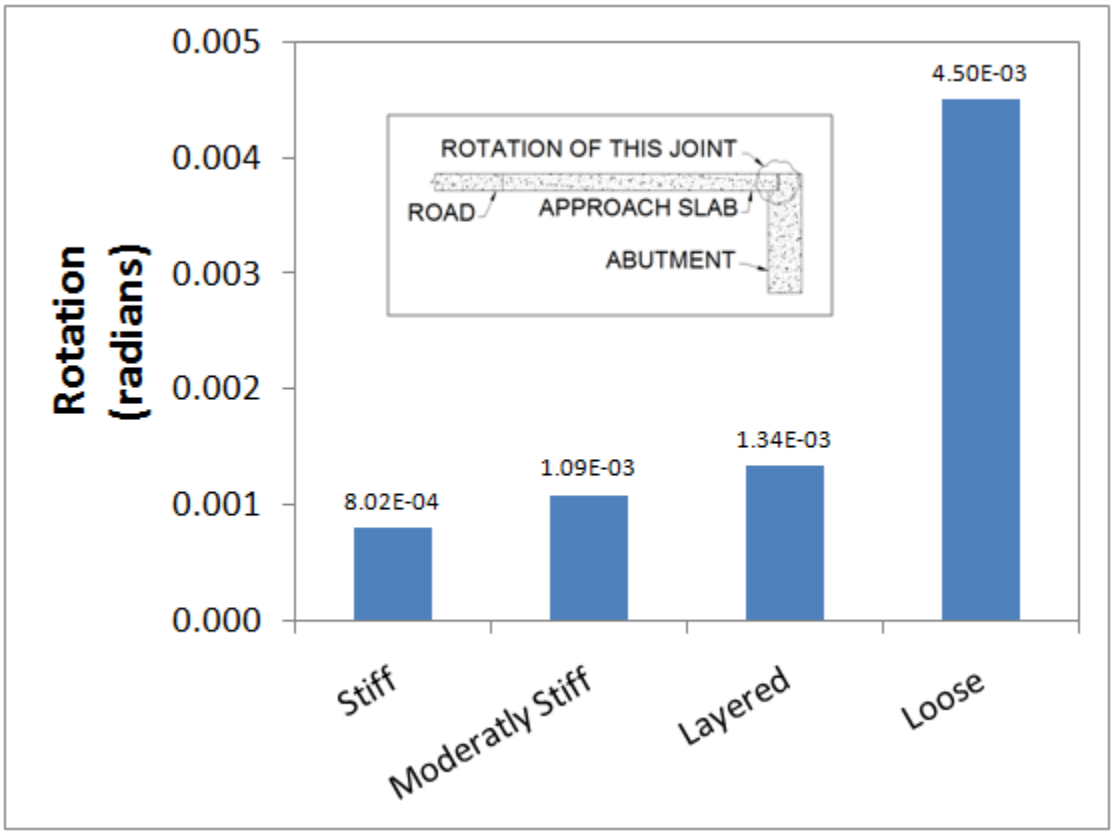

Figure 4.6 – Joint rotation for soil parametric study

4.3.2 Settlement Trench and Abutment Geometry

Three abutment heights were analyzed to determine their impact on the approach slab deformation. Five settlement trench geometries were analyzed for each abutment height. Special consideration was taken to ensure the boundary condition on the lower region of the soil did not interfere with the soil behavior. Figure 4.7 displays the maximum principle strains from the extreme bottom fiber of the approach slab for the 6 ft high abutment. All of the strains were less than the cracking limit (132 με). The maximum

principle strain and corresponding location for each case analyzed with the 6 ft abutment is presented in Tables 4.5 and 4.6.

Table 4-5 – Maximum principle (tensile) strains with location for 6 ft abutment study (132 με is cracking)

Case	Strain	Location
8' Trench	9.87E-05	10'-8 1/4"
6' Trench	8.23E-05	11'-2 1/4"
4' Trench	7.03E-05	11'-8 1/4"
2' Trench	6.82E-05	11'-8 1/4
No Trench	6.84E-05	11'-5 1/4"

Table 4-6 – Minimum principle (compressive) strains with location for 6 ft abutment study

Case	Strain	Location
8' Trench	-1.06E-04	11'-3"
6' Trench	-9.04E-05	11'-9"
4' Trench	-7.92E-05	11'-9"
2' Trench	-7.70E-05	11'-9"
No Trench	-7.71E-05	11'-9"

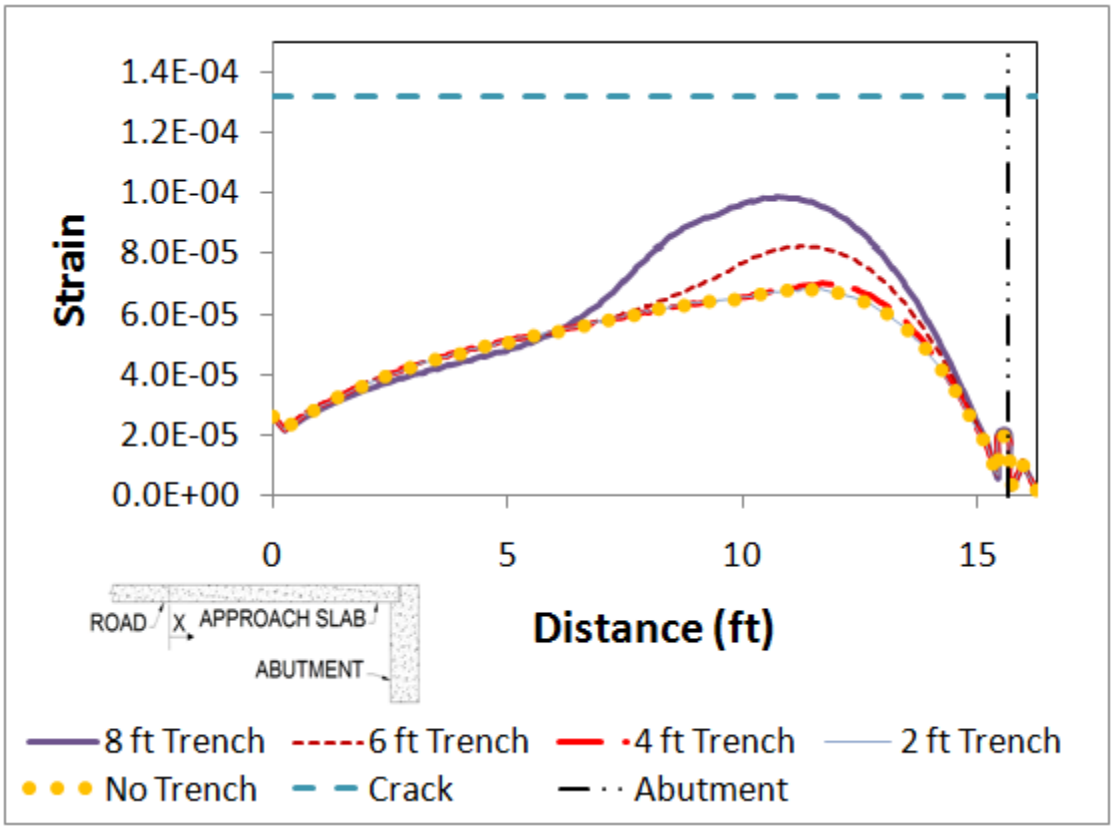

Figure 4.7 – Maximum principle strain of approach slab with a 6 ft high abutment

Figure 4.8 displays the maximum principle strains along the extreme bottom fibers of the approach slab for the 8 ft high abutment. Tables 4.7 and 4.8 display the maximum principle strain and corresponding location for each case analyzed with the 8 ft abutment.

Table 4-7 – Maximum principle (tensile) strains with location for 8 ft abutment study (132 με is cracking)

Case	Strain	Location
8' Trench	1.03E-04	10'-11 1/4"
6' Trench	8.72E-05	11'-2 1/4"
4' Trench	7.64E-05	10'-11 1/4"
2' Trench	7.65E-05	10'-11 1/4"
No Trench	7.67E-05	10'-11 1/4"

Table 4-8 – Minimum principle (compressive) strains with location for 8 ft abutment study

Case	Strain	Location
8' Trench	-1.11E-04	11'-3"
6' Trench	-9.59E-05	11'-0"
4' Trench	-8.44E-05	11'-9"
2' Trench	-8.43E-05	10'-9"
No Trench	-8.45E-05	10'-9"

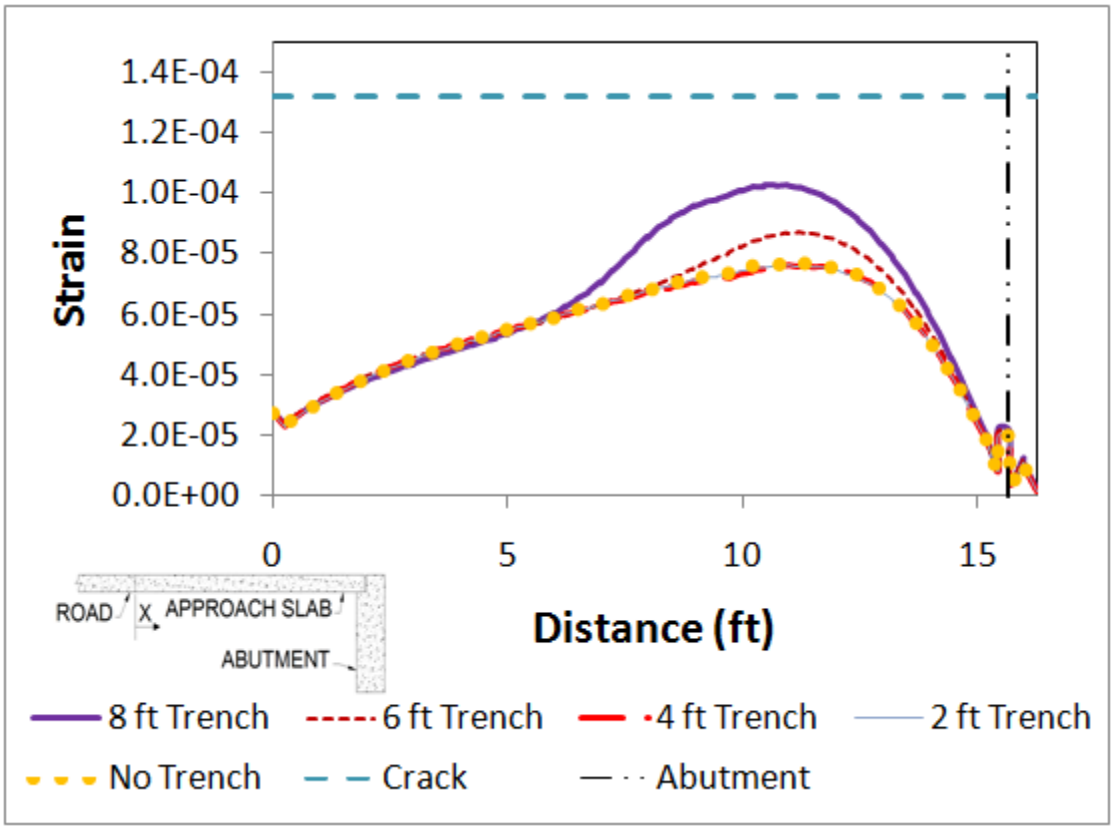

Figure 4.8 – Maximum principle strain of approach slab with a 8 ft high abutment

Figure 4.9 displays the maximum principle strains along the extreme bottom fibers of the approach slab for the 12 ft high abutment. The maximum principle strain and corresponding location for each case analyzed with the 12 ft abutment is presented in Tables 4.9 and 4.10.

Table 4-9 – Maximum principle (tensile) strains with location for 12 ft abutment study (132 με is cracking)

Case	Strain	Location
8' Trench	1.11E-04	10'-5 1/4"
6' Trench	9.73E-05	10'-11 1/4"
4' Trench	9.32E-05	10'-11 1/4"
2' Trench	9.49E-05	10'-11 1/4"
No Trench	9.54E-05	10'-11 1/4"

Table 4-10 – Minimum principle (compressive) strains with location for 12 ft abutment study

Case	Strain	Location
8' Trench	-1.17E-04	10'-6"
6' Trench	-1.02E-04	10'-9"
4' Trench	-9.92E-05	10'-9"
2' Trench	-1.01E-04	10'-9"
No Trench	-1.01E-04	10'-9"

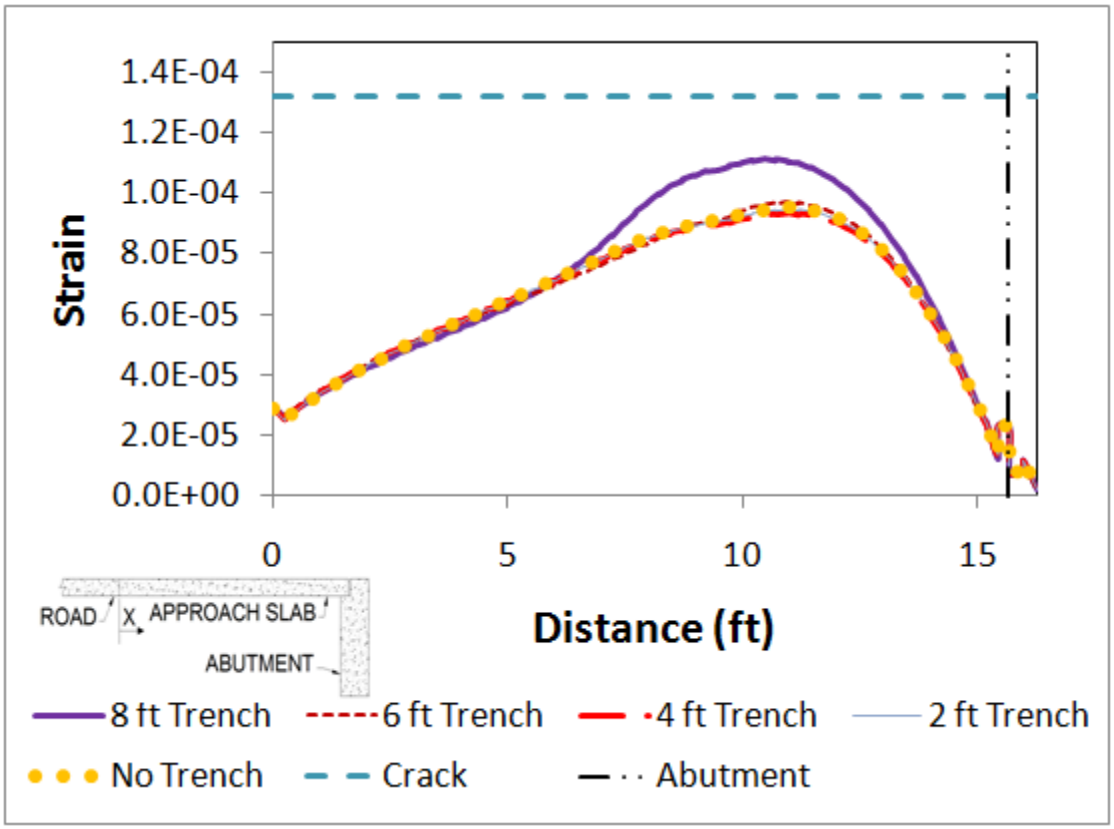

Figure 4.9 – Maximum principle strain of approach slab with a 12 ft high abutment

Figure 4.10 displays the end rotation of the approach slab at the approach slab – abutment interface.

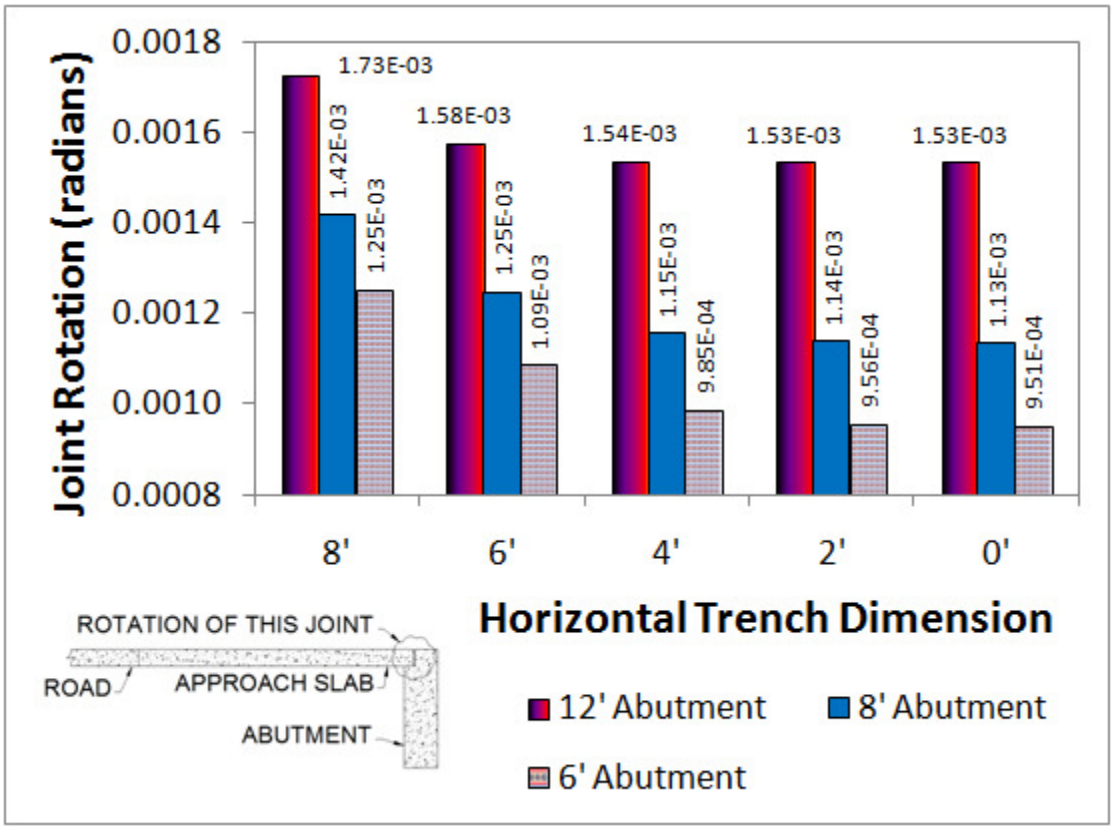

Figure 4.10 – Joint rotations for abutment and settlement trench parametric study

4.3.3 Approach Slab Length

The length of the approach slab was varied from the base model (which had a standard WisDOT length of 15’-8”) to determine how the length of the approach slab affects strain and end rotation near the abutment. Approach slab lengths of 10 ft and 20 ft were analyzed and compared to the 15’-8” long approach slab used in the baseline model. Tables 4.11 and 4.12 display the location and magnitude of the maximum principle compressive strain calculated in the approach slab for each case analyzed.

Table 4-11 – Maximum principle (tensile) strains with location (132 με is cracking)

Case	Strain	Location
20'	8.21E-05	15'-6"
15'-8"	8.23E-05	11'-2 1/4"
10'	7.67E-05	6'-0"

Table 4-12 – Minimum principle (compressive) strains with location

Case	Strain	Location
20'	-9.15E-05	16'-0 3/4"
15'-8"	-9.04E-05	11'-9"
10'	-8.47E-05	6'-6 1/2"

Figure 4.11 shows the maximum principle (tensile) strains of the bottom fiber of each approach slab analyzed.

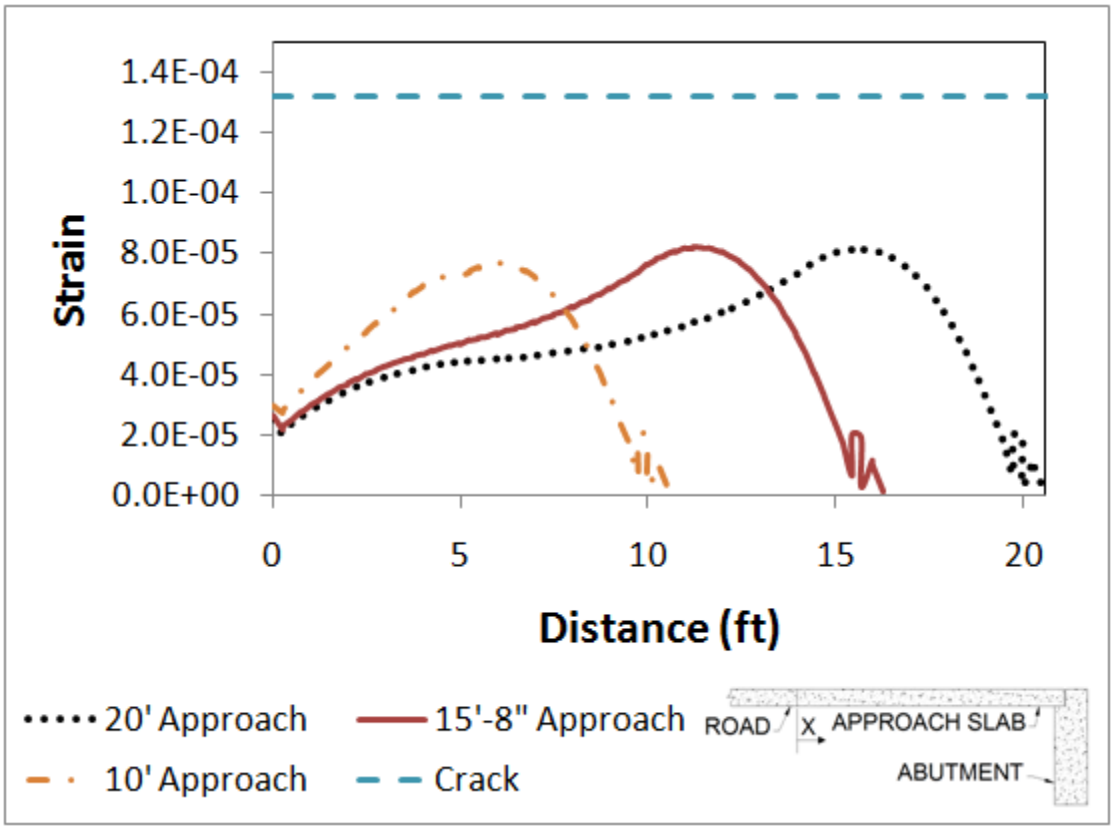

Figure 4.11 – Maximum principle strain of approach slabs with varying length

Figure 4.12 displays the joint rotation of each approach slab.

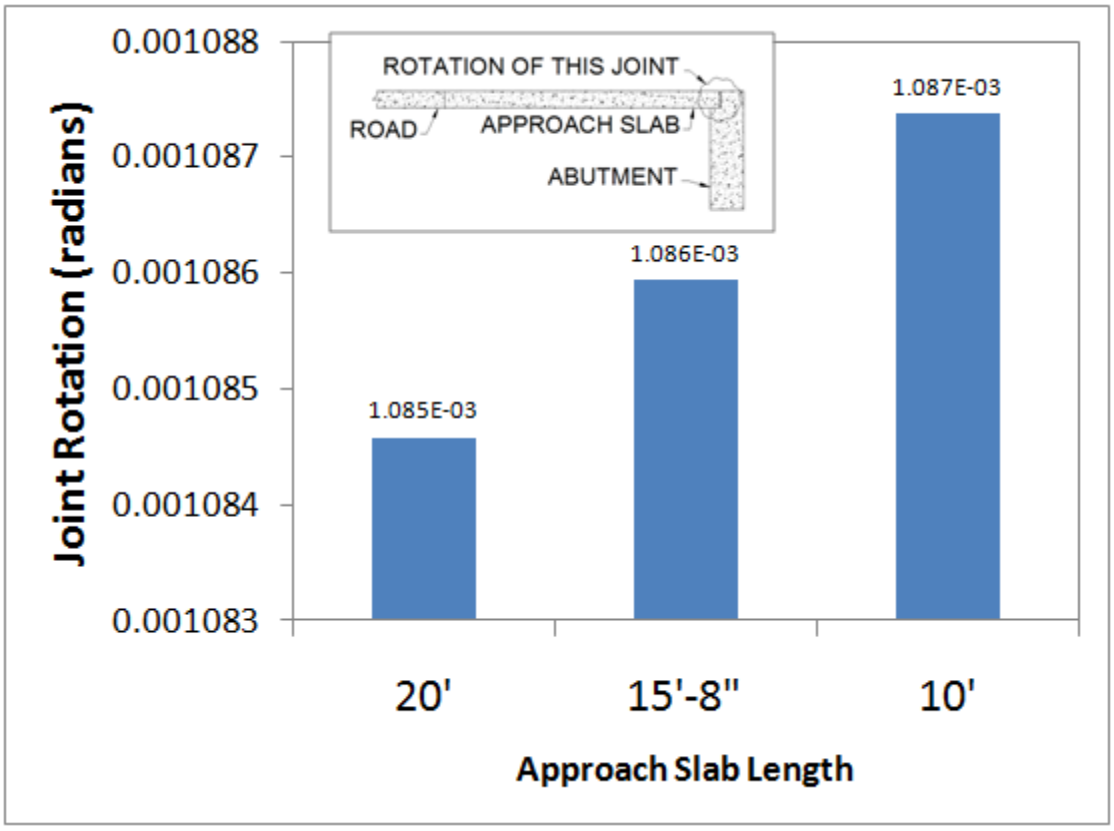

Figure 4.12 – Rotation of approach slab near the abutment for various approach slab lengths

4.3.4 Concrete Stiffness

The 28 day concrete compressive strength used in the baseline analyses was 4000 psi. An analysis was conducted to determine how an increase in the 28 day compressive strength would affect the approach slab. A 28 day compressive strength of 8000 psi that might be provided with precast prestressed approach slabs used in the comparison.

This parametric study investigated the cracking and joint rotation changes if a concrete with a higher compressive stress was utilized. The loose homogeneous soil profile was used for these analyses as this profile had exhibited tensile strains in a previous 4000 psi approach slab that exceeded the cracking strain. The cracking stress in the 8000 psi slab increased to 671 psi compared to 474 psi in the 4000 psi concrete. The cracking strain, however, remained the same at 132 με. The largest maximum principle (tensile) strains were 329 με (250% of cracking) at 10'-2 3/8" and 104 με (79% of cracking) at 9'-2 3/8" for the 4000 psi and 8000 psi concrete, respectively. Clearly the higher strength concrete did not exhibit cracking like the 4000 psi concrete approach slab. The largest minimum principle (compressive) strains were 363 με at 10'-11 3/8" and 109 με at 9'-0" for the 4000 psi and 8000 psi concrete, respectively. Figure 4.13 displays the maximum principle strains from the extreme bottom fiber of the approach slab for each analysis.

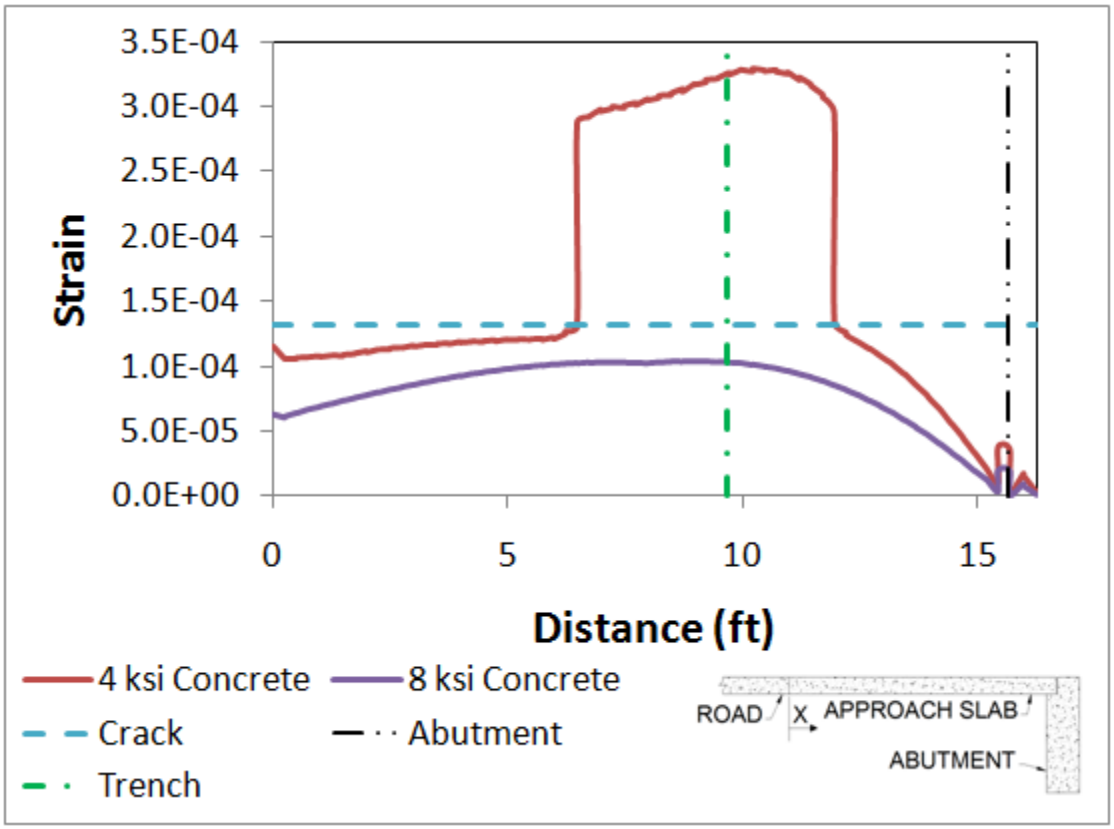

Figure 4.13 – Maximum principle strain of approach slabs with varying concrete stiffness

The maximum end rotation of the high strength approach slab near the abutment was only 66% of that seen in the low strength slab and is compared in Figure 4.14.

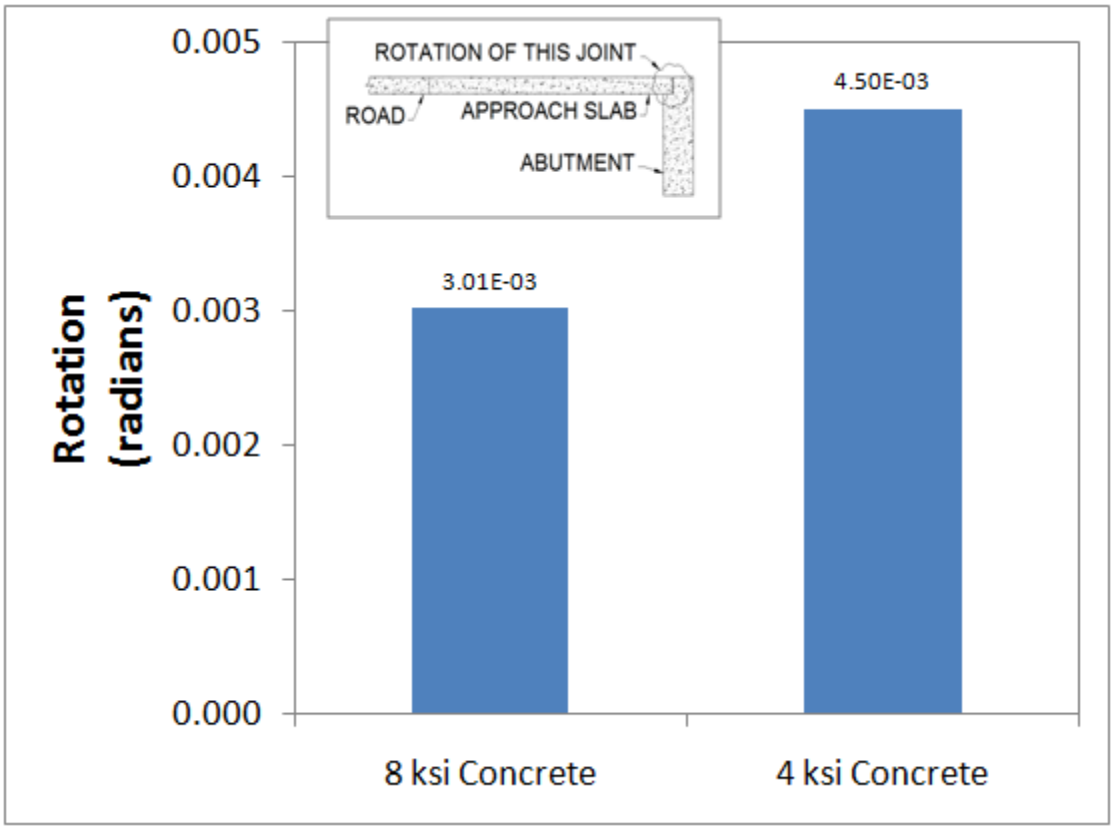

Figure 4.14 – Joint rotation from concrete stiffness parametric study

4.3.5 Joint Restrictions

The constraint placed on the approach slab at the joint between the roadway and the approach slab was investigated to determine its impact on approach slab behavior. The couplings that were considered in this parametric study were:

- Shear Coupling
  - Horizontal and vertical displacement of one member was restrained relative to the other member.

- Moment Coupling
  - Both members were fixed to each other.

- No Coupling
    - Friction alone controlled the surface-to-surface contact.

The control point of the coupling constraint and location of the joint is shown in Figure 4.15.

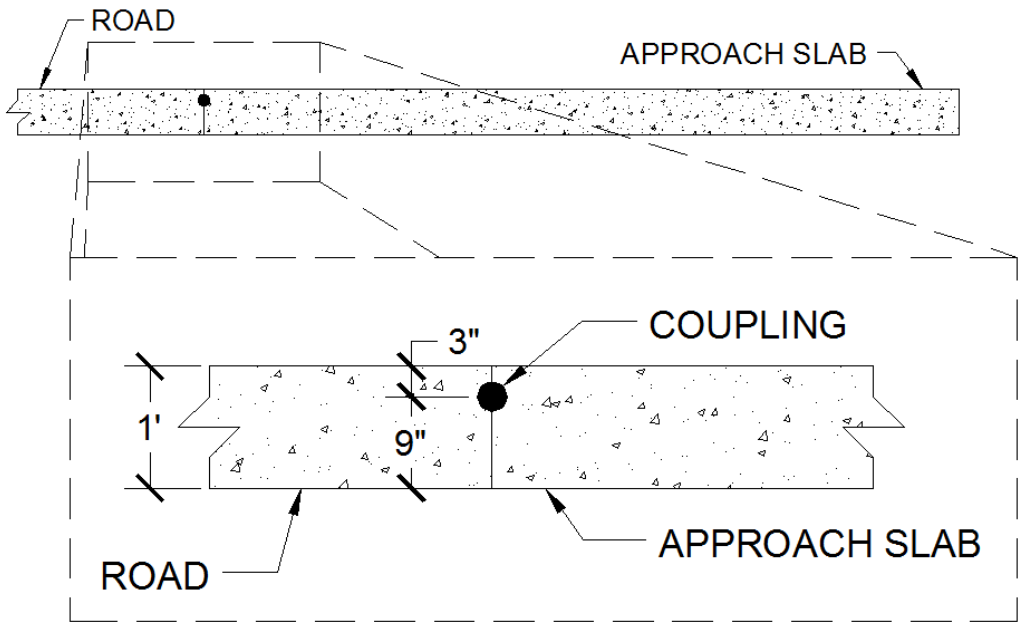

Figure 4.15 – Location of roadway – approach slab coupling

The largest maximum principle (tensile) strain in the approach slab was 82 με at 11’-2 ¼”, 82 με at 11’-2 ¼”, and 81 με at 11’-2 ¼” for the moment, shear, and no coupling cases, respectively. The largest minimum principle (compressive) strain in the approach slab was 90 με at 11’-9”, 90 με at 11’-9”, and 90 με at 12’-0” for the moment, shear, and no coupling cases, respectively. Figure 4.16 displays the maximum principle (tensile) strain along the bottom of the approach slab for each joint restraint.

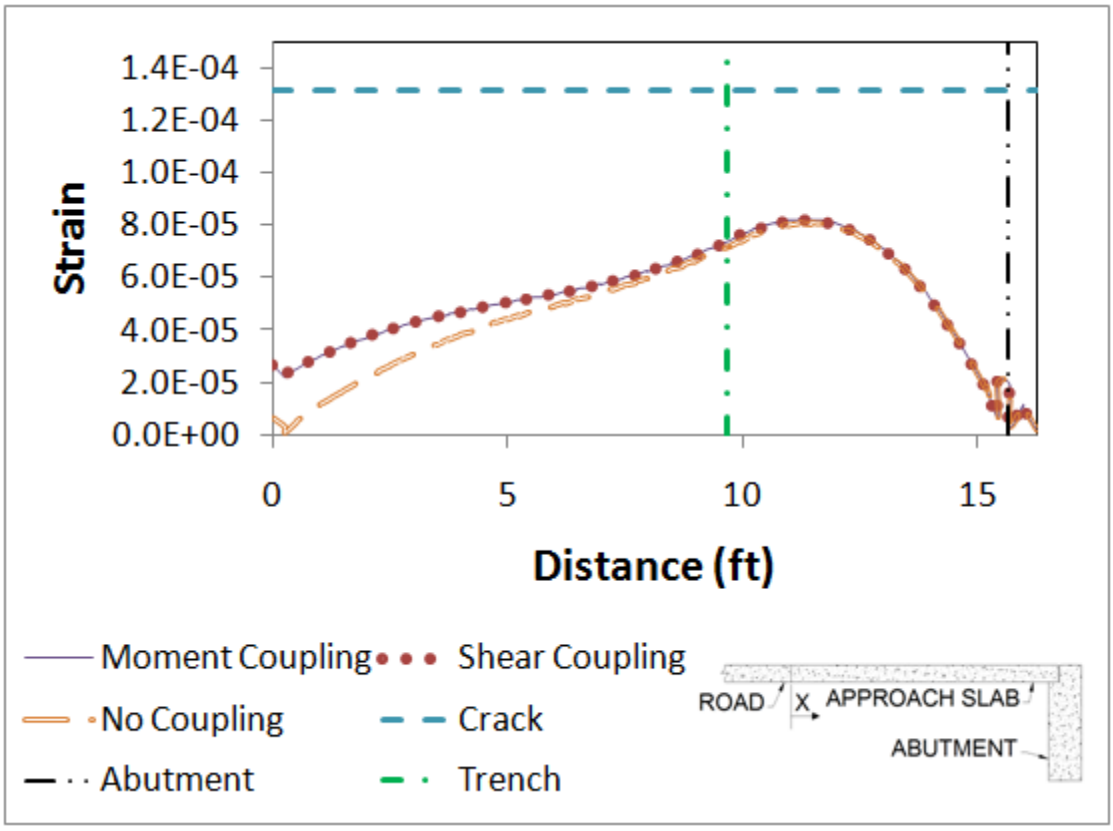

Figure 4.16 – Maximum principle (tensile) strains of approach slab for joint restriction study

Figure 4.17 displays maximum rotational displacements of the joint between the approach slab and abutment for the three parametric studies.

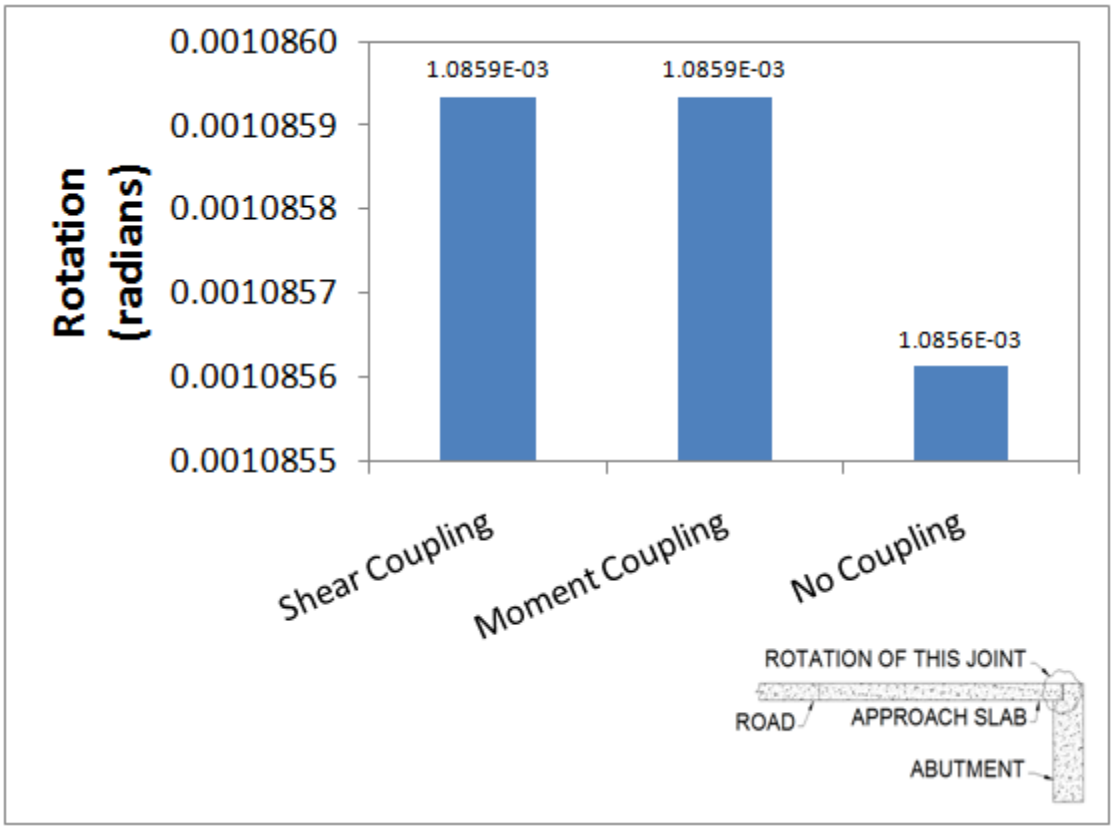

Figure 4.17 – Rotations of the approach-abutment joint determined from the joint restrictions parametric study

The rotation of the end of the approach slab near the roadway was also determined for each case. Figure 4.18 displays this end rotation determined from each analysis.

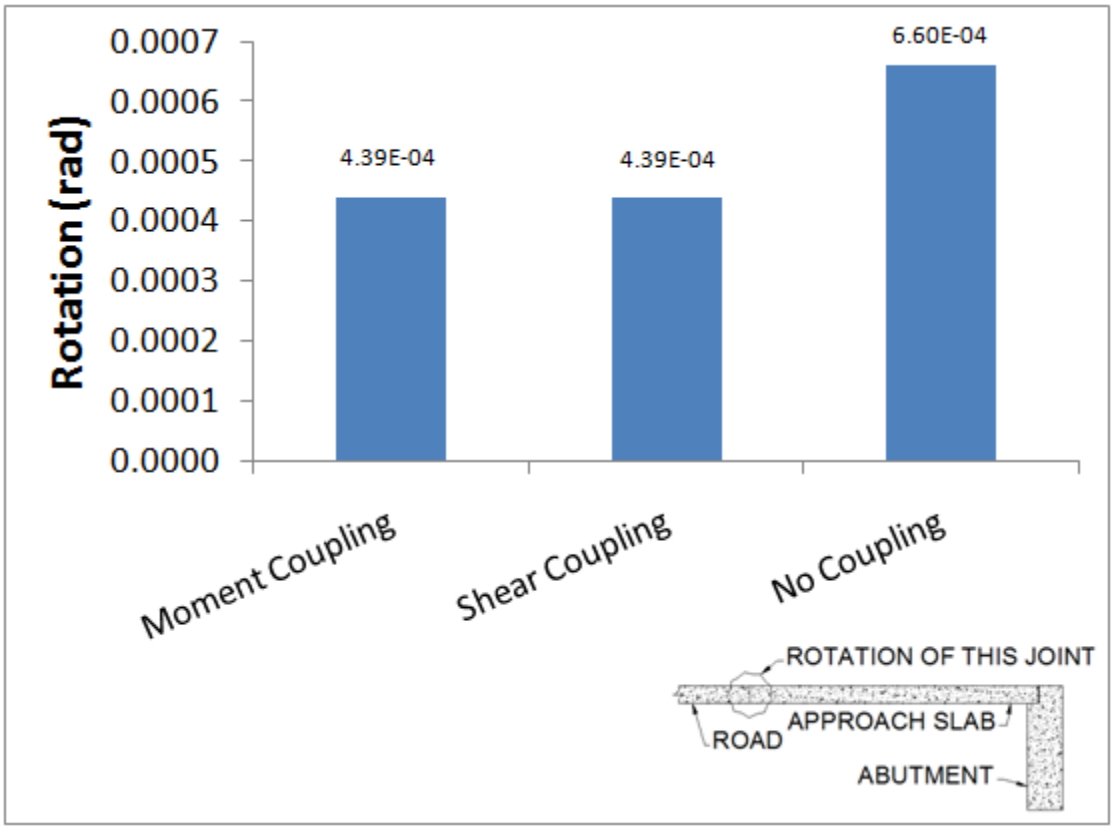

Figure 4.18 – Approach slab end rotation at the roadway-approach slab interface

Chapter 5: Discussion

5.1 Introduction

Results from the analyses performed on the baseline model and subsequent parametric studies were analyzed to determine how the variables affected the behavior of the approach slab. The end rotation of the approach slab at the approach slab-abutment interface, concrete crushing, and concrete cracking were the primary focus of the study. The geometry and material properties used in the baseline model best portrayed the median conditions that may exist at an actual bridge with a compacted clean sand fill. Each analysis was compared to the baseline model to determine the impact of a different parameter on the behavior of the approach slab.

The resulting compressive strain was compared to the concrete crushing strain as defined in section 10.2.3 in ACI 318-08. ACI states crushing will occur when the compressive strain is equal to 0.003 in/in. Concrete crushing was not observed in any of the analyses.

5.2 Assumptions with the Model

The concrete portions of the model utilized elastic properties alone. Assumptions were made on the behavior of the concrete after cracking. The maximum principle (tensile) strain computed from the approach slab was compared to the cracking strain described in Section 3.1.1.2. The moment of inertia of the approach slab was modified if the computed

strain exceeded the cracking strain. It was assumed that the moment of inertia was reduced for the entire region that had exceeded the cracking strain by 33%. This method yielded conservative results (since a lower stiffness was assigned to the cracked approach slab) as the entire region would not crack in a realistic slab. A modified moment of inertia would have better predicted the behavior of the cracked approach slab. The use of the modified moment of inertia was deemed unnecessary due to the uncertainty associated with the behavior of the soil under the approach slab.

The pile was assumed to be rigid for all analyses. This assumption was due to the large variety of geometry and materials used for piles. Actual pile stiffness and deflection was considered to be outside of the scope of this study.

The pile-abutment connection was assumed to act as a rigid connection. This was due to the large variety of pile-abutment connection methods. The pile embedded abutments that Wisconsin frequently used would be well represented by a rigid connection assumption. The stiffness of the pile connection is out of the scope for this project.

The expansion joint placed between the approach slab and abutment was assumed to have little resistance to expansion and contraction. The expansion joint between the approach slab and abutment was modeled as a 1 inch gap. This gap allowed the end of the approach slab to rotate without restraint.

The coupling placed between the roadway and approach slab simulated dowel bars embedded within the concrete to connect the parts together. It was assumed that the dowel bars would be placed at the quarter point in height and would have perfect bond and could resist pullout forces.

5.3 Modified Impact Factor

5.3.1 Introduction

In bridge design, impact factors are applied to axle loads to account for vehicular bouncing that occurs from imperfections in the roadway, approach slab, or deck. The 2007 AASHTO Bridge Design manual recommended a 33% dynamic load allowance increase in each axle load to account for the impact created by those surface imperfections and the natural vibration of the structure. AASHTO uses the dynamic loading factor with the truck wheel loads in all limit states (Strength 1, Strength 2, Strength 5, Service 1, Service 2, Service 3, and Fatigue) that include vehicular loading except for wood bridges.

Modified impact sensitivity factors are defined here differently than the AASHTO factor and were calculated for each analysis using the axle loads and spacing of the AASHTO HL93 tandem truck alone (without the AASHTO dynamic load allowance). These modified impact factors that will be listed, are the factors that the tandem loads needed to be increased by before approach slab cracking would occur. The modified impact factor was

not calculated for cases that exhibited approach slab cracking, since it would be a value less than one.

5.3.2 Methods Used to Determine the Modified Impact Factor

The modified impact factor (hereafter just referred to as “impact factor”) presented is the factor that would be applied to each axle load to cause cracking in the approach slab without including the uniform lane load effects. The impact factor was determined by multiplying the largest maximum principle (tensile) strain observed in the approach slab by a factor that would result in cracking. This factor was defined as the impact factor for the corresponding analysis case and is used to provide a relative measure of how likely the slab is to crack if overloading occurs.

The impact factors presented in this paper should not be used for judging the quality of a design without further testing. This testing should include a more rigorous investigation of soil properties, dynamic loading, lane loading, and additional numerical analyses with the full range of AASHTO trucks applied to the model.

5.4 Base Model Behavior

5.4.1 Results

The strain computed from the numerical analysis of the “base model” did not result in approach slab cracking. The largest maximum principle (tensile) strain determined from

the numerical analysis was 82 με at a distance of 11'-2 ¼" from the left edge of the approach slab. This strain was only 62% of the cracking strain of 132 με as determined in Section 3.1.1.2.

5.4.2 Base Model Discussion

The lower boundary condition on the soil was placed at a depth that minimized ill-conditioning of the concrete members, and the roadway was modeled at a sufficient length to allow the soil to not display adverse effects by the loading of the truck on the roadway (before the truck began to move). The zone of influenced soil (determined by the change in stress of the soil from the introduction of the tandem wheel loads) beneath the loaded truck as it moves in the model can be seen in Figures 5.1-5.3 (all with the same scale). These figures depict the zone of influenced soil beneath the truck at various locations as it was moved across the roadway and approach slab. The soil under the approach slab is affected only when the truck moves close to the approach slab. The zone of influence was approximately 11'-6" deep.

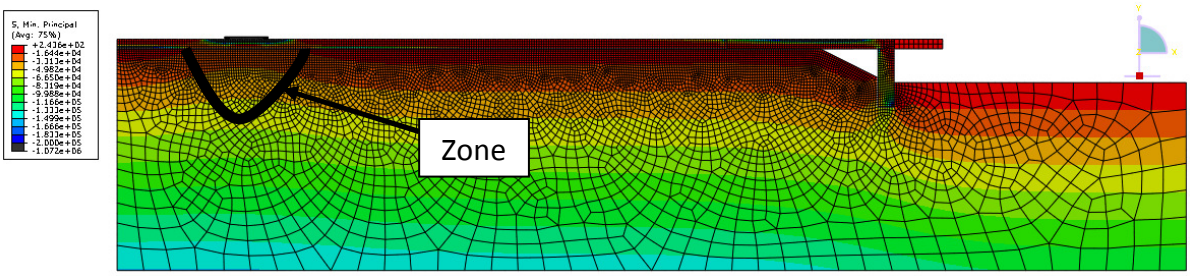

Figure 5.1 – Zone of influenced soil under design vehicle load as the vehicle starts moving

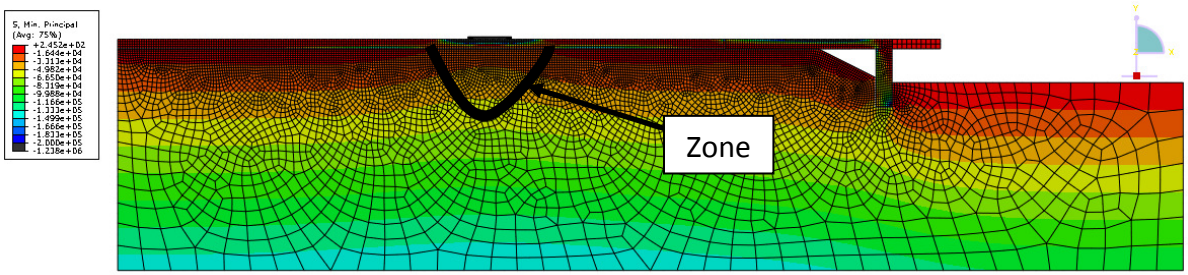

Figure 5.2 – Zone of influenced soil as vehicle moves closer to the approach slab

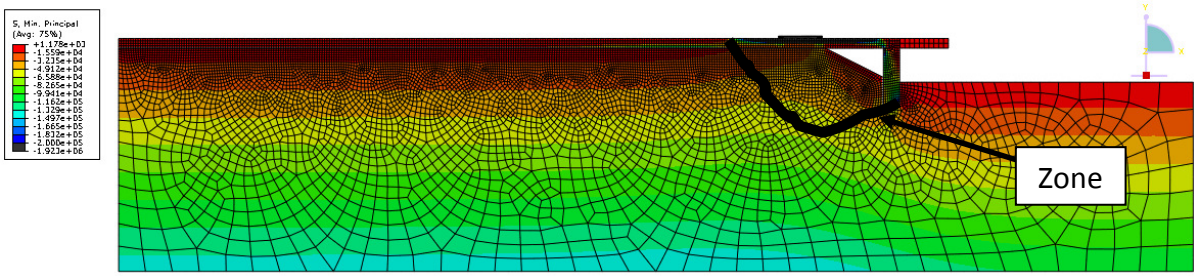

Figure 5.3 – Zone of influenced soil under the approach slab from the design vehicle

The strain at the bottom and top of the approach slab were not equal and opposite for the baseline model. This is due to the presence of axial force created from the frictional restraint between the approach slab and abutment. The axial force shifted the location of the neutral axis up approximately 0.16 inches at the location of the largest maximum and minimum strains. The axial stress was calculated to be approximately 5 psi. The small magnitude of axial stress was ignored for all subsequent analyses.

5.4.3 Approach Slab End Rotation for Base Model

The end rotation of the approach slab was 0.001086 radians near the abutment.

5.4.4 Impact Factor for Base Model

An impact factor that would be required to crack the approach slab was calculated using the method and assumptions outlined in Section 5.3. The impact factor for the base model was 1.60.

5.5 Lane Loading

5.5.1 Introduction

The analysis performed with the standard lane loading alone was only performed with the base model geometry and properties. This analysis was done to get an idea on how much strain would be created in the approach slab from the lane load alone. The lane loading case used a 640 lb/ft distributed unfactored of Service 1 load applied to the roadway and approach slab as defined by AASHTO.

5.5.2 Results

The maximum principle (tensile) strain of the approach slab along the bottom and the end rotation of the joint near the abutment were determined from the numerical analysis. The maximum principle strain of 36 με (27% of cracking) located at a distance of 11’-2 ¼” from the approach slab-roadway interface was calculated from the analysis

resulting in no cracking of the approach slab. The analysis yielded a rotation of 0.000796 radians for the end of the approach slab near the abutment, or 73% of the maximum rotation with the tandem wheel loading.

5.5.3 Lane Loading Discussion

The lane load case was performed with the baseline model geometry and material properties alone. This was done to see the impact of the lane load on the model compared to the effects of the tandem loading. The presence of the lane load alone did not have a substantial impact on the behavior of the model. An impact factor of 3.67 would need to be applied for cracking of the approach slab to occur. This relatively high impact factor serves as evidence that the model is not significantly affected when subjected to lane loading alone.

5.6 Base Model with Tandem and Lane Loading

The model consisting of the lane loading alone was combined with the base model and tandem loading by superposition. Superposition was deemed acceptable because of the following reasons:

- The lane load and base model used the same geometry.
- Linear elastic properties were used to define all concrete parts used within the model.

- Equal plastic deformation of the soil was observed during the application of gravity for each model.
- Plastic deformations produced in the baseline model were observed at two elements near the start of the settlement trench. These deformations were considered negligible.

The largest maximum principle (tensile) strain in the approach slab was 118 με (89% of rupture) measured at a distance of 11’-2 ¼” from datum after superposition had been applied to the two models. Figure 5.4 displays the maximum principle (tensile) strains computed along the bottom fiber of the approach slab for the baseline model with tandem and lane loading.

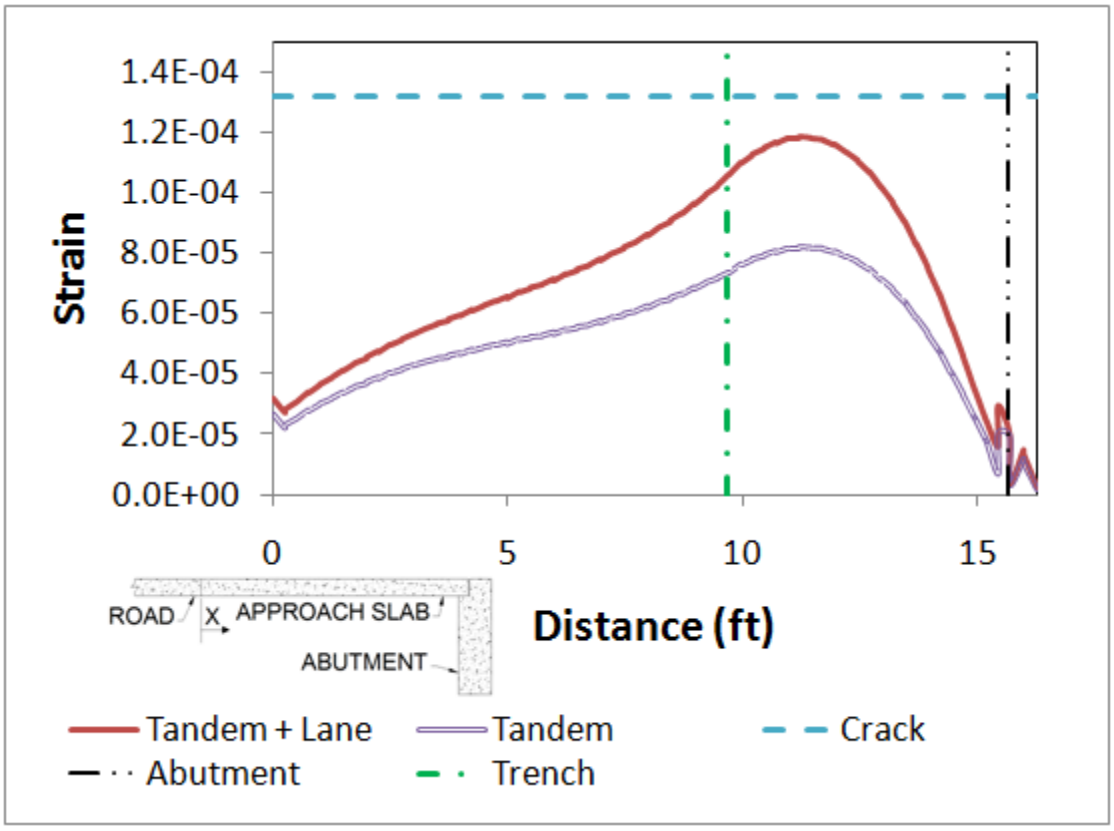

Figure 5.4 – Maximum principle (tensile) strain envelope for baseline approach slab with lane load

5.6.1 Impact Factor for Base Model with Duo Loading

An impact factor was determined for the baseline model with tandem and lane loading. The modified impact factor that would be required for this case would be 1.11 for cracking of the approach slab to occur. This factor is below the actual AASHTO dynamic load allowance factor implying that the actual service loads expected on the approach slab with dynamic effects would exceed the cracking capacity and could result in approach slab deterioration.

The decrease in the impact factor (1.60 to 1.11) states that the lane load has a significant effect on the strain of the approach slab when coupled with the design vehicle. In the remainder of the analyses lane loading will not be included, since it is unlikely that the lane load and the tandem load would be on the approach slab simultaneously.

5.6.2 Approach Slab End Rotation for Base Model with Duo Loading

Superposition was also used to determine a maximum end rotation of 0.001890 radians, or 174% of the baseline model.

5.7 Parametric Study Discussion

5.7.1 Settlement Trench / Void Geometry

5.7.1.1 Results

The geometry of the settlement trench was varied from the baseline model to determine how the settlement trench influenced the behavior of the approach slab. The baseline abutment height of 6 ft was held constant. Three additional settlement trench geometries were analyzed modifying the lengths in the baseline model. Table 5.1 displays the largest maximum principle (tensile) strain with location computed from each analysis. The dimensions presented in Table 5.1 describe the horizontal dimension of the settlement trench. Figure 3.18 displays the geometry of each settlement trench considered in this study.

Table 5-1 – Maximum principle strain with location for settlement trench study (cracking strain is 132 με)

Case	Strain	Location
8' Trench	9.87E-05	10'-8 1/4"
6' Trench	8.23E-05	11'-2 1/4"
4' Trench	7.03E-05	11'-8 1/4"
2' Trench	6.82E-05	11'-8 1/4
No Trench	6.84E-05	11'-5 1/4"

Figure 5.5 displays the maximum principle (tensile) strain envelope for each case analyzed.

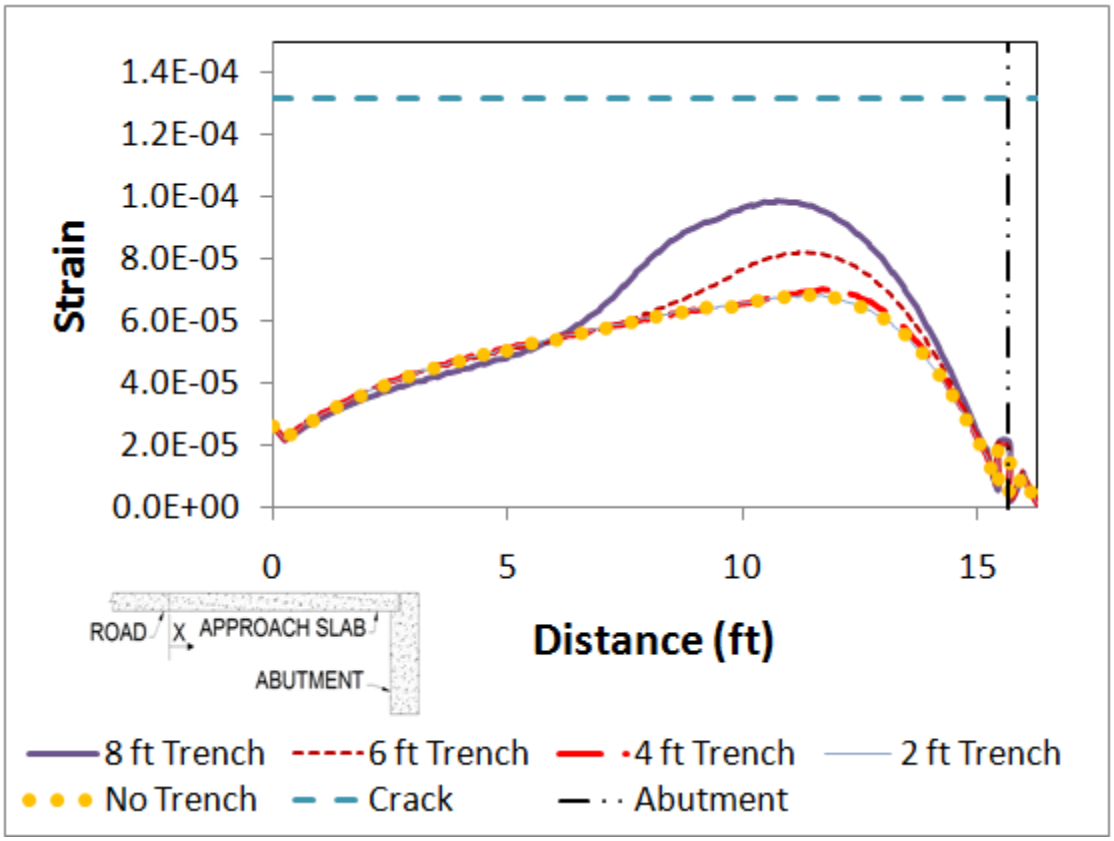

Figure 5.5 – Maximum principle strain envelope for settlement trench study

5.7.1.2 Discussion of Settlement Trench Geometry Study

Results from the settlement trench parametric study suggest the behavior of approach slab is significantly affected when the settlement trench is larger than 4 ft. A 2.7% difference in the largest maximum principle strain was observed between the approach slab with a 4 ft settlement trench and the case without a settlement trench. The difference increased to 15.7% when the 4 ft settlement trench was compared to the 6 ft settlement trench. A difference in strain of 18.1% was observed between the 6 ft and 8 ft settlement trenches.

The principle strain envelopes determined from each analysis depict unique behavioral characteristics for each settlement trench geometry considered. All of the cases exhibited a sharp decrease in strain near the abutment. Each case behaves in a different manner before the sharp decrease in strain. The case with no settlement trench, 2 ft settlement trench, and 4 ft settlement trench exhibited an approximate linear increase in strain from datum to the location of maximum strain. The other cases show a non-linear increase in strain just before the beginning of the settlement trench. This behavior is likely due to the approach slab having the ability to span the smaller settlement trenches better than the larger settlement trenches. The ability of the approach slab to span these distances is dependent on the support of the soil and the stiffness of the concrete.

5.7.1.3 Approach Slab End Rotation for Settlement Trench Geometry Study

The rotation of the end of the approach slab followed the same trend as the strain. The end rotation of the approach slab was relatively unaffected by settlement trenches 4 ft and smaller. Table 5.2 displays the end rotation of the approach slab for each settlement trench analyzed.

Table 5-2 – Approach slab end rotation for settlement trench study

Case	Rotation (rad)
8' Trench	0.001253
6' Trench	0.001086
4' Trench	0.000985
2' Trench	0.000956
No Trench	0.000951

The rotations at the end of the approach slab had a maximum 3.52% difference between the 4 ft settlement trench and no trench, a 9.79% difference between the 6 ft and 4 ft settlement trenches, and a 14.3% difference between the 6 ft and 8 ft settlement trenches.

5.7.1.4 Impact Factor for Settlement Trench / Void Geometry Study

The modified impact factor for each case analyzed is shown in Table 5.3. The impact factor calculated for the tandem to cause cracking in the 8 ft settlement trench is equal to the dynamic load allowance factor recommended by AASHTO. However, this impact factor

was computed without lane loading. It is logical to assume that the presence of the lane load would reduce the impact factor or would have caused earlier cracking of the approach slab.

Table 5-3 – Modified Impact factor for settlement trench study

Trench	Impact Factor
	6' Abutment
8' Trench	1.33
6' Trench	1.60
4' Trench	1.89
2' Trench	1.93
No Trench	1.93

5.7.2 Abutment Height

5.7.2.1 Results

The abutment height parametric study included the abutment height used in the baseline model as well as two additional heights. A total of four different settlement trench geometries were analyzed in combination with each abutment height. The settlement trench geometry and identification follows the guidelines presented in Figure 3.41.

The height of the abutment used in the settlement trench parametric study described previously was the shortest abutment considered in this parametric study. The

results for the baseline model with the 6 ft abutment height can be found in Section 5.4.1 and for other trench geometries in Section 5.7.1.

The second abutment height that was considered in the parametric study was 8 ft. A difference in the largest maximum principle (tensile) strains computed between the 4 ft settlement trench and the trenchless case was 0.27%. The difference in the strains computed between the 4 ft and 6 ft settlement trenches was 13.2%. A 16.2% difference in the strains computed between the 6 ft and 8 ft settlement trenches was observed. Table 5.4 displays the largest maximum principle (tensile) strains computed with the 8 ft abutment with each settlement trench.

Table 5-4 – Maximum principle strain and location for 8 ft abutment (cracking strain is 132 με)

Case	Strain	Location
8' Trench	1.03E-04	10'-11 1/4"
6' Trench	8.72E-05	11'-2 1/4"
4' Trench	7.64E-05	10'-11 1/4"
2' Trench	7.65E-05	10'-11 1/4"
No Trench	7.67E-05	10'-11 1/4"

The last abutment height that was considered in the parametric study was 12 ft. A difference in the largest maximum principle (tensile) strains computed between the 4 ft settlement trench and the trenchless case was 2.28%. The difference in the strains

computed between the 4 ft and 6 ft settlement trenches was 4.30%. A 13.5% difference in the strains computed between the 6 ft and 8 ft settlement trenches was observed. Table 5.5 displays the largest maximum principle (tensile) strains computed for the 12 ft abutment with each settlement trench.

Table 5-5 – Maximum principle strain and location for 12 ft abutment (cracking strain is 132 με)

Case	Strain	Location
8' Trench	1.11E-04	10'-5 1/4"
6' Trench	9.73E-05	10'-11 1/4"
4' Trench	9.32E-05	10'-11 1/4"
2' Trench	9.49E-05	10'-11 1/4"
No Trench	9.54E-05	10'-11 1/4"

Additional plots were created to compare the effect that each abutment height had for a given settlement trench. These plots were designed to mitigate the differences seen between the settlement trench geometries and effectively compare the effects of abutment geometry against each other.

The 8 ft settlement trench was analyzed with each abutment height. A 3.92% difference of the largest maximum principle (tensile) strain was found between the 6 ft and 8 ft abutments. The difference between the 8 ft and 12 ft abutment was 8.22%. The

difference between the 6 ft and 12 ft abutment was 12.13%. Figure 5.6 displays the plot comparing the abutments with a settlement trench of 8 ft.

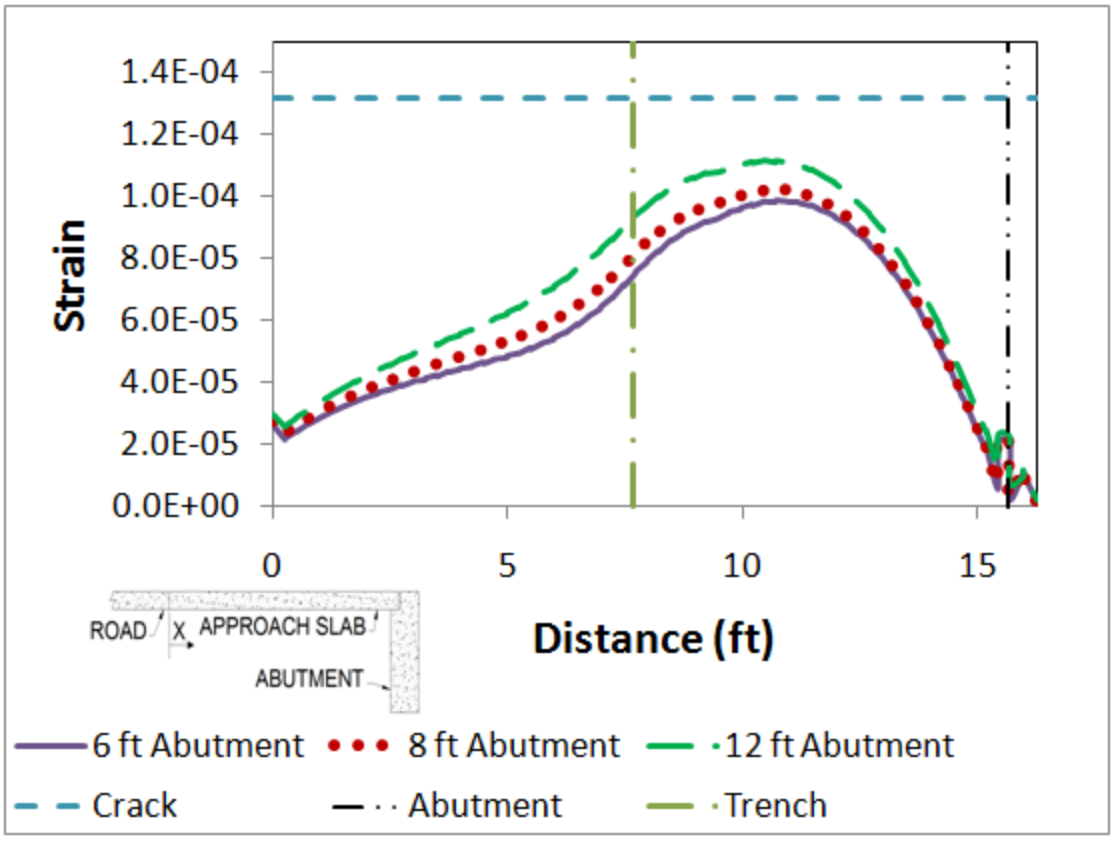

Figure 5.6 – Maximum principle strains for 8 ft settlement trench abutment height study

The 6 ft settlement trench was analyzed with each abutment height. A 5.83% difference of the largest maximum principle (tensile) strain was found between the 6 ft and 8 ft abutments. The difference between the 8 ft and 12 ft abutment was 10.97%. The

difference between the 6 ft and 12 ft abutment was 16.8%. Figure 5.7 displays the plot comparing the abutments with a settlement trench of 6 ft.

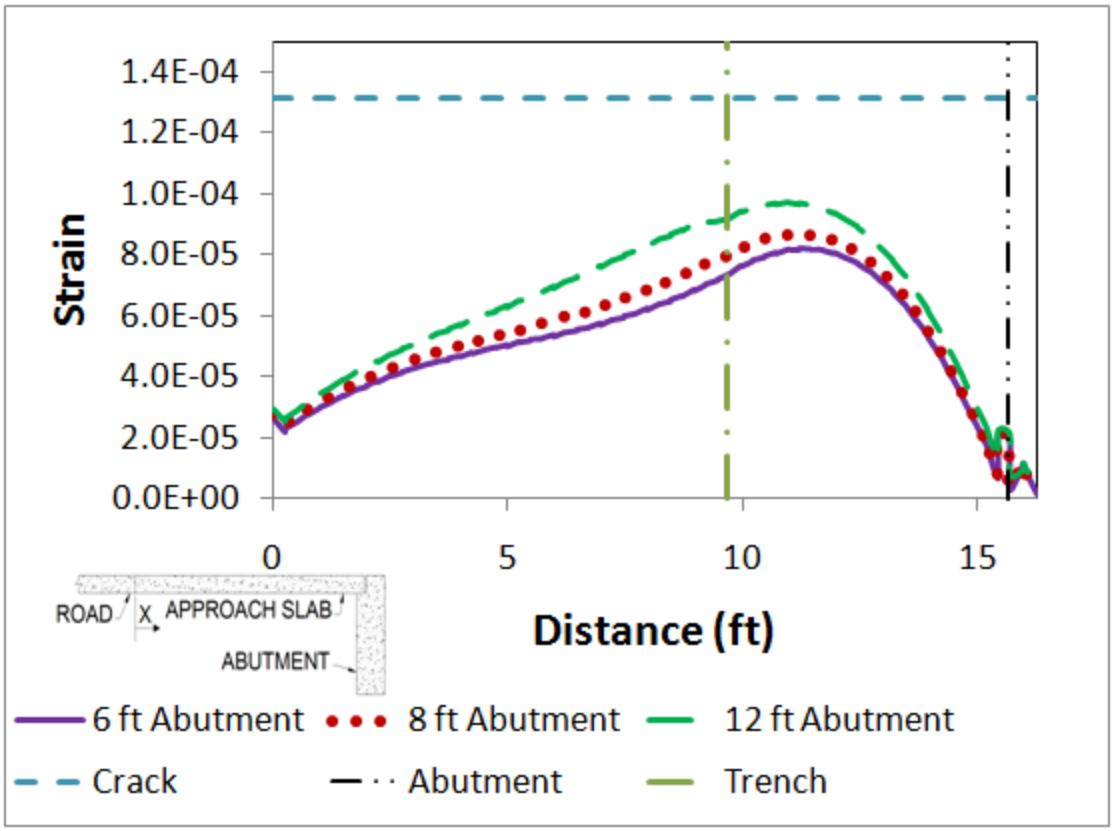

Figure 5.7 – Maximum principle strains for 6 ft settlement trench abutment height study

The 4 ft settlement trench was analyzed with each abutment height. An 8.37% difference of the largest maximum principle (tensile) strain was found between the 6 ft and 8 ft abutments. The difference between the 8 ft and 12 ft abutment was 19.79%. The difference between the 6 ft and 12 ft abutment was 28.0%. Figure 5.8 displays the plot comparing the abutments with a settlement trench of 4 ft.

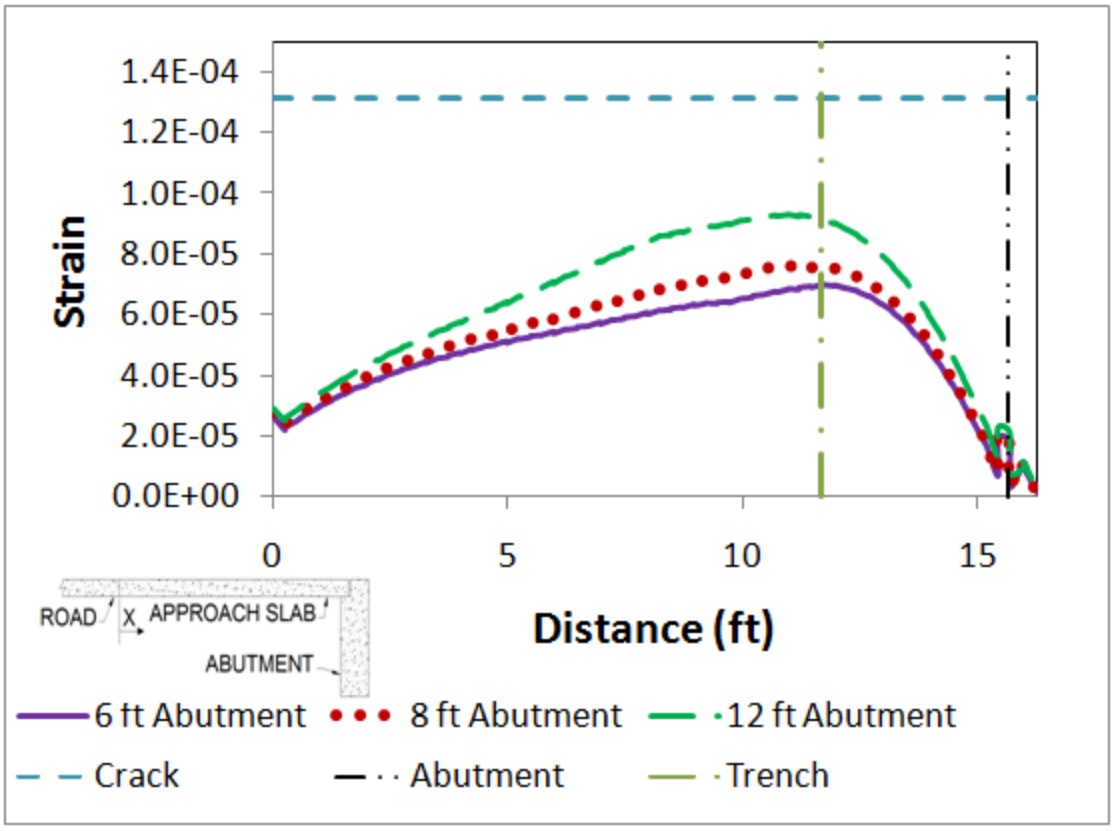

Figure 5.8 – Maximum principle strains for 4 ft settlement trench abutment height study

The 2 ft settlement trench was analyzed with each abutment height. An 11.3% difference of the largest maximum principle (tensile) strain was found between the 6 ft and 8 ft abutments. The difference between the 8 ft and 12 ft abutment was 21.5%. The difference between the 6 ft and 12 ft abutment was 32.6%. Figure 5.9 displays the plot comparing the abutments with a settlement trench of 2 ft.

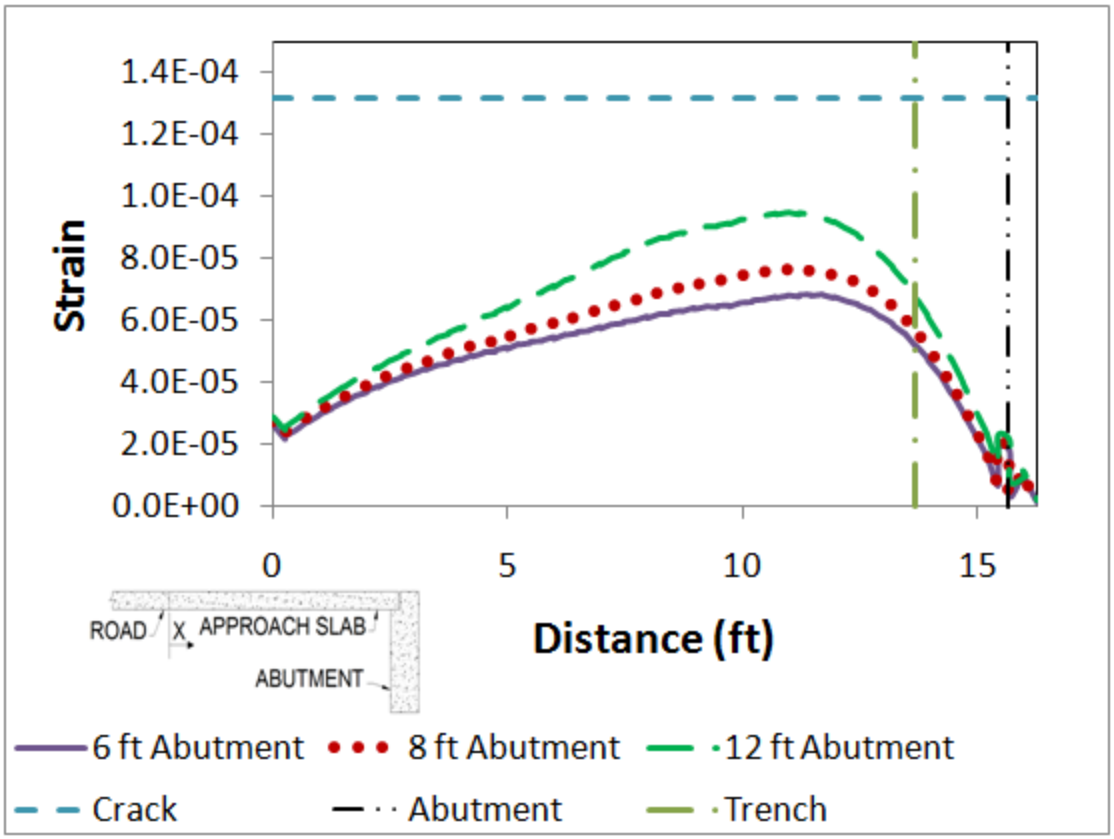

Figure 5.9 – Maximum principle strains for 2 ft settlement trench abutment height study

The 0 ft settlement trench was analyzed with each abutment height. An 11.3% difference of the largest maximum principle (tensile) strain was found between the 6 ft and 8 ft abutments. The difference between the 8 ft and 12 ft abutment was 21.8%. The difference between the 6 ft and 12 ft abutment was 32.9%. Figure 5.10 displays the plot comparing the abutments with a settlement trench of 0 ft.

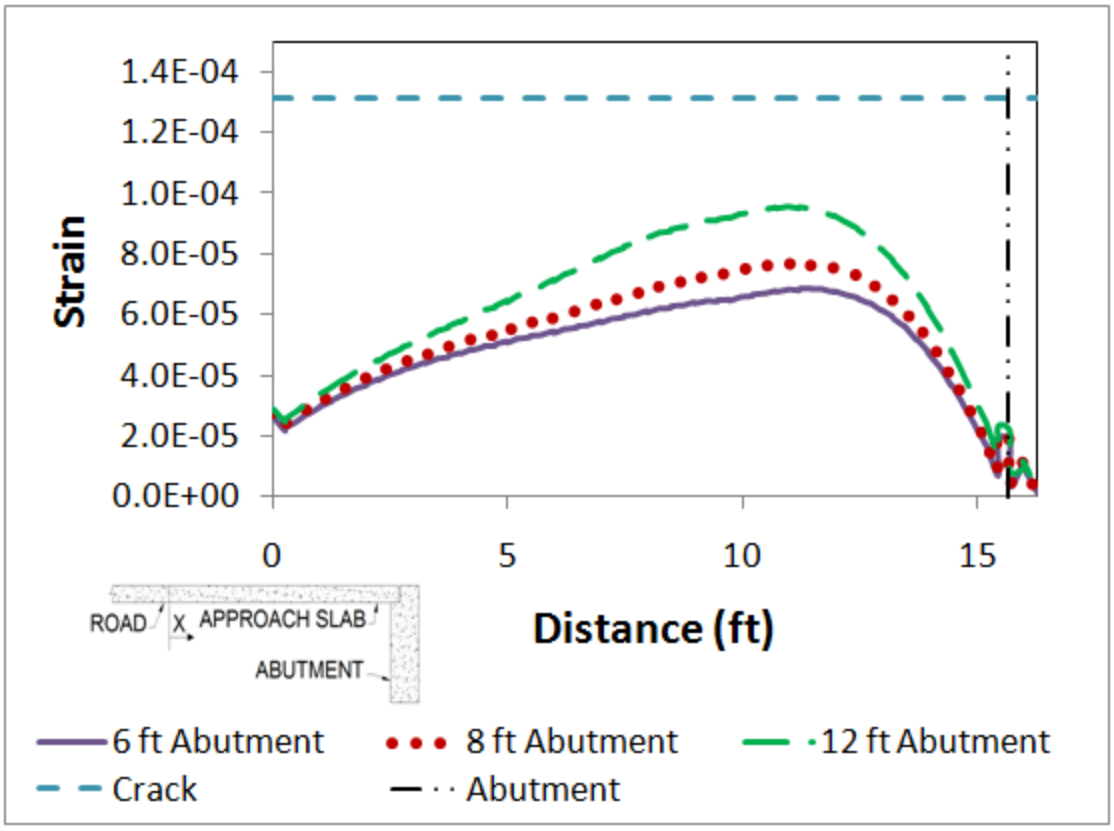

Figure 5.10 – Maximum principle strains for 0 ft settlement trench abutment height study

The largest maximum principle (tensile) strains for each case analyzed is presented in Table 5.6.

Table 5-6 – Largest maximum principle (tensile) strains for abutment height study (cracking strain is 132 με)

Trench	Maximum Principle (Tensile) Strain		
	6' Abutment	8' Abutment	12' Abutment
8' Trench	9.87E-05	1.03E-04	1.11E-04
6' Trench	8.23E-05	8.72E-05	9.73E-05
4' Trench	7.03E-05	7.64E-05	9.32E-05
2' Trench	6.82E-05	7.65E-05	9.49E-05
No Trench	6.84E-05	7.67E-05	9.54E-05

5.7.2.2 Discussion of Abutment Height Study

The height of the abutment did have an effect on the behavior of the approach slab. Higher abutments tended to have a larger influence on the approach slab. The influence that the height of the abutment had on the approach slab seemed to increase as the geometry of the settlement trench decreased. This can be seen by the difference between the strains computed from analyses performed with equal settlement trenches.

Approach slab strain was higher for analyses performed with equal settlement trenches but taller abutments. A difference of 12.13% was observed between the 6 ft and 12 ft abutment analyzed with the 8 ft settlement trench while a difference of 32.9% was observed between the same abutments with no trench present. The soil in the shorter abutment analysis would have less contact with the abutment resulting in a lower contact area of the soil being supported by the weaker force generated from the friction between the soil and abutment.

5.7.2.3 Approach slab End Rotation for Abutment Height Study

The rotation of the end of the approach slab followed the same trend as the strain. End rotations were the largest for taller abutments, regardless of settlement trench size. Figure 5.11 displays the end rotation of the approach slab for each settlement trench analyzed.

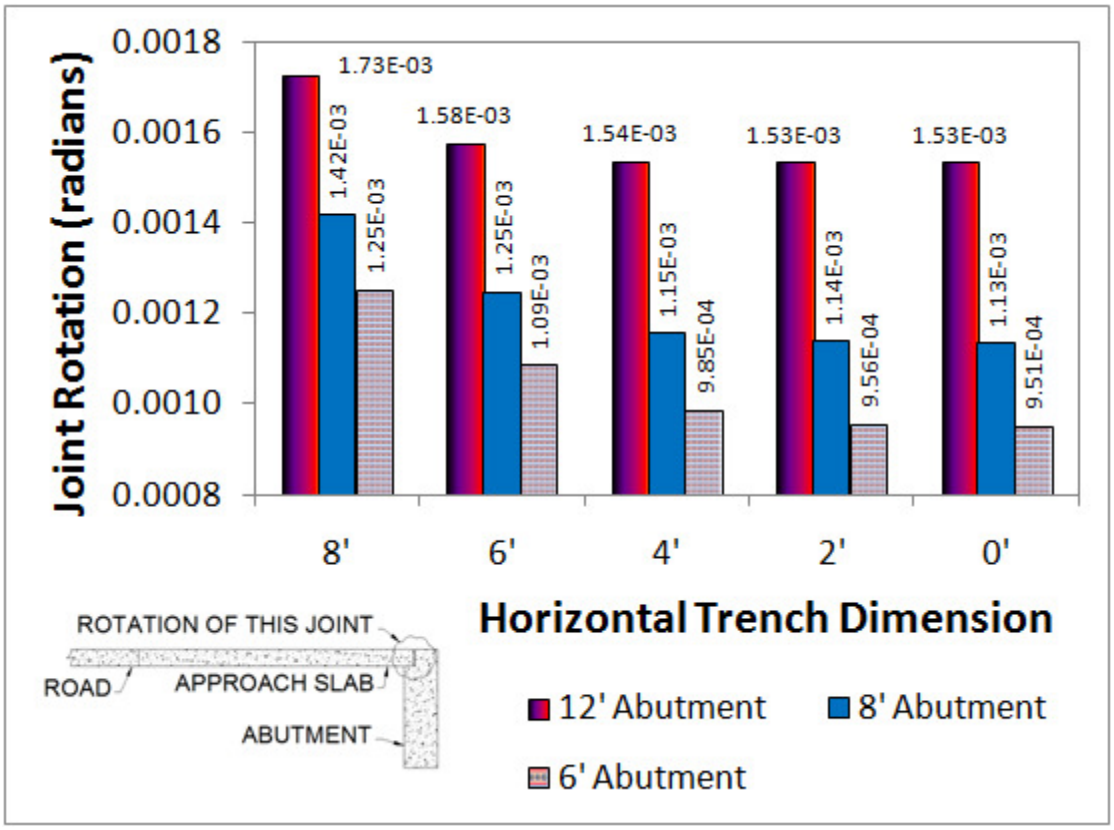

Figure 5.11 – Approach slab end rotation for settlement trench study

5.7.2.4 Modified Impact Factor for Abutment Height Study

The modified impact factor for each case analyzed is shown in Table 5.7. The impact factor calculated for the 8 ft settlement trench cases is less than or equal to the dynamic allowance factor recommended by AASHTO. However, this impact factor was computed without lane loading. It is logical to assume that the presence of the lane load would reduce the impact factor or would have caused cracking of the approach slab.

Table 5-7 – Modified Impact factor for settlement trench study

Trench	Impact Factor		
	6' Abutment	8' Abutment	12' Abutment
8' Trench	1.33	1.28	1.18
6' Trench	1.60	1.52	1.36
4' Trench	1.89	1.74	1.42
2' Trench	1.93	1.74	1.38
No Trench	1.93	1.74	1.37

5.7.3 Approach Slab Length

5.7.3.1 Results

The maximum principle (tensile) strains in the varying approach slabs were determined from the numerical analysis and are presented in Table 5.8. Cracking was not observed for any of the approach slab lengths analyzed. All of the cases used the same geometry that was used in the baseline model.

Table 5-8 – Maximum principle (tensile) strains determined from the approach slab length parametric study (cracking strain is 132 με)

Case	Strain	Location
20'	8.21E-05	15'-6"
15'-8"	8.23E-05	11'-2 1/4"
10'	7.67E-05	6'-0"

The strains from each case were plotted using a different datum than previously shown in Chapter 4. Datum was placed at the abutment for this plot. Figure 5.12 displays the maximum principle (tensile) strains calculated for the bottom of the approach slab.

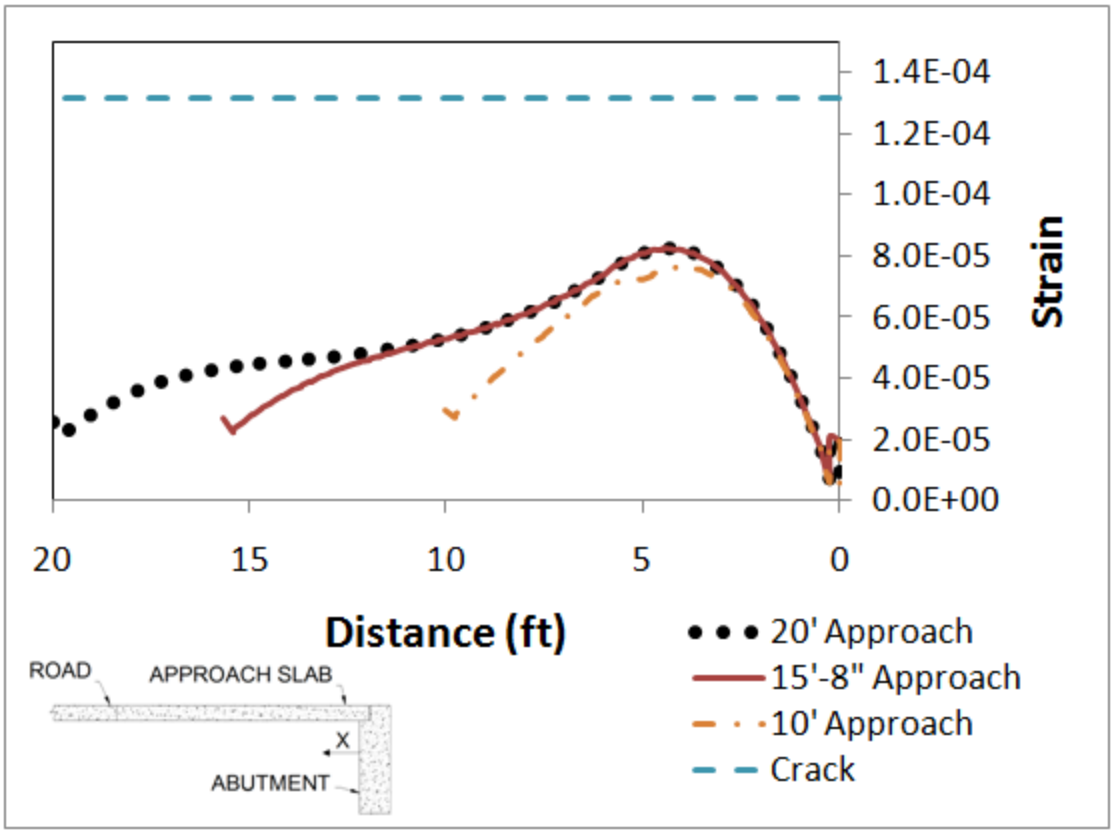

Figure 5.12 – Maximum principle (tensile) strains for the approach slab

5.7.3.2 Approach Slab Length Study Discussion

The maximum strain computed in the 20 ft and 15'-8" approach slab length cases exhibited little variation between each other while the 10 ft approach slab showed a trend similar to the other analyses. A difference of 0.18% was observed between largest maximum principle strains calculated in each case. The difference in the strain determined from each analysis case at locations further away from datum is seen because the plot displays the envelope instead of the strains for a single load case.

The location of the largest maximum principle strain varied by 6 in. in all of the cases analyzed. This behavior can be attributed to the coupling placed at the approach slab-roadway joint. The coupling at this joint transferred vertical, horizontal, and bending forces between the roadway and approach slab. The transfer of these forces minimized the differences observed between the various approach slab lengths.

The difference in the magnitude of the largest maximum principle strain was 6.86% between all of the cases analyzed. The strain in the 10 ft approach slab is smaller than the other two cases. This is due to the loading of the HL93 tandem truck. The HL93 standard truck created higher moments for spans less than or equal to 11 ft. For this reason, the truck that was used did not generate the worst-case loading. The location of the largest maximum principle strains using the modified datum is presented in Table 5.9.

Table 5-9 – Maximum principle (tensile) strains determined from the approach slab length parametric study with revised datum (cracking strain is 132 με)

Length	Strain	Location
20'	8.21E-05	4'-6"
15'-8"	8.23E-05	4'-5 3/4"
10'	7.67E-05	4'-0"

5.7.3.3 Approach Slab End Rotation for Approach Slab Length Study

The end rotation of the approach slab was determined from each analysis. A maximum rotation of 0.001085, 0.001086, and 0.001087 radians was determined for the 20 ft, 15’-8”, and 10 ft approach slabs, respectively.

5.7.3.4 Modified Impact Factor for Approach Slab Length Study

The modified impact factors for the approach slab length parametric study were determined. The impact factors are presented in Table 5.10.

Table 5-10 – Impact factors for approach slab parametric study

Length	Factor
20'	1.60
15'-8"	1.60
10'	1.73

5.7.4 Soil Stiffness

5.7.4.1 Results

The soil stiffness parametric study investigated the influence the soil had on approach slab strain. Four analyses were performed in this parametric study. The largest maximum principle (tensile) strains with locations are presented in Table 5.11.

Table 5-11 – Maximum principle (tensile) strains with location for soil parametric study (cracking strain is 132 με)

Case	Strain	Location
Stiff Soil	7.06E-05	11'-8 1/4"
Moderately Stiff	8.23E-05	11'-2 1/4"
Layered Soil	9.36E-05	10'-11 1/4"
Loose Soil	3.29E-04	10'-2 3/8"

Cracking was predicted in the loose soil analysis (strain was larger than the cracking strain of 132 με). The moment of inertia was modified according to Section 3.1.1.2 to account for the geometrical changes to the cross section from cracking.

5.7.4.2 Soil Stiffness Study Discussion

The soil stiffness parametric studies performed were intended to represent a range of soil properties that could be expected for compacted clean sand backfill that may be present under an approach slab. The layered soil analysis case represented heavy

compaction near the surface and an increase in stiffness due to increases in effective stress with depth.

The moderately stiff soil case was selected to be used as the baseline soil stiffness. The layered soil profile would have been a better representation of the soil encountered under the approach slab but was not used due to the uncertainty associated with the natural soil that would exist under the base course. Section 3.1.1.1 gives further explanation on the choice to use the moderately stiff soil for the baseline model.

Approach slab cracking was observed in the loose soil analysis case alone. The moment of inertia was adjusted for the portions of the approach slab that exceeded the cracking strain as defined by Equation 3.3. Successive iterations were used until all portions of the approach slab that exceeded the cracking strain had the cracked moment of inertia. The reduction of the moment of inertia caused decrease in stiffness which caused a sharp increase in the strain computed from the analysis as shown in Figure 5.13.

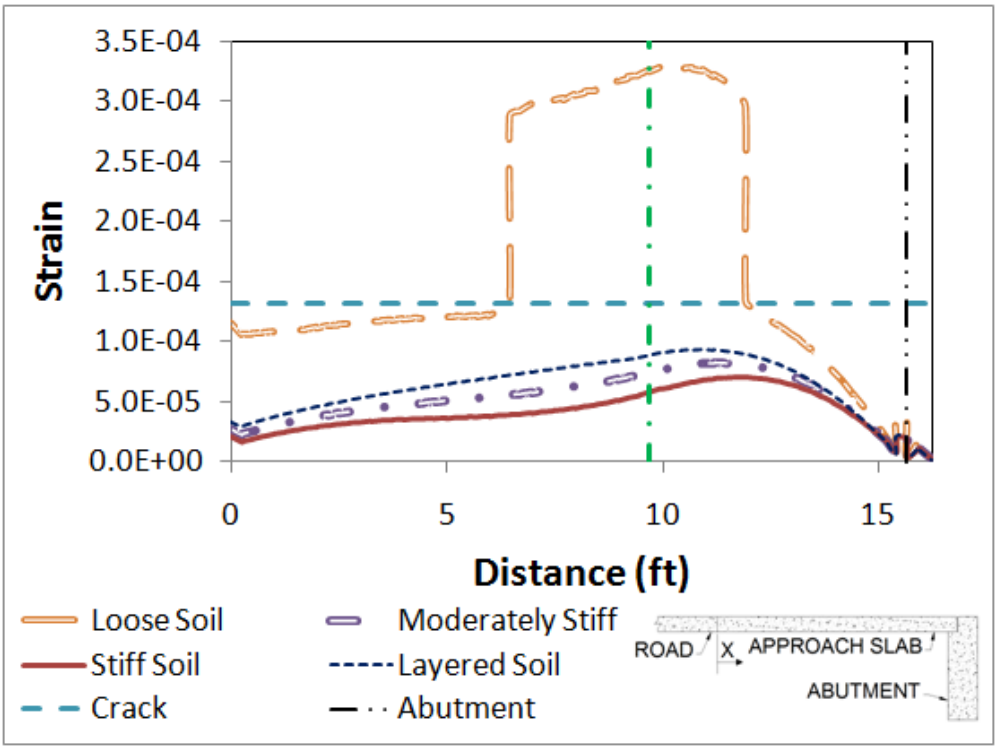

Figure 5.13 – Maximum principle strains for soil stiffness study

The trends shown in Figure 5.13 show a decrease in strain with soil stiffness increases. The difference between the stiff and moderately stiff soil was 15.2%. A 12.9% difference was observed between the layered and moderately stiff case. The location of the maximum strains was shifted further away from the abutment as the soil stiffness decreased. This was due to the approach slab having to 'span' a longer distance when it was supported by looser soil as the soil would provide less support in the loose case.

5.7.4.3 Approach Slab End Rotation for Soil Stiffness Study

End rotation of the approach slab near the abutment was determined from the numerical analysis. The rotation of 0.000802, 0.00109, 0.00134, and 0.00450 radians was determined for the stiff, moderately stiff, layered, and loose soil, respectively.

5.7.4.4 Modified Impact Factor for Soil Stiffness Study

The modified impact factor for each soil analyzed in the soil stiffness parametric study was determined from the strain information collected from each analysis. Table 5.12 displays the impact factor for each soil. The impact factor for the loose soil is not meaningful as the approach slab had cracked from the truck load alone

Table 5-12 – Impact factors for soil stiffness parametric study

Case	Factor
Stiff Soil	1.85
Moderately Stiff	1.60
Layered Soil	1.40
Loose Soil	NA

5.7.5 Concrete Stiffness

5.7.5.1 Results

Two concrete stiffnesses were investigated using the homogeneous loose soil layer. The largest maximum principle (tensile) strain calculated in the numerical analysis with the

baseline model but with the loose soil was 329 με and 104 με (or 250% and 79% of cracking) for the 4000 psi and 8000 psi concrete, respectively. The 4000 psi concrete exhibited cracking while the 8000 psi concrete did not crack.

5.7.5.2 Concrete Stiffness Discussion

The analyses conducted in this parametric study utilized the homogeneous loose soil layer. During the soil stiffness parametric study, approach slab cracking was predicted from the analysis conducted with the loose soil alone. The approach slab analyzed with the higher concrete stiffness did not exhibit any cracking when it was placed on the loose soil. This was due to an increase in the modulus of rupture (formerly shown as Equation 3.2) and stiffness of the concrete. The increase in strength increased the ability of the approach slab to 'span' the void and not be as susceptible to changes in the stiffness of the soil supporting the end of the approach slab.

5.7.5.3 Approach Slab End Rotations for Concrete Stiffness Study

The maximum end rotation of the approach slab was 0.00301 radians for the 8 ksi concrete and 0.00450 radians for the 4 ksi concrete. The rotation of the stronger approach slab was smaller than the rotation of the more flexible approach slab. A 39.6% difference in rotation was observed between the two cases.

5.7.5.4 Modified Impact Factor for Concrete Stiffness Study

The modified impact factor was calculated for the 8 ksi concrete. The 4 ksi concrete cracked under the truck load alone so the factor is meaningless. The calculated impact factor was 1.28 for the 8 ksi concrete without the lane load. This is significant because the analysis was performed on the loose soil and indicates that use of higher strength concrete, such as precast/prestressed slabs, could avoid some of the long term deterioration due to cracking.

5.7.6 Joint Restrictions

5.7.6.1 Results

Constraints placed on the coupling between the roadway and approach slab were varied to determine the impact this restraint had on the behavior of the approach slab. Two constraints were considered in addition to the baseline model. The restraints utilized a moment, shear, and unrestrained coupling placed between the roadway and approach slab. The largest maximum principle (tensile) strain determined from the analysis was 80 με for the unrestrained coupling case and 82 με for both the moment and shear couplings (or 61% and 62% of the cracking strain).

5.7.6.2 Joint Restriction Study Discussion

The shear and moment coupling analyses caused similar behavior in the approach slab. Both couplings used a control point that was placed at the quarter point of the depth. The control point is depicted in Figure 5.14.

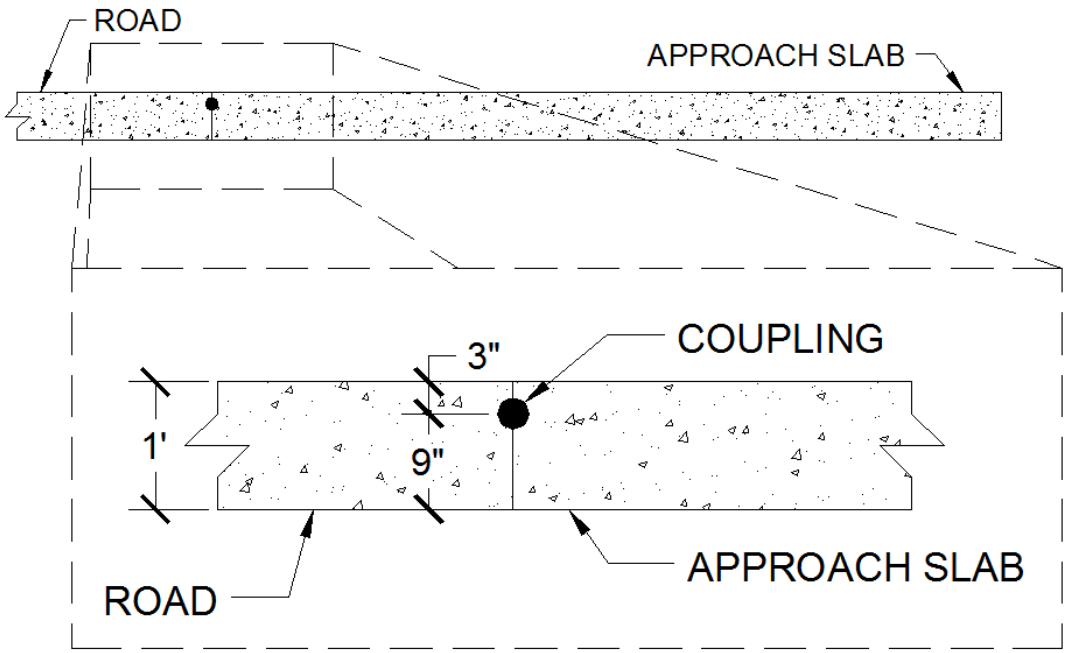

Figure 5.14 – Roadway-approach slab coupling location

The moment coupling effectively joined the end surface of the approach slab to the end surface of the roadway. Vertical, horizontal, and rotational displacements of each surface were coupled together for this analysis. The shear coupling restricted vertical and horizontal displacement of the end of the approach slab relative to the end of the roadway

surface. Rotational displacement of the approach slab about the control point was allowed. No rotational displacement occurred from this analysis due to the location of the control point. The location of the control point created a force couple between the approach slab and roadway. The concrete was sufficiently stiff and resisted deformations from the force couple. This contributed to the shear coupling acting like the moment coupling.

The unrestrained analysis was performed to investigate the behavior of the approach slab if the expansion joint would be relocated to the joint between the roadway and approach slab. The largest maximum principle (tensile) strain for the unrestrained case was 81 με (or 61% of cracking) at a location of 11'-2 ¼" from datum. The decrease in the strain computed in the unrestrained case can be attributed to the approach slab acting more like a simply supported beam. The other models considered in this parametric study induced some bending in the approach slab from the roadway.

The relocation of the expansion joint to this location is common when integral abutments are utilized. The strain computed from the unrestrained case exceeded each restrained case. This is due to excessive movement of the approach slab at the joint between the roadway and approach slab. The absence of any coupling would allow differential movement of each part at the joint location. This differential movement created a 'bump' at the joint between the roadway and approach slab as the truck traversed the approach slab. The maximum end rotation of the approach slab at this joint

was 0.000440 radians for both the moment and shear coupling and 0.000660 radians for the unrestrained case.

5.7.6.3 Approach Slab End Rotations for Joint Restriction Study

The maximum end rotation of the approach slab near the abutment was 0.0010859 radians for both the moment and shear coupling and 0.0010856 radians for the unrestrained case. A difference of 0.03% was computed between the end rotation of the unrestrained and restrained approach slab near the abutment. The difference between the end rotations of the approach slab near the abutment for the three parametric studies is negligible.

5.7.6.4 Modified Impact Factor for Joint Restrictions Study

The shear and moment coupling restrictions placed on the joint between the roadway and approach slab had insignificant effects on the behavior of the approach slab. The modified impact factor that would be assigned to each model was approximately equal to the impact factor assigned to the base model (the impact factor assigned to the base model was 1.60).

The unrestrained model developed smaller strains than the other models performed in the parametric study. An impact factor of 1.65 could be applied to the model before any cracking of the approach slab would be observed.

Chapter 6: Summary, Conclusions, & Future Work

6.1 Summary

6.1.1 Abutment and Settlement Trench Geometry Parametric Study

Abutment height influenced the behavior of the approach slab for all cases analyzed. The reason for the difference in strain observed between the abutment heights could not be attributed to any factors. The difference may have been a result of the location of the location of the lower boundary condition or from the loss of support due to the friction created between the abutment and soil. Strains computed in the approach slab were consistently higher for taller abutments. A 5.83% difference in maximum tensile strain was computed between the baseline model (6 ft high abutment) and the model with an 8 ft tall abutment. The difference between the baseline model and the 12 ft tall abutment increased to 16.8%. Rotations of the end of the approach slab near the abutment also increased with increases in abutment height. A 13.8% and 36.8% difference of rotation was computed between the baseline model and the 8 ft and 12 ft abutment heights, respectively.

The geometry of the settlement trench impacted the behavior of the approach slab. Settlement trenches less than or equal to 4 ft had a small impact on the behavior of the approach slab for the abutment heights considered (6 ft, 8 ft, and 12 ft abutment heights). The largest difference in maximum principle strain computed in the approach slab was less than 3% between models with a 4 ft settlement trench and those without a settlement

trench. The degree to which the larger settlement trenches influenced the approach slab was dependent on the height of the abutment. Taller abutments exhibited larger increases in strain compared to the shortest abutment.

The percent change in maximum tensile strains and approach slab end rotations for each analysis conducted in the settlement trench and abutment geometry parametric study were compared to the base model. The changes in rotation are presented in Figure 6.1 while Figure 6.2 displays changes in maximum tensile strains compared to the base model.

Table 6-1 - Percent change in approach slab end rotation determined from the settlement trench and abutment geometry study to the base model

Variable	Rotation (rad)	Change
6' Abt. Ht. - 8' TR	1.25E-03	15%
6' Abt. Ht. - 6' TR	9.85E-04	9%
6' Abt. Ht. - 4' TR	1.09E-03	NA
6' Abt. Ht. - 2' TR	9.56E-04	12%
6' Abt. Ht. - 0' TR	9.51E-04	12%
8' Abt. Ht. - 8' TR	1.42E-03	30%
8' Abt. Ht. - 6' TR	1.25E-03	15%
8' Abt. Ht. - 4' TR	1.15E-03	6%
8' Abt. Ht. - 2' TR	1.14E-03	5%
8' Abt. Ht. - 0' TR	1.13E-03	4%
12' Abt. Ht. - 8' TR	1.73E-03	59%
12' Abt. Ht. - 6' TR	1.58E-03	45%
12' Abt. Ht. - 4' TR	1.54E-03	41%
12' Abt. Ht. - 2' TR	1.53E-03	41%
12' Abt. Ht. - 0' TR	1.53E-03	41%

Table 6-2– Percent change in approach slab tensile strain determined from the settlement trench and abutment geometry study to the base model

Variable	Max. Strain	Change
6' Abt. Ht. - 8' TR	9.87E-05	40%
6' Abt. Ht. - 6' TR	7.03E-05	17%
6' Abt. Ht. - 4' TR	8.23E-05	NA
6' Abt. Ht. - 2' TR	6.82E-05	3%
6' Abt. Ht. - 0' TR	6.84E-05	3%
8' Abt. Ht. - 8' TR	1.03E-04	25%
8' Abt. Ht. - 6' TR	8.72E-05	6%
8' Abt. Ht. - 4' TR	7.64E-05	7%
8' Abt. Ht. - 2' TR	7.65E-05	7%
8' Abt. Ht. - 0' TR	7.67E-05	7%
12' Abt. Ht. - 8' TR	1.11E-04	35%
12' Abt. Ht. - 6' TR	9.73E-05	18%
12' Abt. Ht. - 4' TR	9.32E-05	13%
12' Abt. Ht. - 2' TR	9.49E-05	15%
12' Abt. Ht. - 0' TR	9.54E-05	16%

6.1.2 Approach Slab Length

The length of the approach slab had a small influence on the behavior of the approach slab. Strain envelopes determined from the analysis of the 20 ft and 15’-8” approach slabs showed similar trends and had a 0.18% difference in peak tensile strains. A 7.04% difference in the largest tensile strain was computed between the 15 ft-8” and 10’ approach slabs. Approach slab end rotation increased as the length decreased. A 0.26% difference in end rotation was predicted between the 20 ft and 10 ft approach slabs.

The location of the largest principle strains computed from the approach slab length parametric study were located within a six inches from each other. This was due to the coupling placed at the roadway-approach slab joint. This restraint transferred vertical, horizontal, and bending forces between the approach slab and roadway.

The percent change in maximum tensile strains and approach slab end rotations for each analysis conducted in the approach slab length parametric study were compared to the base model. The changes in rotation are presented in Figure 6.3 while Figure 6.4 displays changes in maximum tensile strains compared to the base model.

Table 6-3 – Percent change in approach slab end rotation determined from the approach slab length study to the base model

Variable	Rotation (rad)	Change
20'-0" Length	1.08E-03	0.12%
15'-8" Length	1.09E-03	NA
10'-0" Length	1.09E-03	0.13%

Table 6-4 – Percent change in approach slab tensile strain determined from the approach slab length study to the base model

Variable	Max. Strain	Change
20'-0" Length	8.21E-05	0.18%
15'-8" Length	8.23E-05	NA
10'-0" Length	7.67E-05	7%

6.1.3 Soil Stiffness

The soil stiffness parametric study was performed to determine how the upper bound, lower bound, and most common soil would influence the behavior of the approach slab. The general trend observed from the analyses suggested the end rotation and strain in the approach slab decreased as the stiffness of the soil increased. Cracking of the approach slab was observed in the lower soil stiffness case alone.

The percent change in maximum tensile strains and approach slab end rotations for each analysis conducted in the soil stiffness parametric study were compared to the base model. The changes in rotation are presented in Figure 6.5 while Figure 6.6 displays changes in maximum tensile strains compared to the base model.

Table 6-5 – Percent change in approach slab end rotation determined from the soil stiffness study to the base model

Variable	Rotation (rad)	Change
Stiff Soil	8.02E-04	26%
Layered Soil	1.34E-03	24%
Moderately Stiff	1.09E-03	NA
Loose Soil	4.50E-03	314%

Table 6-6 – Percent change in approach slab tensile strain determined from the soil stiffness study to the base model

Variable	Max. Strain	Change
Stiff Soil	7.06E-05	14.15%
Layered Soil	9.36E-05	14%
Moderately Stiff	8.23E-05	NA
Loose Soil	3.29E-04	300%

6.1.4 Concrete Stiffness

The concrete stiffness parametric study investigated how changes in concrete stiffness affected approach slab behavior. This parametric study was performed with the loose soil condition. Concrete cracking was observed with the lower stiffness approach slab but was prevented when the concrete stiffness was increased. End rotation of the approach slab was decreased with the increase in concrete stiffness.

6.1.5 Joint Restrictions

The restrictions placed on the joint between the roadway and approach slab had a minimal effect on the behavior of the approach slab. Moment and shear couplings placed at this joint exhibited no change in the behavior of the approach slab. A decrease in strain but increases in the rotation at each end was observed when the restrictions on the roadway-approach slab joint were removed.

The percent change in maximum tensile strains and approach slab end rotations for each analysis conducted in the joint restrictions parametric study were compared to the base model. The changes in rotation are presented in Figure 6.7 while Figure 6.8 displays changes in maximum tensile strains compared to the base model.

Table 6-7 – Percent change in approach slab end rotation determined from the joint restrictions study to the base model

Variable	Rotation (rad)	Change
No Coupling	1.09E-03	0%
Moment Coupling	1.09E-03	0%
Shear Coupling	1.09E-03	NA

Table 6-8 – Percent change in approach slab tensile strain determined from the soil stiffness study to the base model

Variable	Max. Strain	Change
No Coupling	8.07E-05	2%
Moment Coupling	8.23E-05	0%
Shear Coupling	8.23E-05	NA

6.1.6 End Rotation

The expected range of end rotation of the approach slab near the abutment was determined from the analyses. The maximum end rotation of the approach slab was 0.00450 radians and the minimum end rotation was 0.00080 radians. The rotation was consistently under 0.00200 radians for all of the analyses except those that utilized the homogeneous loose soil layer. Rotations computed with the loose soil layer were assumed to be overly conservative as these loose soil conditions are not likely to occur under the approach slab.

The percent change in maximum tensile strains and approach slab end rotations for each analysis conducted in the soil stiffness parametric study were compared to the base model. The changes in rotation are presented in Figure 6.5 while Figure 6.6 displays changes in maximum tensile strains compared to the base model.

6.1.7 Modified Impact Factor

A modified impact factor was determined for each analysis that did not result in approach slab cracking from the HL93 tandem truck alone. The calculated impact factor for the uncracked analyses ranged from 1.93 to 1.18 with a median impact factor of 1.60. Analyses that resulted in the cracking of the concrete approach slab did not have an impact factor assigned to them.

The impact factor was calculated using results computed from the lane and HL93 tandem truck load analyses. An impact factor of 1.11 was computed for the combined loading.

6.2 Conclusions

6.2.1 Approach Slab End Rotation

The end rotation of the approach slab near the abutment varied depending on geometry and stiffness of the soil and concrete parts used in the analyses. A maximum rotation of 0.0045 radians was computed from the analyses conducted with the 4000 psi concrete stiffness over the loose homogeneous soil layer. The majority of the rotations were below 0.002 radians. The expansion joint between the approach slab and abutment should be design to accommodate a minimum of 0.002 radians of rotation. Analysis cases that computed higher rotations (analyses utilizing the homogeneous loose soil layer) were

assumed to be overly conservative as the loose soil conditions are not likely to occur under the approach slab.

The influential parameters considered in the study were assessed against the base model. Parameters with the largest percent change were considered to be the most influential. An excessively loose soil condition (the homogeneous loose soil layer) was determined to have the largest percent change from the base model. Outside of the loose soil case, the abutment height was the most influential. Taller abutments resulted in more end rotation of the approach slab. The soil stiffness parameter had the lowest significant percent change (larger than 15% change) between the base model. Approach slab length and joint restrictions had little influence (less than 3%) on the behavior of the approach slab.

6.2.2 Approach Slab Cracking

The susceptibility of an approach slab to cracking was influenced by the height of the abutment, soil stiffness, concrete stiffness, and settlement trench geometry. The following conclusions were made concerning the previously mentioned variables:

- Taller abutments increase the likelihood of concrete approach slab cracking. This was true for all settlement trench geometries considered. Differences in strains between the 6 ft and 12 ft abutment heights were approximately three times higher than the differences between the 6 ft and 8 ft abutment.

- The presence of loose soil was the most influential parameter investigated. Aside from the loose soil layer, the influence of this parameter is rather small (the percent change in maximum tensile strain was within 14% from the base model) when compared to other parameters. While the general trend suggested the risk of concrete cracking decreased with increases in soil stiffness, this parameter is not considered to be influential outside of the loose soil case. The stiffness of the soil is recommended not to fall within the loose soil properties to avoid cracking and minimize the influence of the soil on the behavior of the approach slab.

- Cracking was less likely when a concrete with a higher compressive strength was specified for the concrete in the approach slab. The concrete stiffness parametric study predicted concrete cracking when the compressive strength was 4000 psi but did not predict concrete cracking when the compressive strength was increased to 8000 psi. Increasing the concrete strength and stiffness may be an effective means of increasing the durability of the approach slab.

- Settlement trench geometry became influential when the horizontal length of the trench exceeded 50% of the abutment height (for a 10 ft tall

abutment, the horizontal length of the settlement trench would equal 5 ft). A 3% difference in tensile strains was calculated between the no trench case and settlement trenches having a horizontal length equal to 50% of the abutment height. This relatively small difference suggests effective soil compaction (soil compacted to at least 95% standard Procter) near the abutment (a horizontal distance equal to 50% of the abutment height) has little effect on the cracking of the approach slab under conditions similar to those modeled. Further investigations should be conducted before altering any construction practices.

The least influential parameters were identified using the smallest percent change criteria. Approach slab length and joint restrictions placed at the roadway-approach slab interface had little impact (less than a 7% change from the base model) on the behavior of the approach slab.

6.2.3 Modified Impact Factor

The modified impact factor presented in this paper should not be used to check the safety of a design without further testing. This testing should include a more rigorous investigation of soil properties, dynamic loading, lane loading, and additional numerical analyses with the full range of AASHTO trucks applied to the model. One analysis was conducted with the HL93 tandem truck and lane loads applied to the model. Additional

models should be performed that consider the presence of the lane load with the other HL93 design trucks outline from the AASHTO Bridge Design Manual.

6.3 Recommendations for Future Work

6.3.1 Finite Element Analyses

Additional finite element analyses should be performed with the full range of the AASHTO HL93 design trucks. The HL93 standard design truck generates the largest bending moment in simply supported spans of 11 ft and smaller. The HL93 tandem design truck generates the largest bending moment in simply supported spans larger than 11 ft up to 20 ft. The soil supporting the approach slab acted like springs of varying stiffness (due to the presence of the settlement trench) making the actual span unknown. Additional analyses with all of the HL93 design vehicles and the application of the lane load should be performed to determine the full impact of each variable.

It is recommended that future finite element models should be performed considering:

- Skew.
- Multiple lanes.
- Non-linear concrete behavior.
- The use of integral abutments.
- Additional fill and natural soil properties and thicknesses.

6.3.2 Recommendations for Improving Approach Slab Durability

In order to improve the durability of approach slabs, two issues are recommended to be addressed: 1) soil compaction and 2) concrete strength.

A minimum relative density of 52% should be achieved when utilizing Portage Sand (as used in this model) or other granular soils. Additionally, as discussed in Seo (2003), ideal soil compaction is recommended to reach no less than 95% standard proctor.

As shown in the concrete stiffness parametric study, lower strength concrete displayed cracking over loose soil, while the stronger concrete displayed a linear elastic behavior despite the poor soil compaction. Therefore, high strength concretes, utilized in combination with soil compaction techniques that attain 95% standard proctor are recommended to ensure that an approach slabs will be able to provide a 75-year service life.

References

Bolton M D The Strength and Dilatancy of Sands [Report]. - [s.l.] : Geotechnique, 36(1), 65-78, 1986.

Cook Robert D [et al.] Concepts and Applications of Finite Element Analysis [Book]. - [s.l.] : John Wiley & Sons, Inc., 2002. - Vol. IV.

Cosgrove Edward F and Lehane Barry M Cyclic Loading of Loose Backfill Placed Adjacent to Integral Bridge Abutments [Report]. - [s.l.] : International Journal of Physical Modelling in Geotechnics 3, 2003.

CTC & Associates, LLC Concrete Bridge Approach Pavements: A Survey of State Practices [Report]. - Madison : WisDOT Research & Library Unit, 2010.

Edil T. B., Benson C. H. and Bareither C. A. Determination of Shear Strength Values for Granular Backfill Material Used by the Wisconsin Department of Transportation, Report SPR # 0092-05-08 [Report]. - 2007.

FHWA Continuously Reinforced Concrete Pavement [Online] // Federal Highway Administration Pavements Technical Advisory. - U.S. Department of Transportation, June 5, 1990. - October 20, 2010. - http://www.fhwa.dot.gov/pavement/t508014.cfm.

Fredlund D.G and Rahardjo H. Soil Mechanics for Unsaturated Soils [Book]. - [s.l.] : John Wiley & Sons, Inc., 1993.

Gere James M Mechanics of Materials [Book]. - [s.l.] : Brooks/Cole, 2004. - Vol. 6th Edition.

Ha Hunsoo, Seo Jeong Bok and Briaud Jean-Louis Investigation of Settlement at Bridge Approach Slab Expansion Joint: Numerical Simulations and Model Tests [Report]. - College Station : Texas A&M University, 2002.

Hall Kevin D and James Mainey PCC Inputs to Mechanistic-Empirical Pavement Design Guide [Report]. - 2008.

Helwany Sam Applied Soil Mechanics with ABAQUS Applications [Book]. - [s.l.] : John Wiley & Sons, Inc., 2007.

Helwany Sam, Koutnik Therese Ellen and Ghorbanpoor Al Evaluation of Bridge Approach Settlement Mitigation Methods [Report]. - Milwaukee : University of Wisconsin, 2007.

Hoppe Edward J Guidelines for the Use, Design, and Construction of Bridge Approach Slabs [Report]. - Charlottesville : Virginia Department of Transportation, 1999.

Jardine R. J., Lehane B. M. and Everton S. J. Friction Coefficients for Pile in Sands and Silts [Report]. - [s.l.] : Society for Underwater Technology, 1993.

Merritt David K [et al.] Construction of the Iowa Highway 60 Precast Prestressed Concrete Pavement Bridge Approach Slab Demonstration Project [Report]. - Austin : The Transtec Group, Inc., 2007.

Naik Tarun R., Chun Yoon-Moon and Kraus Rudolph N. Investigation of Concrete Properties to Support Implementation of the New AASHTO Pavement Deisgn Guide [Report]. - Milwaukee : University of Wisconsin, 2006.

Puppala Anand J [et al.] Recommendations for Design, Construction, and Maintenance of Bridge Approach Slabs: Synthesis Report [Report]. - [s.l.] : FHWA, 2008.

Schuettpelz C.C., Fratta D. and Edil T.B. Mechanistic Corrections for Determining the Resilient Modulus of Base Course Materials Based on Elastic Wave Measurements [Report]. - [s.l.] : ASCE Journal of Geotechnical and Geoenvironmental Engineering, 136(8):1086-1094, 2010.

Seo Jeong Bok The Bump at the End of the Bridge: An Investigation [Report]. - College Station : Texas A&M University, 2003.

Stark T. K., Olson S. M. and Long J. H. Differential Movement at the Embankment/Structure Interface - Mitigation and Rehibilitation Report No. IAB=H1 [Report]. - Springfield : Illinois Department of Transportation, 1995.

Wahls H. E. NCHRP Synthesis of Highway Practices 159: Design and Construction of Bridge Approaches. [Report]. - Washington D.C. : Tranportation Research Board, National Research Council, 1990.

White David J [et al.] Underlying Causes for Settlement of Bridge Approach Pavement Systems [Journal]. - [s.l.] : ASCE, 2007. - July/August.

Wisconsin Department of Transportation WisDOT Bridge Manual [Book]. - 2009.

Zaman M., Gopalasingam A. and Laguros Consolidation of Settlement of Bridge Approach Foundations [Journal]. - [s.l.] : Journal of Geotechnical Engineerings, ASCE, 1991. - Vol. 117.

Appendix 1 – WisDOT A5 Abutment

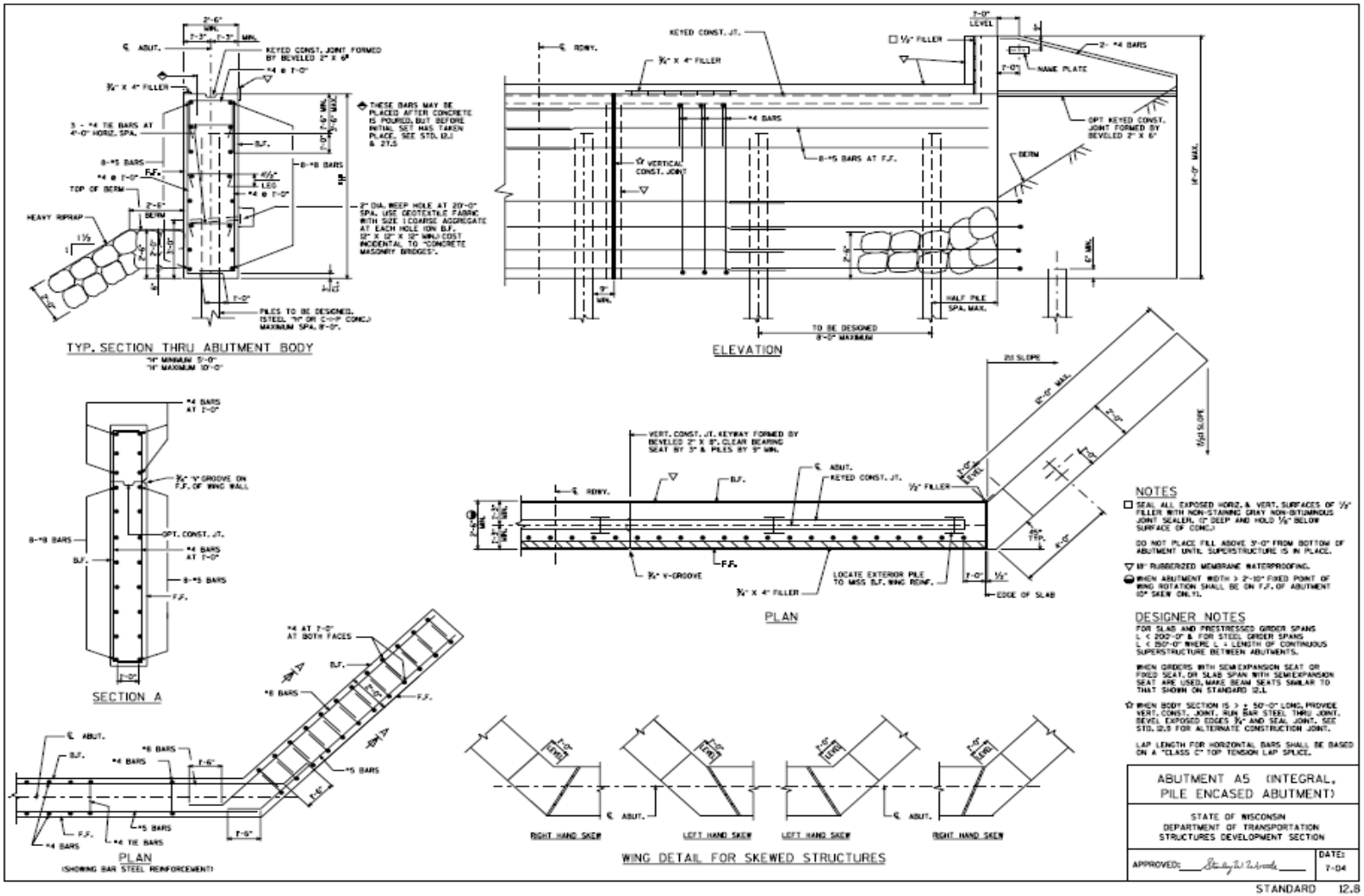

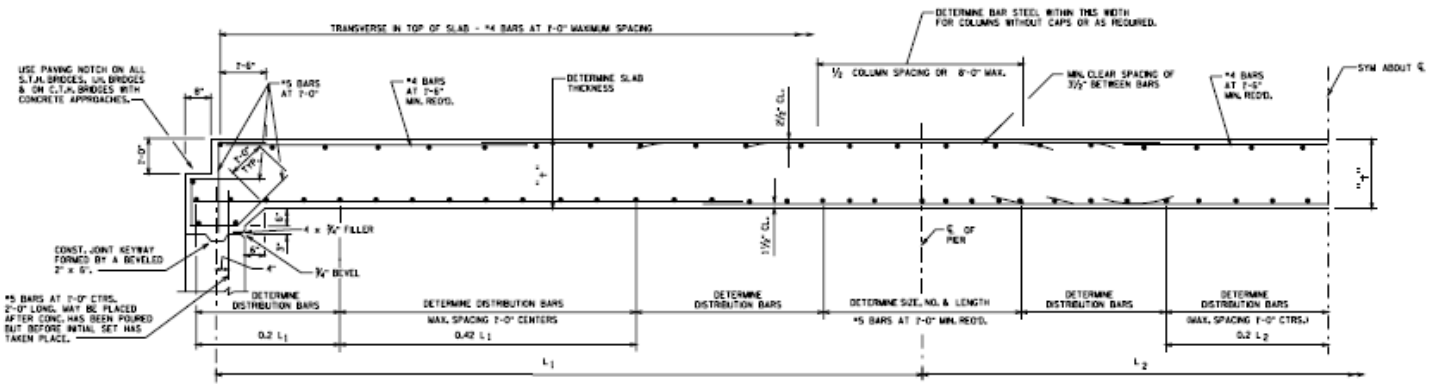

HALF LONGITUDINAL SECTION

PIER CAP OR WALL TYPE PIER
SEE STD. 18.1 FOR COLUMN W/O CAP PIER DETAIL.

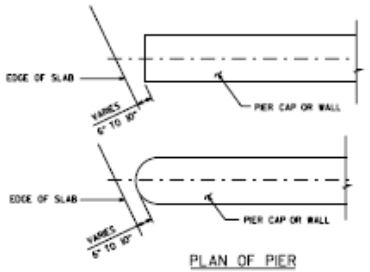

PLAN OF PIER

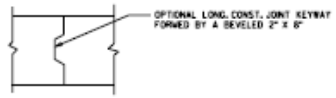

OPTIONAL LONGITUDINAL CONSTRUCTION JOINT

NOTES

TOP TRANSVERSE BARS IN SLAB SHALL BE SUPPORTED BY INDIVIDUAL BAR CHAIRS AT APPROXIMATELY 7'-0" CENTERS EACH WAY. BOTTOM LONGITUDINAL BARS SHALL BE SUPPORTED BY CONTINUOUS BAR CHAIRS AT APPROXIMATELY 4'-0" CENTERS.

ALL SLAB THICKNESS DIMENSIONS ARE MINIMUM. ANY TOLERANCES NECESSARY TO CORRECT CONSTRUCTION DISCREPANCIES ARE TO BE PLUS (+).

PARAPETS SHOWN ABOVE THE HORIZONTAL CONSTRUCTION JOINT SHALL BE POURED AFTER FALSEWORK HAS BEEN RELEASED EXCEPT FOR STAGE CONSTRUCTION.

CAMBER SPANS AS SHOWN TO PROVIDE FOR DEAD LOAD DEFLECTION & FUTURE CREEP. CAMBER DOES NOT INCLUDE ALLOWANCE FOR FORM SETTLEMENT.

Δ ¾" CONTINUOUS DRIP GROOVE TO END 2'-0" AWAY FROM FACE OF ABUTMENT.

DESIGNER NOTES

ALL BAR SPLICES TO BE BASED ON "CLASS C" TENSION LAP SPLICE.

USE OPTIONAL LONGITUDINAL JOINTS WHEN ROADWAY WIDTH IS OVER 52'-0".

FOR BRIDGES LOCATED IN REMOTE AREAS USE OPTIONAL TRANSVERSE JOINT WHEN POUR EXCEEDS 400 C.Y. PLACE KEYED JOINT NEAR POINT OF DEAD LOAD INFLECTION.

ALL TRANSVERSE BAR STEEL REINFORCEMENT SHALL BE PLACED ON THE SKEW.

FLOOR DRAINS ARE TO BE OMITTED FROM THESE UNITS WHERE POSSIBLE. IF FLOOR DRAINS ARE REQ'D., PLACE ONLY AT THE 2/10 & 8/10 PTS. BEND MAIN REBARS PAST DRAINS - DO NOT CUT.

PIER CAP OR WALL TYPE PIERS SHALL BE USED ON MOST STRUCTURES. COLUMN W/O CAP TYPE PIERS (SEE STD. 18.1) MAY BE USED WITH THE APPROVAL OF THE STRUCTURES DESIGN SECTION.

THE MAXIMUM ALLOWABLE SKEW ANGLE OF STRUCTURE SHALL BE 30°.

CONTINUOUS FLAT SLAB

STATE OF WISCONSIN
DEPARTMENT OF TRANSPORTATION
STRUCTURES DEVELOPMENT SECTION

APPROVED: [signature] DATE: 7/99

STANDARD 18.2

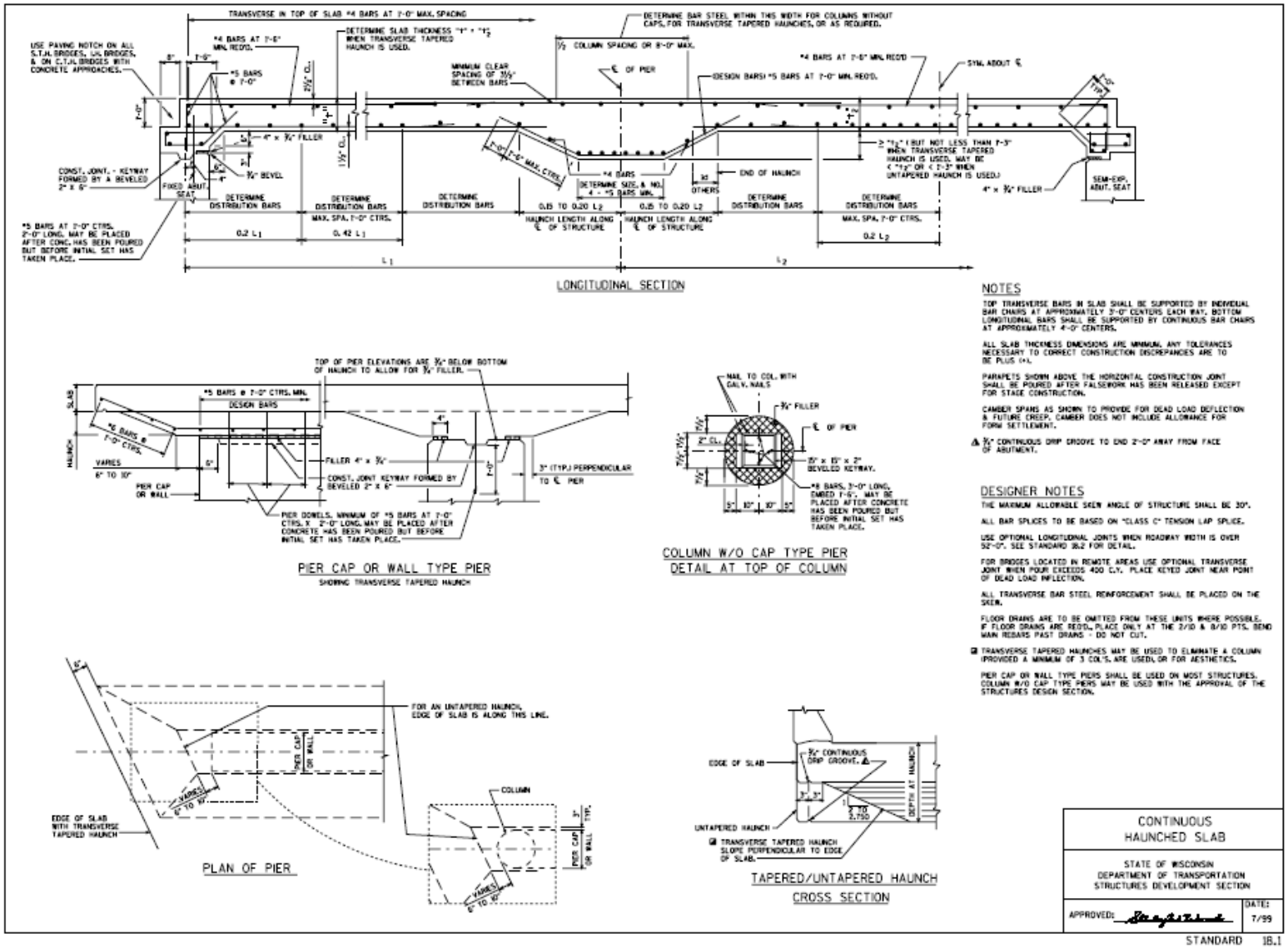

LONGITUDINAL SECTION

PIER CAP OR WALL TYPE PIER
SHOWING TRANSVERSE TAPERED HAUNCH

COLUMN W/O CAP TYPE PIER
DETAIL AT TOP OF COLUMN

NOTES

TOP TRANSVERSE BARS IN SLAB SHALL BE SUPPORTED BY INDIVIDUAL BAR CHAIRS AT APPROXIMATELY 3'-0" CENTERS EACH WAY. BOTTOM LONGITUDINAL BARS SHALL BE SUPPORTED BY CONTINUOUS BAR CHAIRS AT APPROXIMATELY 4'-0" CENTERS.

ALL SLAB THICKNESS DIMENSIONS ARE MINIMUM. ANY TOLERANCES NECESSARY TO CORRECT CONSTRUCTION DISCREPANCIES ARE TO BE PLUS (+).

PARAPETS SHOWN ABOVE THE HORIZONTAL CONSTRUCTION JOINT SHALL BE POURED AFTER FALSEWORK HAS BEEN RELEASED EXCEPT FOR STAGE CONSTRUCTION.

CAMBER SPANS AS SHOWN TO PROVIDE FOR DEAD LOAD DEFLECTION & FUTURE CREEP. CAMBER DOES NOT INCLUDE ALLOWANCE FOR FORM SETTLEMENT.

▲ ¾" CONTINUOUS DRIP GROOVE TO END 2'-0" AWAY FROM FACE OF ABUTMENT.

DESIGNER NOTES

THE MAXIMUM ALLOWABLE SKEW ANGLE OF STRUCTURE SHALL BE 30°.

ALL BAR SPLICES TO BE BASED ON "CLASS C" TENSION LAP SPLICE.

USE OPTIONAL LONGITUDINAL JOINTS WHEN ROADWAY WIDTH IS OVER 52'-0". SEE STANDARD 18.2 FOR DETAIL.

FOR BRIDGES LOCATED IN REMOTE AREAS USE OPTIONAL TRANSVERSE JOINT WHEN POUR EXCEEDS 400 C.Y. PLACE KEYED JOINT NEAR POINT OF DEAD LOAD INFLECTION.

ALL TRANSVERSE BAR STEEL REINFORCEMENT SHALL BE PLACED ON THE SKEW.

FLOOR DRAINS ARE TO BE OMITTED FROM THESE UNITS WHERE POSSIBLE. IF FLOOR DRAINS ARE REQ'D., PLACE ONLY AT THE 2/10 & 8/10 PTS. BEND MAIN REBARS PAST DRAINS - DO NOT CUT.

■ TRANSVERSE TAPERED HAUNCHES MAY BE USED TO ELIMINATE A COLUMN (PROVIDED A MINIMUM OF 3 COL'S. ARE USED), OR FOR AESTHETICS.

PIER CAP OR WALL TYPE PIERS SHALL BE USED ON MOST STRUCTURES. COLUMN W/O CAP TYPE PIERS MAY BE USED WITH THE APPROVAL OF THE STRUCTURES DESIGN SECTION.

PLAN OF PIER

TAPERED/UNTAPERED HAUNCH
CROSS SECTION

CONTINUOUS HAUNCHED SLAB

STATE OF WISCONSIN
DEPARTMENT OF TRANSPORTATION
STRUCTURES DEVELOPMENT SECTION

APPROVED: _____ DATE: 7/99

STANDARD 18.1

Appendix 2 – WisDOT Standard Approach Slab

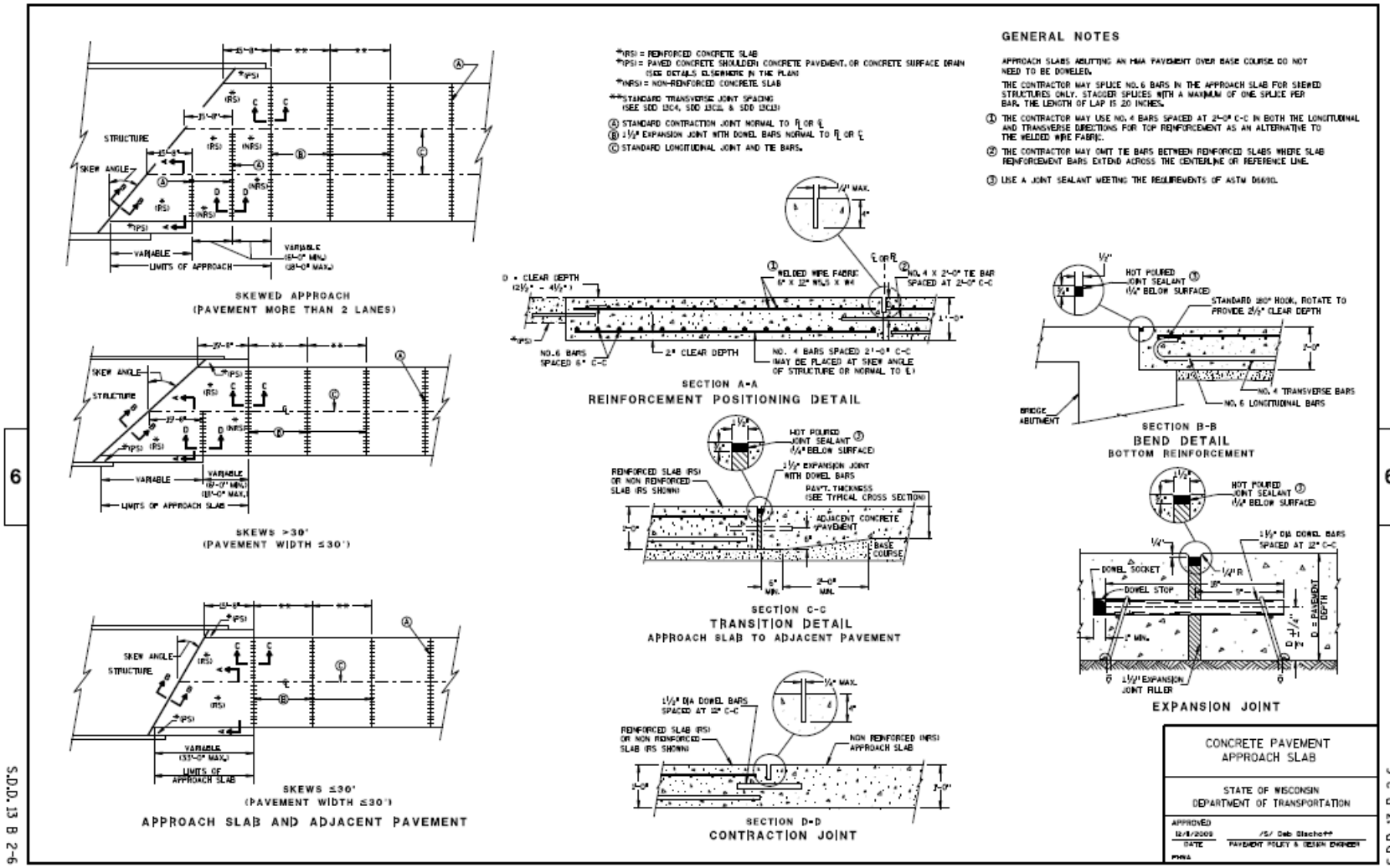

Appendix 3 – Mesh Verification Calculations

The multi mesh extrapolation used Richardson's Extrapolation as defined in the *Concepts and Applications of Finite Element Analysis* by Cook, Malkus, Pleshia, and Witt (CMPW).

From the analysis conducted with 6" elements:

The length of one of the elements: $l_6 := 6in$

The deflection of the control point: $\Delta_6 := 1.7715079in$

The "characteristic length" of the element: $h_{6inchele} := \sqrt{l_6^2 + l_6^2} = 8.4852814 \cdot in$

This is defined in Section 9.6 of CMPW.

From the analysis conducted with 3" elements:

The length of one of the elements: $l_3 := 3in$

The deflection of the control point: $\Delta_3 := 1.7985551in$

The "characteristic length" of the element: $h_{3inchele} := \sqrt{l_3^2 + l_3^2} = 4.2426407 \cdot in$

This is defined in Section 9.6 of CMPW.

From the analysis conducted with 1.5" elements:

The length of one of the elements: $l_{15} := 1.5in$

The deflection of the control point: $\Delta_{15} := 1.8034567in$

The "characteristic length" of the element: $h_{15inchele} := \sqrt{l_{15}^2 + l_{15}^2} = 2.1213203 \cdot in$

This is defined in Section 9.6 of CMPW.

$\phi_1 := \Delta_6$ $h_1 := h_{6inchele}$

$\phi_2 := \Delta_3$ $h_2 := h_{3inchele}$

$\phi_3 := \Delta_{15}$ $h_3 := h_{15inchele}$

Plot the deflection vs. characteristic length raised to the q power. Iterate q until a straight line is plotted.

$q := 2.46688316122129$

$\Phi := \begin{pmatrix} \phi_1 \\ \phi_2 \\ \phi_3 \end{pmatrix}$ $h := \begin{pmatrix} h_1 \\ h_2 \\ h_3 \end{pmatrix}$

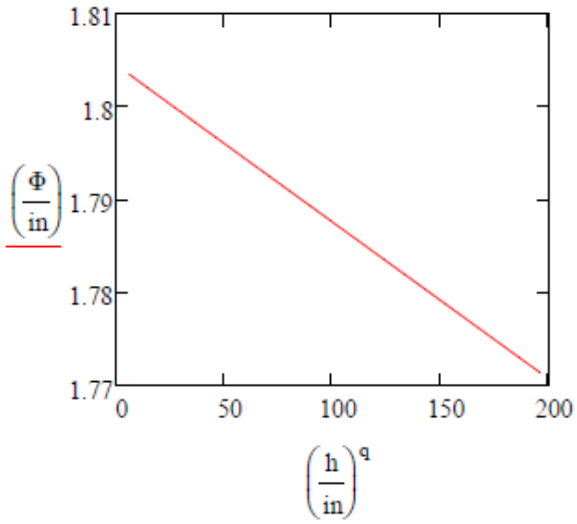

If the above plot is linear, you may proceed to determine the deflection that would be calculated in a model with an infinitely fine mesh.

$$\phi_{infinite} := \frac{\frac{\phi_1}{in}\cdot\left(\frac{h_2}{in}\right)^q - \frac{\phi_2}{in}\cdot\left(\frac{h_1}{in}\right)^q}{\left(\frac{h_2}{in}\right)^q - \left(\frac{h_1}{in}\right)^q}\cdot 1in \qquad \phi_{infinite} = 1.8045278\cdot in$$

Now you can calculate the error between the infinitely fine mesh and the other meshes:

The error in the 6" element mesh: $e_1 := \left|\frac{\phi_1 - \phi_{infinite}}{\phi_{infinite}}\right| = 1.8298353\cdot\%$

The error in the 3" element mesh: $e_2 := \left|\frac{\phi_2 - \phi_{infinite}}{\phi_{infinite}}\right| = 0.3309834\cdot\%$

The error in the 1.5" element mesh: $e_3 := \left|\frac{\phi_3 - \phi_{infinite}}{\phi_{infinite}}\right| = 0.0593555\cdot\%$

Appendix 4 – Slab Deflection Verification Calculations

Multiple beam charts were used from Table 3-23 in the AISC 13th LRFD steel design handbook. Superposition was used to combine the differing load cases together.

Identify/calculate properties used for the calculations:

The 28 day compressive strength of the concrete: $f_c := 4000psi$

The density of the concrete is: $\rho := 145pcf$

Concrete modulus of elasticity: $E := 57000psi \cdot \sqrt{\frac{f_c}{psi}}$

The axle load is: $P := 25kip$

The length of the slab is: $L := 15ft + 8in$

The width of the slab is: $b := 12ft$

The height of the slab is: $h := 1ft$

The moment of inertia is: $I := \frac{b \cdot h^3}{12}$

$I = 20.736 \times 10^3 \cdot in^4$

The self weight of the slab is: $w := b \cdot h \cdot \rho$

$w = 1.74 \times 10^3 \cdot plf$

The coordinates of the axles are:

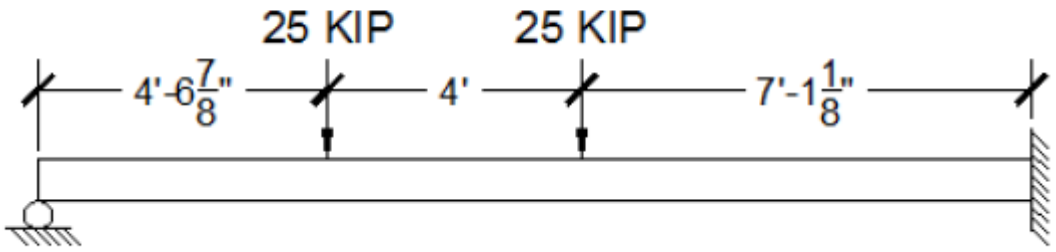

Case 12 in the AISC manual was used to determine the deflection of the slab due to gravity:

$$\Delta_w(x) := \frac{w \cdot x}{48 \cdot E \cdot I} \cdot \left(L^3 - 3 \cdot L \cdot x^2 + 2 \cdot x^3\right)$$

Case 14 in the AISC manual was used to determine the deflection of the slab from a single point load:

Deflection the left axle load:

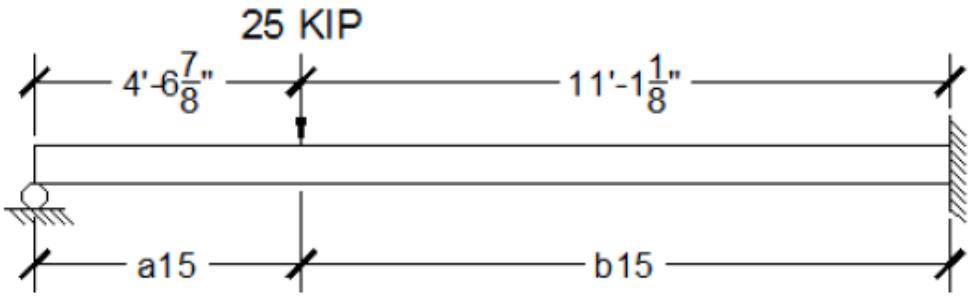

$a_{15} := 4ft + 6.875in$ $\quad$ $b_{15} := 11ft + 1.125in$

$$\Delta_{M15}(x) := \begin{cases} \frac{P \cdot b_{15}^2 \cdot x}{12 \cdot E \cdot I \cdot L^3} \cdot \left(3a_{15} \cdot L^2 - 2L \cdot x^2 - a_{15} \cdot x^2\right) & \text{if } x < a_{15} \\ \frac{P \cdot a_{15}^2 \cdot b_{15}^3}{12 \cdot E \cdot I \cdot L^3} \cdot \left(3 \cdot L + a_{15}\right) & \text{if } x = a_{15} \\ \frac{P \cdot a_{15}}{12 \cdot E \cdot I \cdot L^3} \cdot (L - x)^2 \cdot \left(3L^2 \cdot x - a_{15}^2 \cdot x - 2 \cdot a_{15}^2 \cdot L\right) & \text{if } x > a_{15} \end{cases}$$

Deflection of the right axle:

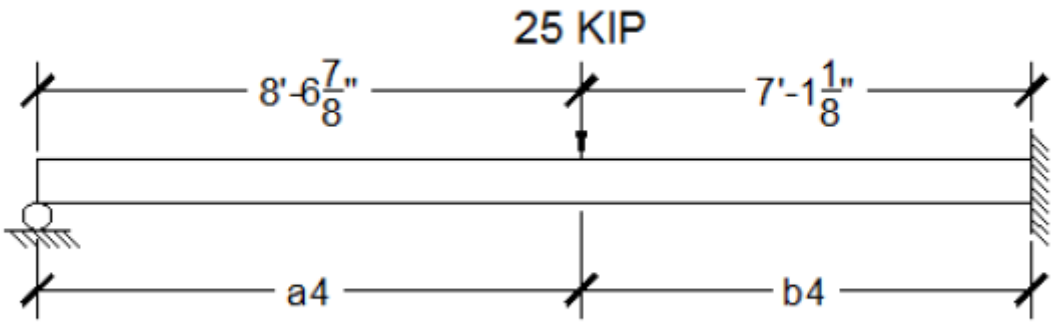

$a_4 := 8ft + 6.875in$ $b_4 := 7ft + 1.125in$

$$\Delta_{M4}(x) := \begin{cases} \frac{P \cdot b_4^{\,2} \cdot x}{12 \cdot E \cdot I \cdot L^3} \cdot \left(3a_4 \cdot L^2 - 2L \cdot x^2 - a_4 \cdot x^2\right) & \text{if } x < a_4 \\ \frac{P \cdot a_4^{\,2} \cdot b_4^{\,3}}{12 \cdot E \cdot I \cdot L^3} \cdot \left(3 \cdot L + a_4\right) & \text{if } x = a_4 \\ \frac{P \cdot a_4}{12 \cdot E \cdot I \cdot L^3} \cdot (L - x)^2 \cdot \left(3L^2 \cdot x - a_4^{\,2} \cdot x - 2 \cdot a_4^{\,2} \cdot L\right) & \text{if } x > a_4 \end{cases}$$

Use superposition to find the total deflection of the slab:

$\Delta(x) := \Delta_w(x) + \Delta_{M15}(x) + \Delta_{M4}(x)$

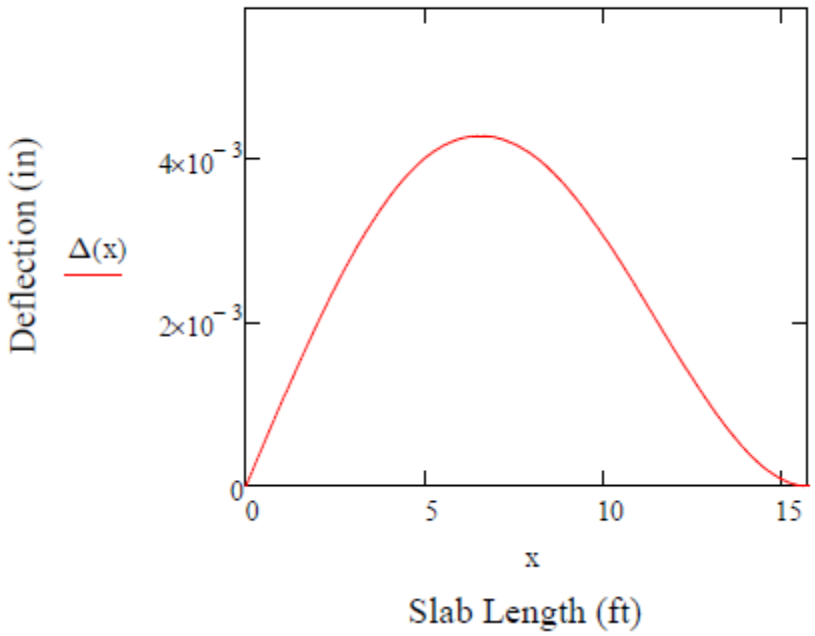

Appendix 5 – Soil Verification Spreadsheet

P	1000	N
B	0.0572	m
H	3.66	m
c	4784	Pa
Tire Load	1000	N

Coorcinates and Stress			
x	Depth (z) (m)	FEM Stress (Pa)	Eqn 3.12 (Pa)
0.0000003	0.000	4405	4783
0.0000025	0.069	2370	1799
0.0000025	0.069	1857	1799
0.0000046	0.138	1171	1133
0.0000046	0.138	1154	1133
0.0000065	0.208	806	797
0.0000065	0.208	805	797
0.0000085	0.278	614	609
0.0000085	0.278	615	609
0.0000106	0.349	493	491
0.0000106	0.349	495	491
0.0000122	0.420	412	409
0.0000122	0.420	413	409
0.0000148	0.493	352	350
0.0000148	0.493	353	350
0.0000169	0.558	313	310
0.0000172	0.568	306	305
0.0000172	0.568	307	305
0.0000198	0.644	270	269
0.0000198	0.644	270	269
0.0000214	0.724	240	239
0.0000243	0.809	215	214
0.0000264	0.882	198	197
0.0000271	0.916	190	190
0.0000271	0.916	190	190
0.0000279	0.925	188	188
0.0000279	0.925	189	188
0.0000308	1.03	168	168
0.0000308	1.03	168	168
0.0000335	1.13	154	154
0.0000367	1.24	141	140
0.0000367	1.24	141	140
0.0000383	1.29	135	135
0.0000417	1.42	123	123
0.0000436	1.49	117	116
0.0000436	1.49	117	116
0.0000485	1.65	107	106
0.0000494	1.67	105	104
0.0000534	1.84	96	95
0.0000585	2.01	87	86
0.0000623	2.13	83	82
0.0000623	2.13	83	82
0.0000623	2.15	82	81
0.0000660	2.27	78	77
0.0000715	2.45	72	71
0.0000765	2.65	68	66
0.0000774	2.66	67	66
0.0000827	2.86	63	61
0.0000891	3.07	59	57
0.0000958	3.30	55	53
0.000103	3.54	52	49
0.000111	3.82	49	46
0.000120	4.14	46	42
0.000130	4.48	43	39
0.000140	4.84	41	36
0.000151	5.24	39	33
0.000163	5.67	38	31
0.000176	6.12	37	28
0.000189	6.57	36	26
0.000201	7.00	36	25

Change in Vertical Stress		
Depth (ft)	Theory (psf)	FEM (psf)
0.000	99.9	92.0
0.227	37.6	49.5
0.227	37.6	38.8
0.454	23.7	24.5
0.454	23.7	24.1
0.682	16.7	16.8
0.682	16.7	16.8
0.912	12.7	12.8
0.912	12.7	12.8
1.14	10.2	10.3
1.14	10.2	10.3
1.38	8.55	8.60
1.38	8.55	8.62
1.62	7.31	7.36
1.62	7.31	7.37
1.83	6.47	6.53
1.85	6.36	6.40
1.85	6.36	6.41
2.11	5.61	5.63
2.11	5.61	5.64
2.33	5.00	5.01
2.65	4.48	4.49
2.89	4.11	4.13
3.00	3.96	3.97
3.00	3.96	3.96
3.04	3.92	3.93
3.04	3.92	3.94
3.39	3.51	3.51
3.39	3.51	3.52
3.71	3.21	3.22
4.05	2.93	2.95
4.05	2.93	2.95
4.24	2.81	2.82
4.65	2.56	2.58
4.90	2.43	2.45
4.90	2.43	2.45
5.40	2.21	2.23
5.49	2.17	2.19
6.02	1.98	2.00
6.60	1.81	1.83
6.99	1.71	1.73
6.99	1.71	1.73
7.05	1.69	1.72
7.44	1.60	1.63
8.05	1.48	1.51
8.69	1.37	1.41
8.72	1.37	1.41
9.39	1.27	1.31
10.1	1.18	1.23
10.8	1.10	1.16
11.5	1.03	1.09
12.5	0.95	1.02
13.5	0.88	0.96
14.7	0.81	0.90
15.9	0.75	0.86
17.2	0.69	0.82
18.5	0.64	0.79
20.1	0.59	0.77
21.6	0.55	0.76
23.0	0.52	0.75

Appendix 6 – Approach Slab End Rotation Sample Calculations

These calculations use the values from the baseline model.

The coordinates of Points A, B, and C were pulled from the model.

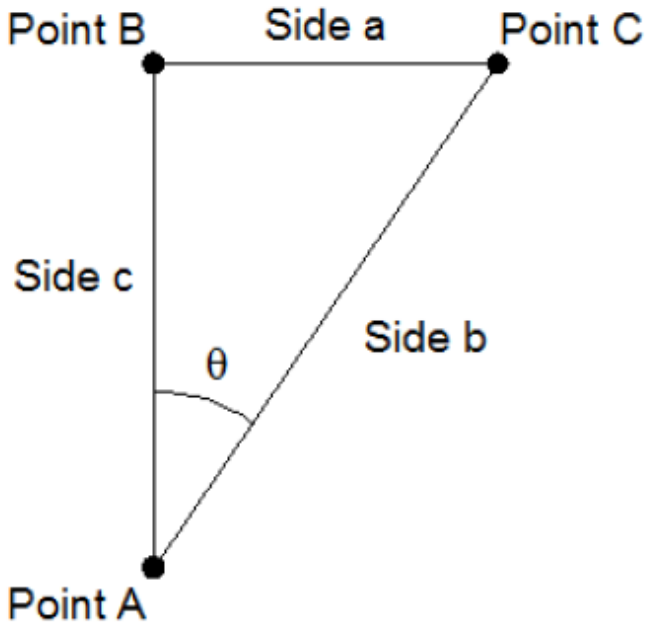

Point A:	$x_A := 0.000168637\text{m}$	$y_A := -0.00516027\text{m}$
Point B:	$x_B := -0.000162356\text{m}$	$y_B := 1\text{ft} + 0.00516009\text{m}$
Point C:	$x_C := x_A$	$y_C := y_B$

The length of each leg was:

Side a: $$a := \sqrt{(x_B - x_C)^2 + (y_B - y_C)^2}$$

$$a = 0.013 \cdot in$$

Side b: $$b := \sqrt{(x_C - x_A)^2 + (y_C - y_A)^2}$$

$$b = 12.406 \cdot in$$

Side c: $$c := \sqrt{(x_B - x_A)^2 + (y_B - y_A)^2}$$

$$c = 12.406 \cdot in$$

The law of cosines was used to determine angle theta:

The law of cosines is: $$a^2 = b^2 + c^2 - 2 \cdot b \cdot c \cdot \cos(\theta)$$

Rewritten to find theta: $$\theta := \operatorname{acos}\left(\frac{b^2 + c^2 - a^2}{2 \cdot b \cdot c}\right)$$

$$\theta = 1.05 \times 10^{-3} \cdot rad$$

Note: The small differences exist between MathCAD and Excel are due to truncation of calculations performed in Excel.